

Design, Modeling and Evaluation of Indoor Visible Light Communication System for Improved Communication & Illumination Performance

Thesis submitted by

Sourish Chatterjee

Doctor of Philosophy (Engineering)

**Department of Electrical Engineering
Faculty Council of Engineering & Technology
Jadavpur University, Kolkata, India**

2024

JADAVPUR UNIVERSITY

FACULTY OF ENGINEERING AND TECHNOLOGY

Index No: 149/22/E

1. Title of the Thesis

“DESIGN, MODELING AND EVALUATION OF INDOOR VISIBLE LIGHT COMMUNICATION SYSTEM FOR IMPROVED COMMUNICATION & ILLUMINATION PERFORMANCE”

2. Name, Designation and Institution of the Supervisor/s:

Prof. Biswanath Roy

Professor, Department of Electrical Engineering
Jadavpur University, Kolkata 700032

3. List of Publications:

(a) International Journal Articles (Published)

1. Chatterjee, S., & Roy, B. (2020). “Design, development and practical realization of a VLC supportive indoor lighting system”, *Light & Engineering*, 28(3). DOI: doi.org/10.33383/2019-048 (SCIE & Scopus Indexed)
2. Chatterjee, S., & Roy, B. (2020). “An approach to ensure joint illumination & communication performance of a forward error corrected indoor visible light communication (VLC) system in presence of ambient light interference”, *Journal of Optical Communications*, vol. 44, no. s1, 2023, pp. s1767-s1776 DOI: doi.org/10.1515/joc-2019-0212 (Impact Factor/CiteScore: NA/3.2)

3. Chatterjee, S., & Sabui, D. (2020). **"Daylight integrated indoor VLC architecture: an energy-efficient solution"**, *Transactions on Emerging Telecommunications Technologies*, 31(9), e3800. DOI: doi.org/10.1002/ett.3800 **(Impact Factor/CiteScore: 3.6/6.4)**
4. Chatterjee, S., Sabui, D., Khan, G. S., & Roy, B. (2021). **"Signal to interference plus noise ratio improvement of a multi-cell indoor visible light communication system through optimal parameter selection complying lighting constraints"**, *Transactions on Emerging Telecommunications Technologies*, 32(10), e4291. DOI: doi.org/10.1002/ett.4291 **(Impact Factor/CiteScore: 3.6/6.4)**
5. Chatterjee, S., Sabui, D., & Roy, B. (2024). **"Mobility Aware Blockage Management of a Multi-user Multi-cell Hybrid Li-Fi Wi-Fi System With Freeform Diversity Receiver"**, *Optics Communications*, 130487 DOI: doi.org/10.1016/j.optcom.2024.130487 **(Impact Factor/CiteScore: 2.4/5.0)**

(b) International Conference Publications

1. Chatterjee, S., & Roy, B. (2021, January). **"Multi-parameter optimization of a hemispheric angle diversity receiver to reduce SINR fluctuation for an indoor MIMO-VLC system."** In *2021 4th Biennial International Conference on Nascent Technologies in Engineering (ICNTE)* (pp. 1-6). IEEE. DOI: [10.1109/ICNTE51185.2021.9487694](https://doi.org/10.1109/ICNTE51185.2021.9487694) **(Scopus Indexed)**
2. Chatterjee, S., Sabui, D. & Roy, B. (2024, January). **"On the Performance of Hybrid LiFi-RF Network Using Freeform Based Angle Diversity Receiver,"** In *2024 3rd International Conference on Control, Instrumentation, Energy & Communication (CIEC)* IEEE. DOI: [10.1109/CIEC59440.2024.10468220](https://doi.org/10.1109/CIEC59440.2024.10468220) **(Scopus Indexed)**

4. List of Patents: None

5. List of Presentation in National/ International Conferences and Workshops:

1. **S.Chatterjee and B.Roy, "Multi-parameter optimization of a hemispheric angle diversity receiver to reduce SINR fluctuation for an indoor MIMO-VLC system,"** 2021 *4th Biennial International Conference on Nascent Technologies in Engineering (ICNTE)*
(Presented the paper at ICNTE-2021 organized by Fr. C. Rodrigues Institute of Technology, Vashi in association with IEEE and IAS on January 15-16, 2021)
2. **S. Chatterjee, D. Sabui and B. Roy, "On the Performance of Hybrid LiFi-RF Network Using Freeform Based Angle Diversity Receiver,"** 2024 *IEEE 3rd International Conference on Control, Instrumentation, Energy & Communication (CIEC)*
(Presented the paper at CIEC-2024 jointly organized by IEEE CSS-IMS Kolkata Chapter and Department of Applied Physics, University of Calcutta during January 25-27, 2024)

JADAVPUR UNIVERSITY

FACULTY OF ENGINEERING AND TECHNOLOGY

"STATEMENT OF ORIGINALITY"

I, **Sourish Chatterjee** registered on **02nd June, 2022** do hereby declare that this thesis entitled "**Design, Modeling and Evaluation of Indoor Visible Light Communication System for Improved Communication & Illumination Performance**" contains literature survey and original research work done by the undersigned candidate as part of Doctoral studies.

All information in this thesis have been obtained and presented in accordance with existing academic rules and ethical conduct. I declare that, as required by these rules and conduct, I have fully cited and referred all materials and results that are not original to this work.

I also declare that I have checked this thesis as per the "Policy on Anti Plagiarism, Jadavpur University, 2019", and the level of similarity as checked by iThenticate software is 4%.



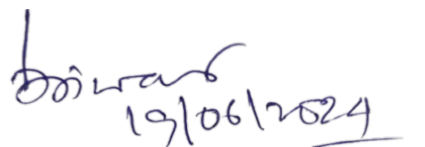
Signature of Candidate:

Date : 19-06-2024

Certified by Supervisor(s):

(Signature with date, seal)

1.




19/06/2024

Professor
Electrical Engineering Department
JADAVPUR UNIVERSITY
Kolkata - 700 032

JADAVPUR UNIVERSITY
FACULTY OF ENGINEERING AND TECHNOLOGY

CERTIFICATE FROM THE SUPERVISOR/S

This is to certify that the thesis entitled *“Design, Modeling and Evaluation of Indoor Visible Light Communication System for Improved Communication & Illumination Performance”* submitted by *Mr. Sourish Chatterjee*, who got his name registered on *02nd June, 2022* for the award of **Ph.D. (Engg.)** degree of Jadavpur University is absolutely based upon his/her own work under the supervision of *Prof. Biswanath Roy* and that neither his/her thesis nor any part of the thesis has been submitted for any degree/diploma or any other academic award anywhere before.

1. 

Signature of the Supervisor
and date with Office Seal

2.

Signature of the Supervisor
and date with Office Seal
(If more than one Supervisor)

Professor
Electrical Engineering Department
JADAVPUR UNIVERSITY
Kolkata - 700 032

Acknowledgement

"The function of education is to teach one to think intensively and to think critically. Intelligence plus character - that is the goal of true education."

- Martin Luther King Jr.

First and foremost, I wish to acknowledge the countless moments that laid the foundation of thoughts long before the journey of research commenced. In those days, I wandered unaware of this technology, its existence a distant rumor, yet I could sense the potential of data transmission through light. How, precisely, remained a mystery even to me, but the seed of the idea nestled within. I remember sharing this notion with a friend, met with little more than a passing glance. Perhaps someone, unseen, was already orchestrating the stage. Be it a solitary guide or the divine hand, my gratitude reaches out to him.

When the ball started to roll he was the first person to whom I approached for guiding me to do research in this unexplored domain. My gratitude, an unending river, flows to my guide, **Prof. Biswanath Roy**, who journeyed alongside, in every facet of this odyssey. Especially, I will never forget the financial assistance received from Prof. Biswanath Roy during the COVID tempest, a lifeline through the storm that delayed my official registration. I vividly reminisce about the days when **Prof. Salil Kumar Sanyal** (Retired) from the Department of Electronics and Telecommunication at Jadavpur University generously provided me with technical guidance to prepare the manuscript of my first paper. The invaluable inputs he shared will forever resonate in my life. Thank you so much, sir, sincere regards to you.

In the tapestry of my learning, though small my thread may seem, its essence weaves from the wisdom of one with whom my physical paths never crossed so far. Yet his scholarly aura, a beacon of enlightenment, guides my path. **Prof. Harald Haas**, "The Father of LiFi", your research, a symphony of enlightenment, resonates within me. Each article, a sacred manuscript, illuminates my way. In moments of adversity, your work becomes my solace, my sanctuary. Want to convey my deepest gratitude and respect to you, Sir.

Despite my deep affinity for VLC research, I found myself unable to dedicate my full time to this field due to the absence of research funding. To support myself, I delved into other research projects focused on clean energy transition. Thankfully, I had the privilege of working under the esteemed guidance of another eminent researcher, **Prof. Joyashree Roy**, a Distinguished Professor at the Asian Institute of Technology, Thailand.

I extend my heartfelt gratitude to Professor Roy for affording me the opportunity to gain global research exposure. Going beyond the technical knowledge, I gleaned invaluable lessons in research etiquette from her mentorship.

Better late than never, I had the chance to interact with another unparalleled research mind, **Prof. Amitava Chatterjee**, Jadavpur University as a member of my research advisory committee. Despite the brevity of our meetings, his insightful comments, foresight, and invaluable suggestions greatly contributed to enhancing the final segment of the thesis. I hold great respect and gratitude towards Prof. Chatterjee for his generosity. I only wish I could have had more opportunities to benefit from his wisdom.

In the realm of implementing this study, amid my struggles to procure necessary software and other resources, bountiful support emerged from my friend **Deblina**, a dedicated research scholar from IIT Delhi. It is with heartfelt sincerity that I extend my profound appreciation to her. Deblina, your unwavering collaboration, along with the respected **Prof. Gufran S. Khan**, IIT Delhi as co-researchers, has been outstanding.

I express my heartfelt gratitude and appreciation to **Prof. Xiping Wu** from University College Dublin for his invaluable support in modeling light-path blockage, a crucial aspect of the last segment of this thesis. Special thanks to **Prof. Saswati Majumdar**, EE Department, JU for her kind encouragement and help.

A massive thank you to my incredible mom for her endless love, support, and encouragement throughout this journey. Big thanks to all my fellow research buddies and other awesome pals, especially **Dr. Vishwanath** (Love to call him Raja who helped in one of my experiment), **Sangita**, **Dr. Snehasish**, **Deepanjan da**, **Asmita**, **Prasenjit** and countless others. Your support has been superb on this journey! A heartfelt thank to all my students at IIE Kalyani for the invaluable lessons I've learned while teaching them—you've enriched my life more than you know.

During my tenure of over three years with the Global Change Programme at Jadavpur University (**GCP-JU**), I was immersed in a secure and vibrant atmosphere. I wish to extend my sincere gratitude to the coordinator of GCP-JU **Prof. Anupam Debsarkar**. I am also thankful to **Arijit** and **Suman da** for their support and camaraderie.

Last but not the least, a huge shoutout to my loyal sidekick, **Maharaja!** Whether I'm buried in books or deep in thought, you're always right there, keeping me company with your wagging tail and unconditional love. Thanks for being the best study buddy a researcher could ask for. You rock, **Maharaja!**

S. Chatterjee
19-06-2024

Abstract

Looking beyond conventional wireless networks, **VLC** holds significant potential to revolutionize the way we perceive data transmission. Moreover, the lighting industry is undergoing a transformation towards a 'light-as-a-service' (LaaS) business model, where lighting infrastructure is repurposed into a wireless communication network. This transformation can enable **VLC** systems to access a frequency spectrum 1000 times larger, facilitating greater cell densification in the future communication and lighting landscape. Both **VLC** and its networked counterpart are expected to play a crucial role in the evolution of data transmission, especially in the context of upcoming 6G networks, the Internet of Everything, and Industry 4.0 applications. The central theme of the thesis revolves around the design, modeling, and assessment of indoor **VLC** Systems. The aim is to overcome the shortcomings observed in current indoor **VLC** system designs, particularly from a lighting perspective. This work seeks to provide constructive solutions that enable the harmonious integration of communication and illumination, fostering improved joint performance in these aspects.

The initial phase of the research focuses on exploring the interferences arising from artificial ambient light sources and their integration with natural daylight in indoor environments. In indoor environment, all the light sources may not always used for both communication and illumination purposes. Also there is a need for dimming to make the system energy efficient as per the available daylight. This study introduces a forward error-corrected receiver configuration capable of effectively mitigating the impact of ambient light interferences. The proposed methodology involves employing a Tail Biting convolution encoder in the transmitter's encoding section and a Viterbi decoder in the receiver's decoding section to enhance bit error rate performance. Additionally, this research segment presents a stand-alone prototype for **VLC** that integrates daylight and supports dimming. The proposed system exhibits a remarkable energy-saving capability, reaching up to 37.29% under maximum daylight conditions. The investigation extends to assessing the performance of both illumination and communication under varying daylight conditions. Furthermore, the short-term Flicker Severity Index is experimentally evaluated and compared against the threshold level specified by the International Electrotechnical Commission.

The next phase of this research focuses on designing an indoor multi-cell **VLC** system, which is crucial for utilizing the collective channel capacity from multiple optical sources /APs concurrently. Within the framework of indoor **VLC** multi-cell operation,

CCI emerges as a major challenge when signals from one AP interfere with those from neighboring APs. The extent of this interference is closely tied to the distribution and HPBW of the installed APs. Moreover, the receiver structure and FOV play crucial roles in controlling CCI, as they can significantly degrade SINR performance. The primary objective of this segment is to analyze the impact of different transmitter configurations and receiver FOVs, considering a simple PD receiver. A design-centric methodology, based on multiple criteria decision modeling (MCDM), is proposed to determine the optimal transmitter configuration and receiver FOV under lighting constraints. This optimal selection ensures improved SINR performance with a simple PD receiver. Additionally, a hemispheric angle diversity receiver (HADR) structure is adopted to enhance both lighting and communication performances. It has been demonstrated that the optimal design of HADR not only improves the average SINR value across the CF but also reduces spatial fluctuations, resulting in a significantly high consistency factor.

In the final segment of this thesis, the focus shifts towards designing a heterogeneous Li-Fi network. This endeavor aims to tackle practical challenges stemming from light path blockages and user mobility. With regard to multi-user association, this segment also imparts the motivation behind the adoption of an improved version of ADR (called FDR) in a hybrid Li-Fi Wi-Fi network (HLWNet). Based on different mobility scenarios and blockage conditions the performance of the proposed HLWNet has been evaluated. A Li-Fi channel model with FDR and a rule-based resource allocation algorithm (RBRA) has also been proposed for the purpose. Nevertheless, the network data quality of the multi-user system has been estimated in terms of packet loss, latency, and fairness index.

The customizations and contributions outlined in various stages of this research are pivotal for the future adaptation of this eco-friendly technology in indoor environments. As communication and lighting industries increasingly prioritize this green technology and intertwine their efforts, the insights and innovations from this research will prove fruitful in driving the commercial success of VLC and Li-Fi.

S. Chandra
19-06-2024

Lay Summary

The rapid growth of IoT devices and mobile data use raises concerns about limited RF spectrum for wireless communication. Optical wireless tech. like **VLC** and **Li-Fi** offer sustainable, uninterrupted connectivity, especially indoors. However, the primary objective of the **VLC** access points is to provide quality illumination, leading to a trade-off between lighting and communication. This study explores designs to enhance communication performance within lighting constraints.

In indoor spaces, multiple WLEDs are commonly used for lighting. However, not all of these lights may be used for transmitting data, either due to cost or other requirements. When some lights are not used for data transmission, the regular room light could interfere with the optical signals they produce. Another issue is adjusting the brightness of these lights according to the amount of natural light available, which helps to save energy. This study initially addresses these challenges by proposing a design to reduce interference from ambient light. Additionally, it suggests creating a standalone prototype for **VLC** that can work with daylight and adjust brightness to save energy. Using multiple transmitters (luminaires) in a setup known as multi-cell **VLC** holds significant promise for enhancing data transfer speed and fairness among all individuals within the room. However, when you have these multiple transmitters close together, they can cause interference with each other, which is called co-channel interference (**CCI**). This interference often limits how well the communication works. Finding ways to reduce this interference without messing up the lighting is another important problem. A part of the thesis also looked at how different setups with diverse transmitter configurations affect things. Finally, it suggested the best solution that balances everything to reduce interference while still keeping the lighting good. The last segment of this thesis deals with more granular problems like light path blockage and multi-user random mobility which are very crucial for future commercialization. For seamless connectivity of all the mobile users, a specially tailored receiving front-end called freeform diversity receiver is suggested in a hybrid LiFi-WiFi network. Compared to the state-of-the-art schemes, the proposed solution exhibits significant improvement in terms of complexity, QoS and average user throughput.

Contents

I	INTRODUCTION	I
1.1	Setting the Scene	1
1.2	Motivation	2
1.3	Contribution	4
2	BACKGROUND OF VLC SYSTEM & STATE OF THE ART	7
2.1	LED & Its Use As Optical Transmitter	7
2.1.1	Different Types of LED	8
2.1.2	Radiation Characteristics	9
2.1.3	LEDs with High-Speed Communication and Lighting Potential: Chal- lenges	9
2.2	VLC Receiver	11
2.3	Modulation Techniques	12
2.3.1	Modulation with Single Carrier	12
2.3.2	Multi Carrier Modulation	13
2.4	Multi-Cell VLC System	14
2.4.1	Existing barriers with multi-cell VLC	14
2.5	Hybrid LiFi-RF System	15
2.6	Lighting Constraints	15
3	MITIGATION OF AMBIENT LIGHT INTERFERENCE	17
3.1	Introduction	17
3.1.1	Ambient Light Interference	18
3.1.2	Research Gap	18
3.2	Luminaire Arrangement	19
3.3	System Model	19
3.3.1	Channel Model	20
3.3.2	Transmitter Design	22
3.3.3	Receiver Architecture	22
3.4	Forward Error Correction	24
3.4.1	Tail Biting Convolution Code	24
3.4.2	Viterbi Decoder	25
3.5	Results	26

3.5.1	Illumination Performance	26
3.5.2	Communication Performance	28
3.6	A Special Case: Design with Office Environment and Infrastructure	31
3.6.1	Office Geometry and Design Parameters	31
3.6.2	System Performance	32
3.7	Summary	33
3.8	Research Output	34
4	DAYLIGHT INTEGRATED INDOOR VLC SYSTEM	35
4.1	Introduction	35
4.2	System Design	36
4.2.1	Overall Block Diagram	36
4.2.2	Mathematical Framework For Dimming Control Mechanism . . .	37
4.3	Optical Dimmable Transmitter	39
4.3.1	Integrated Data Enabled LED Driver	39
4.3.2	Dimming Control Mechanism	40
4.3.3	OOK Modulator	43
4.4	Optical Receiver	43
4.4.1	Shot Noise	44
4.4.2	Thermal Noise	45
4.5	System Performance	46
4.5.1	Average Horizontal Illuminance	46
4.5.2	Short Term Flicker Severity	48
4.5.3	Energy Efficiency	49
4.5.4	Signal to Noise Ratio	50
4.5.5	BER Performance	50
4.6	Discussion	52
4.7	Summary	53
4.8	Research Output	54
5	OPTIMAL TRANSMITTER CONFIGURATION & RECEIVER FOV	55
5.1	Introduction	55
5.1.1	HPBW and CCI	56
5.1.2	Research Gap	56
5.2	System Model	58
5.2.1	Room Geometry and Luminaire Configuration	58
5.2.2	Luminous Intensity Distribution	59
5.2.3	Average spatial SINR	60
5.3	Proposed Methodology	63
5.3.1	Selection of Optimal FOV	65
5.3.2	Effect of Altering HPBW	66
5.4	MCDM Under Lighting Constraints	68
5.4.1	Closeness Coefficient	70
5.5	Results	71

5.5.1	Best transmitter configuration	71
5.5.2	SINR Distribution	72
5.5.3	validation and comparison	75
5.6	Summary	75
5.7	Research Output	78
6	ADOPTING RECEIVER DIVERSITY TECHNIQUES	79
6.1	Introduction	79
6.1.1	Importance of Receiver Diversity From Lighting Perspective	80
6.2	Angle Diversity Receiver for VLC	80
6.3	HADR Architecture With Optimal FOV	81
6.3.1	Random Rotation Angle	82
6.3.2	Design Principles	83
6.3.3	Impact of RRA	84
6.3.4	Reducing Fluctuations of Spatial SINR Distribution	86
6.4	A Step Forward: Design of Improved ADR with Freeform Surface	89
6.4.1	FDR Geometry	90
6.4.2	Improved SINR Performance	90
6.5	Summary	91
6.6	Research Output	92
7	MOVING TOWARDS HYBRID LI-FI WI-FI SYSTEM	93
7.1	Introduction	93
7.2	System Overview	94
7.2.1	LiFi Channel Model With Freeform Diversity Receiver	94
7.2.2	WiFi Channel Model	98
7.2.3	Channel Capacity	99
7.2.4	LOS Path Blockage	99
7.3	Mobility Model and Scenario	99
7.3.1	Random Waypoint Model	99
7.3.2	Scenario Formulation	100
7.4	Distributed Resource Allocation	100
7.4.1	Maximizing System Throughput With Optimal Resource Allocation	101
7.4.2	Rule Based Resource Allocation (RBRA)	101
7.4.3	User Throughput	102
7.5	HLWNet Quality of Service	103
7.5.1	Packet Loss Ratio	103
7.5.2	Latency	104
7.5.3	Fairness Index	105
7.6	Results and Analysis	105
7.6.1	SINR Distribution	106
7.6.2	Effect of No. of Users	107
7.6.3	Impact of LOS Blockage	108

7.6.4	Evaluation of Quality of Service	109
7.6.5	QoS Improvement With RBRA	110
7.6.6	Advancement Beyond Prior Research	114
7.7	Summary	115
7.8	Research Output	116
8	CONCLUSIONS, LIMITATIONS AND FUTURE RESEARCH	117
8.1	Summary and Conclusions	117
8.2	Limitations and Future Research	119
APPENDIX A OTHER PUBLICATIONS ON VLC		121
REFERENCES		123

List of Figures

1.1	Estimated spectrum surplus/deficit through to 2040	2
2.1	Modulation bandwidth of different LED chips	8
2.2	LED Beam Lambertian Pattern	10
2.3	Data transmission rate & LOP SH-LED and μ LED at different offset . . .	11
3.1	Arrangement of evenly distributed luminarie groups	19
3.2	Block diagram of forward error corrected VLC system	20
3.3	Block diagram of the proposed FEC-equipped data transmitter	22
3.4	Receiver architecture of proposed VLC system	23
3.5	Magnitude response of FIR filter (Low pass) used in receiver	24
3.6	Block diagram of the convolution encoder	25
3.7	Decoding technique for Tail Biting Convolution code	26
3.8	Distribution of horizontal illuminance over the working plane	27
3.9	Distribution of optical received power: direct component	27
3.10	Distribution of optical received power: direct with reflected component . .	28
3.11	Power spectrum of internal noise of photodetector	28
3.12	Distribution of SINR at different location inside the room	29
3.13	Transmitted and Received waveform for sample random binary data	30
3.14	Variation of BER with SINR (dB)	30
3.15	Obtained BER at different location inside the room	31
3.16	Li-Fi enabled LED lighting system in office cubicle (3-D view)	32
3.17	Intensity distribution of the optical sources	32
3.18	Variation of BER and SINR in different Ambient Light Intensity	33
4.1	VLC supportive daylight integrated indoor lighting scheme	37
4.2	Generalized block diagram of the proposed system	37
4.3	Luxeon LED Module used for designing optical source	38
4.4	Overall circuit diagram of transmitter involving dimming control and OOK modulator	40
4.5	Transfer characteristics of the designed interfacing circuit for dimming . . .	42
4.6	Variation of external bias current and LED current with ambient daylight .	42
4.7	Circuit diagram of Optical Receiver	44
4.8	AC transfer characteristic of TIA	44
4.9	Variation of ambient daylight during different time in a day	47

4.10	Obtained Average horizontal illuminance incorporating dimming control	47
4.11	Cumulative Probability Function of the signal for 10 min observation time	48
4.12	Relative Horizontal Illuminance & Energy Savings at different test time	50
4.13	Signal to noise ratio over the task area (at 1 PM)	51
4.14	Transmitted and received waveform at 100 kHz frequency	51
4.15	Distribution of Bit Error Rate over the task area	52
4.16	Percentage power-saving and BER performance at different test time	53
5.1	Schematic representation of CCI	56
5.2	Plan view of luminaire deployment arrangements	58
5.3	Downlink indoor Li-Fi channel model	61
5.4	Proposed methodology to determine optimal transmitter configuration and receiver's FOV	65
5.5	Relational dependency between spatial coverage probability and receiver's FOV	67
5.6	Variation of communication performance metrics with transmitter's HPBW	68
5.7	Effect of varying HPBW on lighting parameters	69
5.8	Closeness-Coefficients for different transmitter configuration	72
5.9	Performance indicating metrics at best transmitter configurations of different luminaire arrangements	73
5.10	SINR distribution without any optimization in transmitter configuration and FOV (Non-optimal scheme)	73
5.11	SINR distribution with only optimal transmitter semi-angle (sub-optimal scheme)	74
5.12	SINR distribution of the proposed scheme with optimal transmitter configuration & receiver's FOV	74
5.13	Monte-Carlo ray tracing (Zemax) with optimal transmitter configuration	75
5.14	SINR performance at different room positions along the x-axis	76
5.15	Comparative results of average SINR and overall uniformity	76
5.16	Distribution of horizontal illuminance (Iso-lux)for optimal transmitter configuration	77
6.1	Structure of HADR (a) 3-D View (b) Side View.	81
6.2	Illustration of Random Rotation Angle (Θ_{RRA}).	82
6.3	Variation of Average SINR with Ψ_C for different values of β	84
6.4	Impact of RRA on $SINR_{dev}$ at $\beta = 30^\circ$	85
6.5	SINR distribution over the CF using HADR at $\beta = 30^\circ$	86
6.6	Relational dependency of spatial SINR distribution with Inclination angle (β) at optimal FOV.	87
6.7	Variation of spatial SINR deviation with RRA	87
6.8	SINR distribution over the CF using HADR optimal design	88
6.9	FDR Structure with four co-planar RUs	89
6.10	Quadruple arrangement of RUs: Top view	89
6.11	Perspective view of RU	90
6.12	SINR performance of FDR compared to existing receiver	91

7.1	FDR structure	94
7.2	LiFi channel and Off-axis quadrilateral FoV of FDR	97
7.3	SINR distribution	106
7.4	Effect of increasing no. of user on average user throughput	107
7.5	Average user throughput as a function of N_U and blockage (<i>ScenRM</i>)	108
7.6	Cumulative density function of achieved user data rate for $N_U = 4$	108
7.7	Cumulative density function of achieved user data rate for $N_U = 10$	109
7.8	Impact of occupation rate of blockage on user throughput	110
7.9	Packet loss against data arrival rate ($N_U = 4, 6, 8, 10$)	111
7.10	Latency versus data arrival rate ($N_U = 4, 6, 8, 10$)	111
7.11	Packet loss using RBRA with respect to ORA ($N_U = 6, 10$)	112
7.12	Reduction in HO and improvement in fairness index adopting RBRA	113
7.13	System Throughput using RBRA with respect to ORA	114

List of Tables

3.1	Design parameters for simulation (room and luminaires)	20
3.2	Receiver Specification	23
3.3	Lighting performance over different task area	33
4.1	Design Parameters of Transmitter	41
4.2	Component values of designed optical receiver	45
5.1	Parameters used for different luminaire deployment arrangements	59
5.2	Simulation parameters for VLC receiver	63
5.3	Normalized Relative Weight (AHP)	71
6.1	HADR performance simulation parameters	86
6.2	Designed parameters of FSE	91
7.1	FDR indicator matrix parameters definition	96
7.2	HLWNet Simulation Parameters	106
7.3	Comparative outcome of existing studies	115

Abbreviation

A:

AR : Augmented Reality
AFE : Analog Front-end
ADR : Angle Diversity Receiver
AP : Access Point
APD : Avalanche Photo Diode

AHP : Analytic Hierarchy Process
ADT : Angle Diversity Receiver
ASE : Area Spectral Efficiency
ACO-OFDM : Asymmetrically
Clipped OFDM

B:

BER : Bit Error Rate

BA-LED : Broad Area LED

C:

CSK : Color Shift Keying
CCI : Co-channel Interference

CI : Consistency Index
CF : Communication Floor

D:

DD : Direct Detection
DFT : Discrete Fourier Transform

DCO-OFDM : Direct Current Biased
OFDM

F:

FEC : Forward Error Correction
FDR : Freeform Diversity Receiver

FOV : Field Of View
FIR : Finite Impulse Response

H:

HADR : Hemispheric Angle Diversity Receiver
HPBW : Half Power Beam Width
HLWNet : Hybrid LiFi WiFi Network

I:

ICI : Intercell Interference
ISI : Intersymbol Interference
IM : Intensity Modulation

ISO : International Organization for
Standardization
IC : Integrated Circuit

ISP : Internet Service Provider

IOT : Internet of Things

L:

LED : Light Emitting Diode

LC : Light Communication

LOS : Line of Sight

LOP : Light Output Power

LiFi : Light Fidelity

M:

MIMO : Multiple Input Multiple Output

M-QAM : M-ary Quadrature Amplitude Modulation

MCDM : Multiple Criteria Decision Making

MISO : Multiple Input Single Output

MINLP : Mixed Integer Non-linear Programming

N:

NEP : Noise Equivalent Power

NLOS : Non-line of Sight

O:

OOK : On-Off Keying

OFDM : Orthogonal Frequency
Division Multiplexing

OWC : Optical Wireless
Communication

ORA : Optimal Resource Allocation

P:

PAM : Pulse Amplitude Modulation

PIN : Positive-Intrinsic-Negative

PPM : Pulse Position Modulation

PWM : Pulse Width Modulation

Q:

QOS : Quality Of Service

R:

RF : Radio Frequency

RBRA : Rule Based Resource
Allocation

RRA : Random Rotation Angle

RU : Receiving Unit

RWP : Random Waypoint

S:

SBC : Select Best Combining

SNR : Signal to Noise Ratio

SINR : Signal to Interference plus Noise Ratio

SHR : Space to Height Ratio

SSS : Signal Strength Strategy
SCM : Single Carrier Modulation

T:

TIA : Transimpedance Amplifier
TB : Traceback Block
TOPSIS : Technique for Order of Preference by Similarity to Ideal Solution

V:

VR : Virtual Reality
V2V : Vehicle To Vehicle
VLC : Visible Light Communication
V2I : Vehicle To Infrastructure

W:

WiFi : Wireless Fidelity
WLED : White LED

DEDICATED TO UNSUNG HEROES OF OUR NATION –
THE ORDINARY PEOPLE WHOSE RESILIENCE, EVERY-
DAY STRUGGLES, AND UNWAVERING SPIRIT FORM
THE BACKBONE OF OUR SOCIETY.

“Whatever we are now is the result of our acts and thoughts in the past; and whatever we shall be in the future will be the result of what we think and do now.”

Swami Vivekananda

1

Introduction

1.1 SETTING THE SCENE

OVER the past two decades, remarkable progress has been observed in the field of wireless communication, transforming it into an indispensable part of both our professional and daily lives. The level of data sharing and connectivity achieved during this period has exceeded even the most optimistic predictions from just a few years ago. This remarkable advancement can be attributed to the evolution of mobile communication, spanning from 2G to beyond 5G^(1,2,3,4), coupled with significant strides in edge computing—from laptops to smartphones, Smart TVs to tablets⁽⁵⁾. The emergence of the Internet of Things (IoT) and the broader concept of the Internet of Everything (IoE) have extended connectivity not only to humans but also to machines^(6,7). In the upcoming days, we anticipate a surge in progressive applications and innovative services that will reshape our reality. Notably, technologies like augmented-reality (AR) and virtual-reality (VR) already making significant strides⁽⁸⁾, promising enhanced social experiences within virtual environments, allowing users to interact more immersively and realistically. These high-precision applications are projected to demand data rates on the order of terabits per second (Tb/s). Furthermore, the vision of Industry 4.0 involves highly automated⁽⁹⁾ and interconnected manufacturing processes, where reliable and low-latency wireless connectivity plays a pivotal role. Communication technologies such as Vehicle-to-Infrastructure (V2I) and Vehicle-to-Vehicle (V2V)⁽¹⁰⁾ are poised to become the cornerstones of the transportation sector.

To accommodate such scientific advances and foster economic development, bandwidth and spectrum availability will be critical in the coming decades. Projections for 2030 indicate an estimated annual increase in global data approaching one yottabyte, with a simultaneous tenfold increase in general computing power, reaching up to 3.3 zettaflops^(11,12). This exponential growth⁽¹³⁾ underscores the need for continued advancements in communication infrastructure to meet the escalating demands of an increasingly connected and data-driven

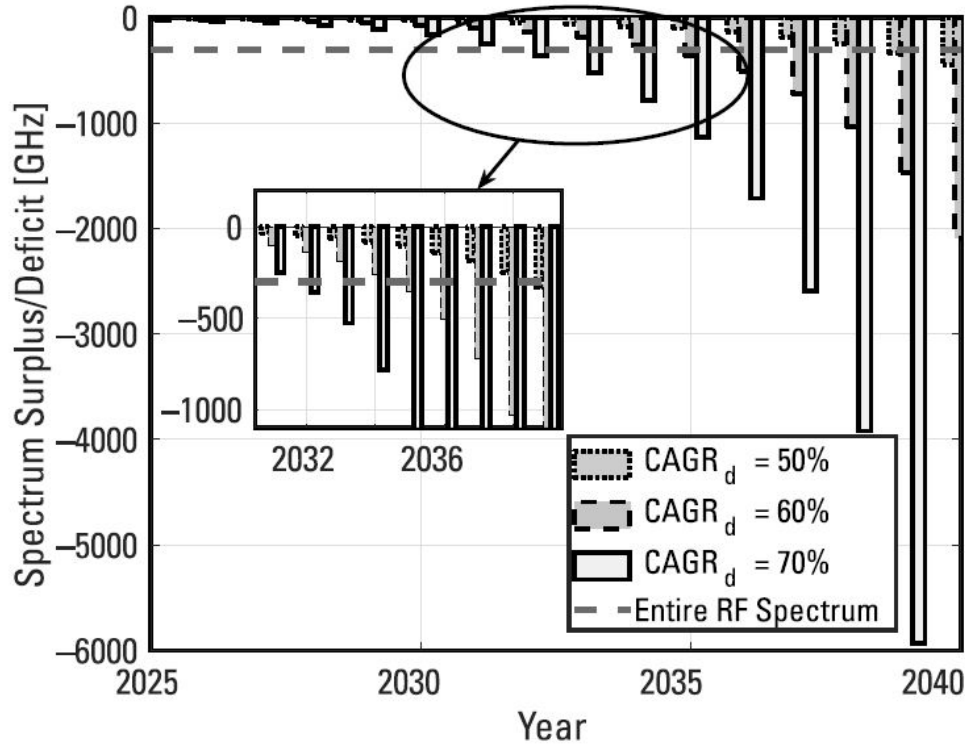


Figure 1.1: Estimated spectrum crisis through to 2040⁽¹⁴⁾

world.

1.2 MOTIVATION

So far, wireless connectivity is solely dependent on radio-frequency (RF) technologies with a limited bandwidth of almost 3 THz⁽¹⁵⁾. Thus, the increasing demand for wireless services, driven by emerging technologies and the growing number of connected devices, poses a risk of spectrum scarcity. Serious concerns are coming up for resources like RF spectrum. The adequacy of RF spectrum to future-proof wireless communications remains a significant and ongoing challenge for the telecommunications industry. Figure 1.1 depicts the spectrum shortage as estimated by Tezcan and Haas for the next 15 years⁽¹⁴⁾. As per this article⁽¹⁴⁾, by 2035, the entire RF spectrum will be in use. So, the regulatory authority, technological innovators, scientists and other communication engineers are making a constant effort to address this unprecedented crisis. The importance of the leftover part of the huge electromagnetic spectrum gradually increases to establish new wireless communication technologies. Already, optical communication technology is deployed worldwide as a main enabler for high-speed broadband connectivity⁽¹⁶⁾. So, exploiting the remainder part of the huge optical spectrum for free space communication is a reasonably insightful and judicious approach to expanding future wireless connectivity without overburdening the RF spectrum. Compared with the RF spec-

trum, the visible light spectrum is itself 1000 times wider^(17,18,19) and the lighting infrastructure is almost everywhere⁽²⁰⁾. Most importantly, LEDs are taking the driver seat and they can be used as an optical transmitter^(21,22). With the advent of LEDs, visible light communication (VLC) emerged as a potential alternative^(23,24) and currently penetrating the wireless communication market.

VLC is the backbone of OWC where intensity modulation of light is used to transfer the data. With the help of optical modulators, optical sources (LEDs), and optical receivers (photo-detector with front-end), this green technology can offer high-speed, short-range connectivity especially suitable for the indoor environment⁽²⁵⁾. Li-Fi is the newest member of the OWC family. This bidirectional technology is a total network counterpart of VLC that uses optical links for seamless connectivity. In both VLC and Li-Fi, optical sources serve as access points for data transfer, even though their primary purpose is to provide quality illumination^(26,27). Most of the research in this domain is heavily focused on the communication perspective. Researchers carried out research in the direction of finding an optimum modulation scheme in terms of data rate and BER for point-to-point VLC link. The most common and widely used modulation technique is binary on-off keying (OOK)^(28,29). In addition to OOK, pulse-position-modulation (PPM), and higher-order PPM^(30,31) are employed to realize a VLC system with intensity modulation and direct detection. However, often these modulation techniques suffer from inter-symbol interference. In contrast, multi-level quadrature-amplitude-modulation (M-QAM) and optical orthogonal frequency division multiplexing (O-OFDM) exhibit robustness against ISI^(32,33,34). Actually, in these modulation techniques, the duration of the symbol is considerably large with respect to RMS delay spread of the optical channel. Apart from modulation techniques, research has been carried out on multiple input multiple output (MIMO) VLC systems^(35,36) and different receiver technologies.

In spite of potential contributions in the communication field, those studies did not address the primary objective of VLC-based system in a comprehensive way. So many crucial research questions were still on the surface that need to be addressed both from a lighting and communication perspective. Daylight integration with VLC system can improve the overall energy efficiency. The entire thesis is dedicated to figuring out the trade-off between lighting and communication parameters while designing an indoor VLC/ Li-Fi system. Although VLC and Li-Fi are often used interchangeably, there is a significant difference between these two. Li-Fi can be considered a networked counterpart of VLC. So, Li-Fi system can be designed with VLC downlink and uplink or VLC downlink and RF/IR uplink. In the case of an indoor VLC system, horizontal illuminance and uniformity are the key lighting parameters while data rates, bit-error-rate, signal-to-noise ratio etc are the parameters under scanner from the communication point of view. The data rate can be sufficiently improved by adopting the multi-cell framework where ambient light interference and co-channel interference are other areas of concern. Apart from that, both the transmitter and receiver configurations have a direct or indirect effect on communication and lighting parameters. Unlike the RF femtocell, the Li-Fi AP covers a relatively small area of more or less 2-3 m in diameter. This can potentially accomplish an elevated bandwidth reuse and superior spectral efficiency. Nevertheless, the system performance is restricted due to inter-channel interference (ICI) from the adjacent APs. This noise is maximum at the edge of the cell and can be tackled by beamforming

. However, beamforming by reducing the semi-angle of an optical transmitter is not always a good alternative as it significantly deteriorates the lighting performance in terms of overall uniformity. To overcome this ICI without sacrificing the lighting requirement MIMO techniques can be adopted in the **Li-Fi** receiver structure. A highly uncorrelated MIMO channel is obtained by using an angle diversity receiver (ADR) where multiple photodiodes (PDs) are pointed toward different directions. Still there exists enough research opportunity to improve the spatial **SINR** performance of the system by optimizing different parameters. Despite all these efforts from different directions, so many practical problems like light path blockage, random receiver orientation, and chipset integration into handheld gadgets stand as a barrier between this promising technology and the mass market.

1.3 CONTRIBUTION

To meet the expanding demand of numerous wireless communication applications with increasing mobile data traffic, Visible Light Communication & its networked counterpart **Li-Fi** have evolved as a propitious green communication technology to provide ubiquitous connectivity. The thesis focuses on the design, modeling, and evaluation of indoor **VLC** Systems to address limitations of existing indoor **VLC** system design from a lighting perspective and propose amicable solutions to achieve joint communication and illumination performances. Specifically five research objectives have been addressed:

- The setback associated with ambient light interference is managed by designing a forward error-corrected indoor **VLC** system.
- A daylight integrated energy efficient **VLC** system prototype has been designed and developed.
- A design-centric methodology is developed to improve the multi-cell indoor **VLC** system by estimating the optimal transmitter and receiver configuration under lighting constrain.
- Optimized the design of a hemispheric angle diversity receiver to improve the average **SINR** and reduce the **SINR** fluctuation of an indoor MIMO **VLC** system.
- Introduced the channel model with a compact freeform-based receiving front-end (Freeform Diversity Receiver) for improving the **SINR** performance of a multi-cell **Li-Fi** system. Also, the performance of the proposed receiving front-end is evaluated in a mobility-aware multi-user HLWNet environment.

In pursuit of the central research objectives outlined above, various minor contributions have been made. Addressing the first objective, a configuration featuring Forward Error Correction (FEC) at both the transmitter and receiver has been introduced. Specifically, a tail-biting convolutional encoder and Viterbi decoder have been meticulously designed for the

encoding and decoding sections, respectively, aimed at enhancing the bit error rate. Additionally, in the context of an indoor environment with ambient light illuminants, a comprehensive evaluation of joint communication and illumination performances has been conducted. This evaluation encompasses key metrics such as Signal-to-Interference-plus-Noise Ratio (**SINR**), Bit Error Rate (BER), horizontal illuminance, and uniformity. The assessment has been carried out on evenly spaced grid points over the working plane, providing insights into the system's performance under varying conditions.

In case of the second objective, a cost-effective data-enabled LED driver circuit has been conceptualized and implemented. This circuit is designed to be adaptable to ambient daylight conditions, allowing it to regulate the LED current through a dimming control mechanism. The incorporation of this feature enhances energy efficiency by adjusting the LED brightness based on the available ambient light. Furthermore, the performance of the proposed prototype has undergone comprehensive evaluation. Various metrics, including short-term flicker severity, energy efficiency, average horizontal illuminance, signal-to-noise ratio, and bit error rate, have been rigorously assessed. This thorough analysis provides a holistic understanding of the system's capabilities and effectiveness, shedding light on its performance across different parameters.

Addressing the third research objective, an in-depth study of a multi-cell Visible Light Communication (**VLC**) channel model has been conducted and reported, aiming to estimate the average Signal-to-Interference-plus-Noise Ratio (**SINR**) within an indoor environment. The investigation involves the use of a simple Photodiode (PD) receiver. The study delves into the critical aspect of simultaneously optimizing the transmitter configuration and the receiver's field of view. This exploration is undertaken to achieve a highly uncorrelated channel, a crucial factor for enhancing communication performance in a multi-cell **VLC** system. The results obtained through analytical methods are also validated using an optical ray tracing tool, Zemax. This validation ensures the reliability and accuracy of the analytically derived outcomes, providing a robust foundation for understanding the intricacies of the multi-cell **VLC** channel model.

Regarding the fourth research objective, an angle diversity receiver structure is adopted instead of ordinary PD considered so far. To be specific, by adapting this multiple-input multiple-output (MIMO) structure, we work on hemispheric angle diversity receiver (HADR) to improve the data rate further. In connection with the spatial **SINR** distribution, the significance of the random rotation angle, FOV, and inclination angle of HADR is first explored. Then, the optimal HADR structure is designed to combat the spatial **SINR** fluctuation by analyzing the impact of different parameters.

For the final research objective, a novel receiver structure named Freeform Diversity Receiver (FDR) is designed, leveraging the advantages offered by freeform optics. In contrast to the Angle Diversity Receiver (ADR), this off-axis receiver is characterized by a more compact size and superior Signal-to-Interference-plus-Noise Ratio (**SINR**) performance. A **Li-Fi** channel model with FDR is proposed where off-axis and rectangular FOV is contemplated instead of symmetrical FOV. Adopting this channel model, the performance of an indoor hybrid **Li-Fi-Wi-Fi** system has been evaluated in the presence of light path blockage for different multi-user mobility scenarios. Moreover, a rule-based resource allocation algorithm has been

developed for multi-user applications.

“ You can’t connect the dots looking forward; you can only connect them looking backwards. So you have to trust that the dots will somehow connect in your future.”

Steve Jobs

2

Background of VLC System & State of the Art

WAY BACK in 1880, just after the invention of the telephone, Sir Alexander Graham Bell along with his assistant Charles Sumner Tainter used light to transmit sound signals wirelessly. They developed a device that used a thin mirror that vibrated in response to sound waves. The mirror reflected a beam of light onto a distant receiver, where it was detected and converted back into sound. They called the system as “Photophone”. This remarkable invention unveiled the pathway of modern optical wireless communication technology⁽³⁷⁾. Despite this innovative idea, the project did not achieve any commercial success and for the next 120 years, researchers did not pay any attention to carry forward this idea in reality. The invention of blue LEDs by Shuji Nakamura in the early 1990s revolutionized the lighting industry⁽³⁸⁾. Blue LEDs, when combined with red and green LEDs or phosphors, can produce white light which is now widely used in various applications, from residential lighting to commercial and outdoor lighting. In 2004, Professor Nakagawa in Japan proposed the fundamental structure of an indoor visible light communication system using white LED⁽³⁹⁾. Inspired by this study, Professor Harald Haas coined the term ‘Li-Fi’ in TED talk Global, 2011. Thereafter, researchers around the globe have come to know the role of overhead lighting in high-speed data communication. In the last decade, both LED technology and VLC has continued to evolve and has witnessed significant advancements.

2.1 LED & ITS USE AS OPTICAL TRANSMITTER

In last two decades, especially in last few years solid state lighting technology has been evolved in a rapid way. Solid-state lighting, particularly LED lighting has gained widespread acceptance and market penetration across the globe. With the rising awareness about energy conservation and environmental sustainability, there has been a substantial shift from traditional

lighting sources to LED lighting in homes, offices, commercial establishments, and public spaces. LEDs can be modulated at very high speed that human eye can't detect. At the same time it can provide sufficient illumination. It creates a great opportunity for the communication industry to utilize this ubiquitous lighting infrastructure as an access point for indoor wireless communication.

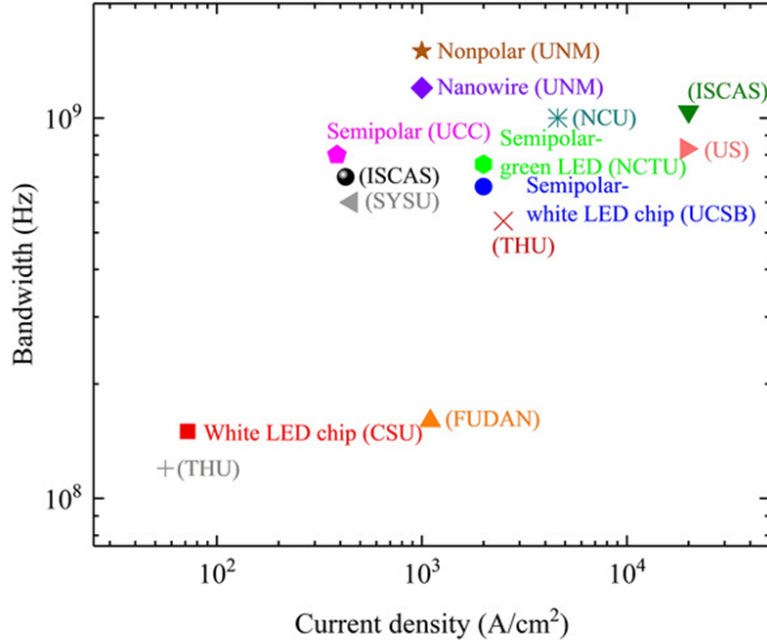


Figure 2.1: Modulation bandwidth of different LED chips at a specific current density⁽⁴⁰⁾.

2.1.1 DIFFERENT TYPES OF LED

Typically, each lamp comprises more than one LED which is regulated by a controlling or driver circuit. The driver circuit's main function is to convey data by modifying the flowing-in current, consequently altering the intensity of light. The flowing-in current should fall within the LED's dynamic range to ensure linear proportionality between input current and output (light intensity). White LED (WLED), known for accurately representing objects without distorting their actual colors, is commonly employed for both illumination and communication. Two prevalent design schemes for WLEDs are observed. In one design scheme, a blue LED with a yellow Phosphor coating⁽⁴¹⁾ is used. Color mixing of three LEDs (red, green, and blue)⁽⁴²⁾ is employed in other cases. Due to its affordability and straightforward implementation, the first kind of LED, featuring a blue LED and yellow phosphor layer, is widely adopted for designing WLEDs than the RGB type. However, in comparison to RGB, it offers a lower bandwidth due to the slower absorption and emission from the phosphor layer coating. Data rates up to 1Gbps could be attained with this type of WLED⁽⁴¹⁾. In contrast, the RGB scheme exhibits superior communication performance by employing the CSK tech-

nique, which modulates the signal using three LEDs of different chromaticity. This approach enables achieving data rates of up to 3.4 Gbps⁽⁴²⁾.

The primary constraint on the frequency response of LEDs is determined by the lifespan of minority carriers and the junction capacitance of the diode⁽⁴³⁾. To enhance the modulation bandwidth of LEDs, light-emitting chips with dimensions in the micrometer range have been incorporated. Micro-LEDs, leveraging GaN, have been suggested for achieving high-speed VLC and communication through polymer optical fibers (POFs)⁽⁴⁴⁾. These devices predominantly emit light within the wavelength range of 370 to 520 nm and can be paired with wavelength converters to generate white light^(44,45).

Recent research in this direction revealed that 7.91 Gbps data rate can be attained by employing a lone μ LED alongside the OFDM modulation format⁽⁴⁶⁾. In another study, a blue series-biased μ LED, comprising 3×3 elements with a diameter of 20 μ m each has been reported. This transmitter exhibits an outstanding data rate of 10 Gbps even at a 5 m distance⁽⁴⁷⁾. Micro-LED devices in semi-polar configurations, specifically in the blue and green spectra, featuring a diameter of 60 μ m, showcase notable bandwidth capabilities at low current densities. These devices hold promise for integration into energy-efficient VLC systems⁽⁴⁸⁾. Modulation bandwidth of different LED chips at a distinct current density is shown in Figure 2.1⁽⁴⁰⁾.

2.1.2 RADIATION CHARACTERISTICS

The optical data radiation pattern from an optical source (LED) depends on the intensity distribution of that light source on a particular plane. In general, the Lambertian radiation model is conceived to represent the intensity distribution of a single LED. In the Lambertian distribution, the radiant intensity (or power per unit solid angle) of the transmitter is proportional to the cosine of the angle between the surface normal and the direction of observation. Considering a point LED source with radiant output power P_s , the radiated power through a solid angle $d\Omega$ is computed as:

$$dP_r = \frac{m+1}{2\pi} \times \cos^m \alpha P_s d\Omega \quad (2.1)$$

Here, m defines the shape of the beam, known as the Lambertian mode number. Using different epoxy lens or other optical arrangements the shape of the beam can be altered. The angular spread of radiated optical power is also defined by the half power beam angle/ width. This is an angle where the optical intensity reduces by a factor of 2.

This is clearly shown in Figure 2.2 where three different Lambertian beam patterns with mode numbers 1, 11 and 45 have been shown.

2.1.3 LEDs WITH HIGH-SPEED COMMUNICATION AND LIGHTING POTENTIAL: CHALLENGES

In section 2.1.1, it has been previously described that the modulation bandwidth of micro-LEDs with less than 100 μ m active area shows significant promise for Li-Fi applications. However, in contrast to broad area LEDs (BA LEDs), the light output power (LOP) of micro-LEDs is currently considerably low. BA LEDs are generally highly suitable for lighting appli-

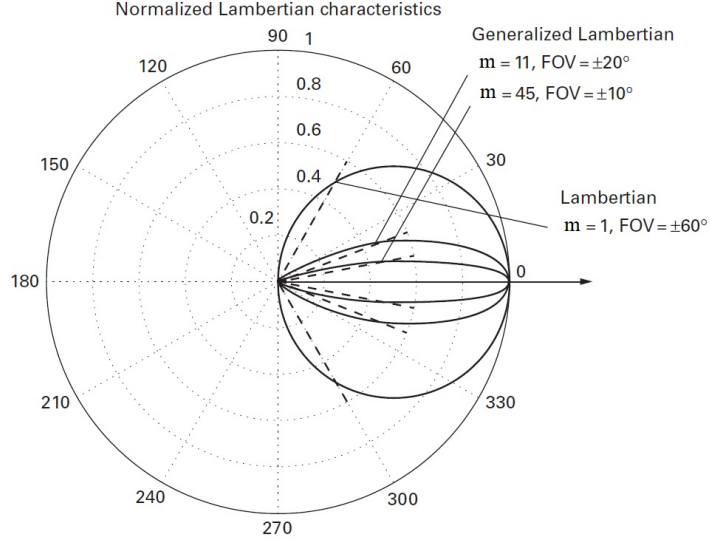


Figure 2.2: LED Beam Lambertian Pattern.

cations due to their higher efficacy. However, the modulation bandwidth of these LEDs is limited to the range of 10-40 MHz due to their lower recombination rate. Therefore, current research efforts are focused on improving both the LOP and modulation bandwidth of LEDs so that they can be simultaneously utilized for both illumination and communication purposes. Careful consideration of state-of-the-art research on micro-LEDs for VLC applications reveals several challenges, summarized as follows:

- *Quantum Confinement Stark Effect (QCSE):*
QCSE arises from strong polarization effects observed in III-nitride LEDs. There are two types of polarization effects: a) spontaneous polarization and b) piezoelectric polarization. These polarization effects cause deformation in the energy band structure^(49,50), resulting in a reduction of the overlapping area of the electron-hole wave function⁽⁵¹⁾. Consequently, this phenomenon, known as QCSE, reduces the recombination rate of free carriers. A lower recombination rate leads to a larger carrier lifetime and consequently lower modulation bandwidth. To mitigate this situation, a high current density in the range of kA/cm^2 is required. While this may be beneficial from a communication perspective, it simultaneously decreases power efficacy, which is undesirable from a lighting standpoint.
- *Droop Effect:*
The droop effect in micro LEDs refers to a phenomenon where the efficiency of the LED decreases as the current passing through it increases. This phenomenon is particularly significant in micro LEDs, characterized by their small size⁽⁵²⁾. The droop effect primarily occurs due to non-radiative recombination of charge carriers within the LED structure at high current densities^(50,40). As the current density increases, the rate of non-radiative recombination also increases, leading to a decrease in the efficiency of light emission. Consequently, this decrease in efficiency results in a lower light output

for a given amount of electrical power supplied to the LED. The droop effect poses a challenge for micro LED technology, especially in applications requiring high brightness and efficiency⁽⁵³⁾. Researchers and engineers are continually working to mitigate this effect through various methods, such as optimizing the LED structure, improving heat dissipation, and developing novel materials with enhanced carrier mobility and reduced non-radiative recombination rates.

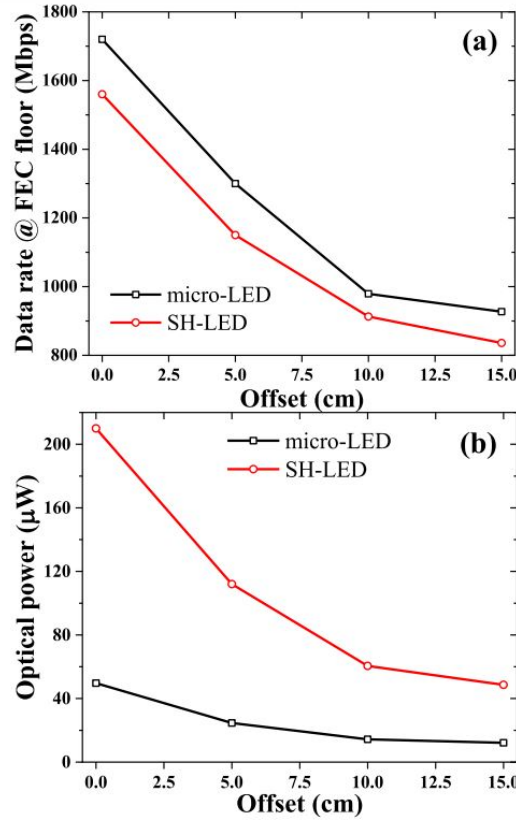


Figure 2.3: Data transmission rate & LOP SH-LED and μ LED at different offset⁽⁵⁴⁾.

Very recently, a GaN based hybrid LED device (SH-LED) is proposed⁽⁵⁴⁾ where μ LED & BA-LED are connected in series configuration to obtain higher LOP and modulation bandwidth. Figure 2.3 shows the practically obtained data rate and optical power at different offset. Here, the offset defines the area coverage of a particular LED. Using the SH-LED, substantial improvement in LOP has been observed compared to micro-LED. Also the decrement in data rate is sufficiently low compared to BA-LEDs.

2.2 VLC RECEIVER

Direct detection (DD) with the help of a photodetector (PD) is the prevalent detection technique in case of VLC system. In proportion with the instantaneously received optical power,

a PD generates current which is treated as a received signal after the optical to electrical conversion. The dimensions of PDs typically span from hundreds to thousands of micrometers. Given that the light interference pattern exists in the micrometer range⁽⁵⁵⁾, the PD has the potential to average the received interference, and as a result, Doppler shift is not encountered. PDs play a crucial role as a leading technology in **VLC** receivers, primarily due to their swift response. This rapid response capability allows for modulation bandwidths to reach at the order of gigahertz. Silicon (Si) PDs, with a typical spectral response peaking in the wavelength window of 0.8-0.9 μm and a cutoff wavelength of 1.1 μm , are widely used. Alternatively, germanium or III-V alloys like InGaAs cater to PDs with spectral responses at longer wavelengths.

Two primary categories of PDs have garnered considerable attention in the context of **VLC**: the PIN and the APD. PIN PDs provide benefits over APDs, including higher temperature tolerance and lower cost. In contrast, APDs excel in detecting lower levels of optical power due to their internal gain mechanism, operating at a higher reverse voltage than PIN PDs. Consequently, APDs find use in scenarios with low-intensity received radiation, while PIN PDs are suited for high-received irradiance. Nevertheless, a significant drawback of APDs arises from the considerable shot noise generated by the high photocurrent induced by ambient light or the information signal. In a standard **VLC** receiver setup, utilizing PD necessitates a reverse bias, introducing an extra power consumption aspect to the process. An alternative strategy for designing a **VLC** receiver involves employing photovoltaic cells^(56,57). These devices operate passively, generating electrical energy solely from an optical bias. A pioneering solar panel receiver design capable of concurrently harvesting power at mW levels and facilitating **VLC** with data rates in the order of Mb/s is introduced for the first time in Reference⁽⁵⁸⁾. A significant drawback of most Silicon (Si) solar cells is their restricted bandwidth, typically in the kHz range, owing to their extensive area and consequent large capacitance.

2.3 MODULATION TECHNIQUES

Within this segment, an overview of digital modulation techniques commonly employed in **VLC/Li-Fi** is presented. **VLC**, relying on electromagnetic radiation for information transmission, can leverage modulation techniques typically utilized in RF communication, albeit with essential adaptations. Furthermore, owing to the utilization of visible light for wireless communication, it introduces a range of distinctive and specific modulation formats.

2.3.1 MODULATION WITH SINGLE CARRIER

In case of **VLC**, standard single-carrier modulation techniques encompass OOK, PPM, PAM, PWM, and optical spatial modulation^(59,60). OOK stands out as a widely recognized and uncomplicated modulation scheme, offering a favorable balance between system performance and implementation complexity. Its inherent characteristic of transmitting data by alternately activating and deactivating the LED allows for inherent dimming support. As outlined in IEEE 802.15.7^(61,62), two main approaches are considered to accomplish OOK dimming: (A) implementing symbol compensation and (B) refining the ON/OFF levels.

In contrast to OOK, another single carrier modulation technique, PPM exhibits greater power efficiency while sacrificing spectral efficiency. By adjusting the width of signal pulses in accordance with a designated brightness level a modified form of PPM is introduced, called VPPM^(59,61). Another noteworthy SCM scheme, known as optical spatial modulation⁽⁶³⁾, harnesses the concept of spatial modulation, demonstrating improved efficiency in terms of both power consumption and bandwidth utilization for indoor OWC.

2.3.2 MULTI CARRIER MODULATION

When the demand for higher data rates escalates, SCM schemes like PPM, OOK and PWM encounter distortion in the transmitted signal at the non-linear LED front-end. Moreover, inter-symbol interference is also induced due to the dispersive nature of optical wireless channels.

Hence, for high-speed VLC, attention is directed towards multi-carrier modulation (MCM). In terms of bandwidth efficiency, MCM has an edge over SCM but at the cost of reduced energy efficiency. One prevalent and widely adopted form of MCM in Li-Fi networks is Orthogonal Frequency Division Multiplexing (OFDM)^(64,65,66,67,68). Over a set of orthogonal subcarriers, parallel information concurrently flows in this modulation technique. To construct an OFDM modulator, an inverse DFT block can be employed, efficiently realized through the use of inverse fast Fourier transform (IFFT), followed by a DAC. Consequently, the signal generated by OFDM is inherently complex and bipolar in nature. Unfortunately, intensity of light cannot be negative. So, the signal flows to LED must be unipolar. The unipolar signal can be obtained by adopting mainly two techniques.

DCO-OFDM employs a positive direct current (DC) bias to generate unipolar signals^(69,70,71). While this approach leads to an elevation in overall electrical power consumption, it does not result in any additional reduction in spectral efficiency^(72,73). ACO-OFDM addresses the challenge of VLC (non negative intensity of light) by utilizing only the odd subcarriers in the OFDM spectrum and clipping the time-domain signal at zero. The asymmetric clipping ensures that the resulting signal remains non-negative while still maintaining the orthogonality of the subcarriers^(74,75). This reduces the impact of clipping distortion to even subcarriers, which carry no information, thereby preserving data integrity on the odd subcarriers. ACO-OFDM enables high spectral efficiency and robustness against multipath effects, making it well-suited for VLC environments where LEDs act as both transmitters and illumination sources. Both DCO-OFDM and ACO-OFDM use Hermitian Symmetry property to make OFDM signal real. This design choice results in a halving of the spectral efficiency in ACO-OFDM. However, due to the minimal necessity for a DC bias in ACO-OFDM, it proves to be more energy-efficient compared to DCO-OFDM^(75,76). Another technique has recently been used in many studies where the elements from both DCO-OFDM and ACO-OFDM have been considered. This hybrid approach is termed as Asymmetrically Clipped Direct Current Biased OFDM or ADO-OFDM^(77,78). ACO-OFDM is implemented on the odd subcarriers while DCO-OFDM is applied to the even subcarriers. In some cases, ADO-OFDM demonstrates superior power efficiency compared to both DCO-OFDM and ACO-OFDM^(79,80).

In addition to the aforementioned MCM techniques, several other variants such as RPO-OFDM⁽⁸¹⁾, AHO-OFDM⁽⁸²⁾, and flip-OFDM^(83,64) have been reported. These MCM tech-

niques have been investigated to improve data rate under dimming conditions.

2.4 MULTI-CELL VLC SYSTEM

In indoor environments, multiple optical sources, such as LEDs, are frequently employed to achieve high-quality illumination. The utilization of multiple LEDs consistently enhances the overall uniformity of horizontal illuminance. Simultaneously, the data rate can be significantly improved by employing all lighting sources as distinct APs, particularly in multi-user scenarios^(84,85). A multi-cell **VLC** system refers to a communication infrastructure that utilizes visible light to transmit data across multiple cells or areas. Each cell typically consists of one or more light sources (such as LED luminaires) equipped with **VLC** transmitters and receivers.^(86,87) These cells are interconnected to form a network, enabling communication between different locations within a given area. The advantages of the multicell **VLC** system are:

- Increased Coverage and Capacity
- Seamless Mobility
- Improved Throughput
- Redundancy and Reliability
- Enhanced Quality of Service

2.4.1 EXISTING BARRIERS WITH MULTI-CELL VLC

Despite having so many advantages, the multi-cell **VLC** system suffers from one major drawback called co-channel interference (**CCI**)^(88,89,90). This setback arises when signals from an AP interfere with signals from the other AP. In a multi-cell optical network, each lighting device can act as a **VLC** AP. Frequently, in order to fulfill lighting requirements, such as achieving an overall uniformity of horizontal illuminance, coverage zones may overlap, leading to interference. It's noteworthy that in certain literature, this type of interference is also referred to as intercell interference (**ICI**)^(91,92,93). To date, various methods have been proposed^(94,95,96,97,89,98) to combat **CCI**. In these studies, non-imaging (**NI**) receivers are predominantly used compared to imaging receivers⁽⁹⁷⁾⁽⁹⁹⁾ that suffer from the large size of the array and high complexity of the systems. For a cell-free **VLC** network, Liu *et al.* proposed a joint AP grouping and user clustering method to reduce interference⁽⁹⁸⁾. In⁽⁹⁵⁾, the decentralized cooperation technique is used to counter **CCI**. This study hasn't considered the random user mobility, or multi-user system throughput and achieves a maximum of 30 dB **SINR**. Younus *et al.* proposed a wavelength division multiplexing (**WDM**) technique in conjunction with sub-carrier multiplexing tones to achieve a high data rate⁽⁹⁶⁾. Addressing the acute interference management problem a novel shared frequency reuse technique is proposed by Ibrahim *et al.* in association with two resource allocation algorithms⁽⁸⁹⁾. Cutting-edge research domain like **RIS** is also used to improve the communication performance of **VLC** system in the

presence of **CCI**⁽⁹⁴⁾. In spite of their contribution, related practical challenges like light path blockage, user mobility, network service quality, and illumination performance are not addressed in those studies⁽⁹⁴⁾⁽⁹⁶⁾⁽⁸⁹⁾. Most importantly, the **SINR** value is always on the lower side.

2.5 HYBRID LiFi-RF SYSTEM

Recent research highlights numerous benefits of **Li-Fi** over its RF counterpart. These include i) its suitability for deployment in RF-restricted areas such as underwater^(100,101) and hospitals⁽¹⁰²⁾; ii) the absence of licensing requirements for its operation; and iii) the capability to offer secure wireless communications⁽¹⁰³⁾, as light does not penetrate opaque objects. However, LiFi does have limitations: i) its coverage is relatively limited, usually spanning a few meters with a single AP; and ii) it is vulnerable to connectivity loss when the light path is obstructed. The communication performance not only degrades due to light path blockage but also due to frequent handover when the user moves inside the indoor environment. Considering both the mobility and light path blockage, network throughput needs to be determined for a practical indoor **Li-Fi** system⁽¹⁰⁴⁾. To counteract the mobility and light path blockage problem, coordination between **Li-Fi** and WiFi has been studied in recent days^(105,106,107,108,109). Hybrid **Li-Fi-RF** typically refers to a concept that combines two different wireless communication technologies (**Li-Fi** and RF/Wi-Fi) in a complementary manner^(60,110) to provide enhanced connectivity options^(111,112,113,114,115,116). However, most of these studies have been performed using a single PD receiver where degradation in **SINR** performance is more severe compared to a system with ADR. In Ref⁽¹¹⁷⁾, ADR is considered in a hybrid **Li-Fi-RF** heterogeneous network.

IEEE 802.11BB STANDARD

To introduce **Li-Fi** into the mass market, a new Light Communication (LC) standard has been developed through collaborative efforts from nearly 25 research and commercial entities. This initiative led to the amendment of the established IEEE 802.11 standard, resulting in the creation of IEEE 802.11bb. This standard is specifically designed for fully networked **Li-Fi** solutions, placing a strong emphasis on handover and mobility support. Major stakeholders in this standardization effort include internet service providers (ISPs), telecom operators, lighting companies, industrial manufacturers, as well as aviation companies. Shifting the center frequency of the baseband waveforms outputted by Wi-Fi chipsets by a few megahertz is the primary proposition of IEEE 802.11bb at the PHY layer⁽¹¹⁸⁾. The potential to reduce the form factor, cost, and energy consumption of **Li-Fi** systems lies in the availability of suitable chipsets for **Li-Fi**-enabled devices. This approach might expedite the integration and adoption of **Li-Fi** technology by device manufacturers and network operators.

2.6 LIGHTING CONSTRAINTS

VLC distinguishes itself from most other communication technologies due to its dual functionality, serving both communication and ambient lighting purposes^(119,120). In an indoor

environment, the main purpose of all the APs responsible for data transmission is to ensure good quality of lighting (QoL). Therefore, numerous constraints are imposed from a lighting perspective during the design of the **VLC** system/**Li-Fi** network. To date, only a few studies have considered the importance of both lighting and communication. The two key criteria from a lighting perspective are average horizontal illuminance and overall uniformity. In the initial phase of adoption, when the cost of LED lighting fixtures incorporating **VLC** technology is high for enabling ultra-dense deployments, it is anticipated that only one **VLC** transmitter will be placed per room. In a study⁽¹²¹⁾ conducted by Alexis et al., it is evident that when utilizing a single optical source, indirect illumination outperforms direct illuminance in terms of homogeneous data rate. Contrary to this, in recent times, smart lighting has entered the scene, utilizing multiple LEDs. The primary focus of this smart lighting system is to enhance energy efficiency through dimming and daylight integration. Ensuring high-integrity color quality that satisfies human perception is the other area of concern in smart lighting^(121,120). When designing the **VLC** system to meet smart lighting requirements, four distinct constraints are imposed⁽¹²²⁾: communication quality, power variation, transmission power, and the metamerism constraint.

The co-design of intelligent lighting and connectivity with light (SmartVLC) is crucial and beneficial. However, it is still in its early stages of development. SmartVLC proves advantageous in areas experiencing unpredictable weather conditions during daylight hours, including cities like London and Amsterdam⁽¹²³⁾. The foundational principles of SmartVLC may serve as inspiration for additional research endeavors at the system level, concentrating on the collaborative design of intelligent lighting and communication systems.

“No one undertakes research in physics with the intention of winning a prize. It is the joy of discovering something no one knew before.”

Stephen Hawking

3

Mitigation of Ambient Light Interference

3.1 INTRODUCTION

AMBIENT LIGHT interference is a significant challenge in visible light communication (VLC) systems. To transmit data, VLC uses the visible light spectrum, typically using White LEDs (WLEDs) as the light source. However, the presence of ambient light can interfere with the transmission of data, leading to errors in communication. This chapter tackles the issue of interference from ambient light in an indoor VLC system, aiming to optimize both communication and illumination within an office setting. It introduces an innovative VLC architecture featuring an appropriate arrangement of WLED luminaires designed to reduce the variation of SINR throughout the room. The channel model along with the transmitter and receiver architecture is illustrated in section 3.3. Luminaires are divided into two categories: data-transmitting illuminants and those meant solely for lighting. The data-transmitting illuminants handle both data transmission and illumination, while the other group provides only ambient lighting to ensure high-quality illumination. The proposed forward error-corrected receiver configuration eliminates ambient light noise from the luminaires used for ambient lighting. A tail-biting convolutional encoder and a Viterbi decoder are employed in the transmitter's encoding section and the receiver's decoding section, respectively, to enhance the bit error rate. This is clearly described in section 3.4. In section 3.5, the results obtained through DIALux and MATLAB simulation to evaluate illumination and communication performances are analyzed. As an extension of this study, a more realistic office environment with cubicles and corridors is considered as indoor space and the corresponding lighting and communication performances are estimated in section 3.6. Section 3.7 concludes the chapter by discussing the relevance of this study.

3.1.1 AMBIENT LIGHT INTERFERENCE

The evolution of WLED as a potential optical transmitter has been noteworthy in recent years, especially for short-range LOS communication. Apart from data transmission capability, these LED sources are also used for illumination purposes^(124,119). However, in addition to data-transmitting LEDs, additional light sources are required to achieve the desired lighting quantity and quality throughout the indoor environment as per international standards. In the detection of transmitted data, the light generated by these illuminants imparts noise^(125,126,127,128). IEEE 802.15.7 standard also adheres to this issue of impairment due to ambient light noise⁽¹²⁹⁾ which is severe when the brightness of these additional sources changes to meet dimming requirements. So, consideration of this ambient light noise is highly recommended to design an energy-efficient lighting solution with a data transmission feature for an indoor environment.

3.1.2 RESEARCH GAP

So far very few attempts have been reported to eliminate the ambient light interference in a VLC system. In⁽¹²⁵⁾ simulation of a VLC system is done using OPTISYSTEM, considering fluorescent light noise. In a recent work⁽¹²⁶⁾ by Chang, Hu and LEE proposed a method to eliminate the ambient noise using a Schmitt trigger and a high pass filter. The reference voltage of the Schmitt trigger is kept at constant which limits the system to deal with variable low-frequency light noise. If the noise voltage exceeds the threshold then the receiver can't detect the bit stream accurately. System accuracy of their proposed system^(125,126) is not reported in a quantitative manner. In another work⁽¹²⁷⁾, Adiono et al. proposed a VLC Analog Front End (AFE) receiver to eliminate ambient light noise. However, they didn't consider any practical indoor environment and BER distribution over different positions in a room. Furthermore, they have achieved minimum BER in the order of 10^{-3} , which is not sufficient in modern communication aspect⁽¹³⁰⁾. The average voltage tracking method⁽¹²⁸⁾ has been proposed by Pham et al. to counteract ambient light interference. They claimed that robust interference rejection is possible inside a $5\text{m} \times 5\text{m} \times 3\text{m}$ room to establish an error-free communication with OOK modulation at a SINR of -2.7 dB. This work didn't address the BER issue. Moreover, luminaire arrangements of data sources and ambient light sources have not been clearly demonstrated. This arrangement has a significant impact on reducing the SINR fluctuation⁽¹³¹⁾ from different locations in the room for multi-user visible light communications. These discussions indicate the possible research gaps that exist in the recent research of indoor VLC systems considering ambient light noise as listed below-

- reprehensible luminaire arrangement leads to wide SINR fluctuation across a room which in turn restricts the mobility
- considering ambient light interference, there is enough scope to improve BER at different receiver locations inside a room
- The illumination performance of the indoor environment needs proper attention as per international standard

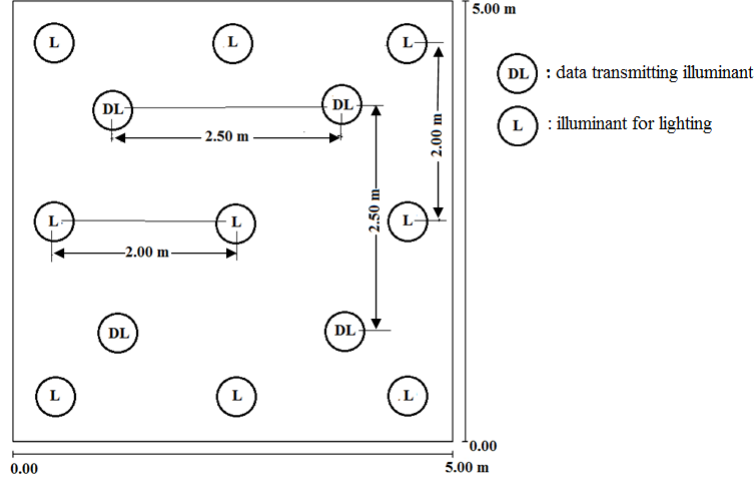


Figure 3.1: Arrangement of evenly distributed luminarie groups, $z=3\text{m}$

3.2 LUMINIAIRE ARRANGEMENT

In an indoor VLC system, room model, classically expressed as $(L \times W \times H)$, is one of the key elements to inspect. It directly affects the quantity, allotment of LED luminaire and communication eminence as well⁽¹³²⁾. In this study, a common office room model⁽³⁹⁾ of square configuration ($5\text{m} \times 5\text{m} \times 3\text{m}$) has been taken to facilitate the analysis of results and subsequent comparison with earlier works. Room surface reflectance of ceiling, walls and floor are taken as 70%, 60% and 20% respectively. In the case of office lighting, ISO standard suggests a minimum of 300 Lux average illuminance (E_m) with a minimum of 0.70 uniformity of illuminance (U_0) over a horizontal work plane. Considering a commercial indoor downlighter of luminous flux 1140 lm, thirteen ceiling-mounted luminaires are required to achieve the required illuminance level and uniformity as per the ISO standard⁽¹³³⁾. This estimation is done by using well well-known Lumen formula⁽¹³⁴⁾. Among these thirteen luminaires, nine are dedicatedly used only for ambient lighting purposes and the rest act as a data-transmitting hotspot that transmits encoded binary packet data at a rate of 100 Mbps. The details and specifications of all the luminaires and room used in the present study are tabulated in Table 3.1.

These data-transmitting luminaires also contribute light to achieve the required horizontal average illuminance with good uniformity. Here, in order to reduce **SINR** fluctuation the ceiling of the room is subdivided into four equal segments, and four data transmitting luminaires (DL) are mounted at the center of each segment, while the remaining nine luminaires (L) are arranged uniformly across the ceiling to achieve uniform light distribution. The arrangement of all of these luminaires is shown in Figure 3.1.

3.3 SYSTEM MODEL

The overall building block of designed VLC system is illustrated in Figure 3.2. Here the incoming binary serial data (b_i) initially processed through the transmitter and optically modu-

Table 3.1: Design parameters for simulation (room and luminaires)

Parameter	Specification
Room Dimension(m)	$5 \times 5 \times 3$
Reflectance of ceiling, wall, floor	0.7, 0.6, 0.2
Mounting height of luminaires from working plane(m)	2.15
Luminaire wattage(W)	11.7
Luminous Flux (Lumen)	1140
Number of luminaire	13
Number of luminaire used for both data transmission and illumination (DL)	4
Number of luminaire used for illumination (L)	9
Height of working plane above floor(m)	0.8

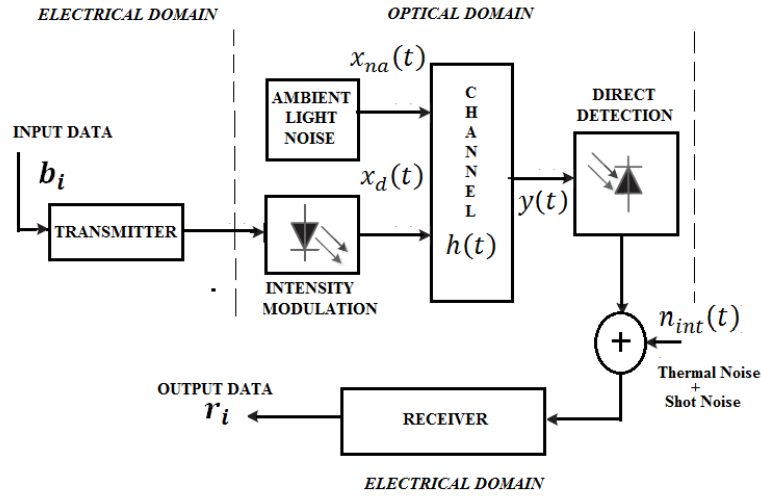


Figure 3.2: Block diagram of forward error corrected VLC system

lates the data transmitting WLEDs. The ambient light noise along with optically modulated data propagates through the channel before it has been received by the photo-detector. Since the channel characteristic plays an important role to set up an efficient VLC system, modeling of channel is essential^(135,136) in order to understand the characteristics of visible light channels and thus to design well-performing communication systems. Integral components of the proposed system are described in the subsequent sections.

3.3.1 CHANNEL MODEL

The basic channel model of our designed system is given as:

$$y(t) = [x_d(t) + x_{na}(t)] * h(t) \quad (3.1)$$

Here, $y(t)$ = Received signal by the photo-detector (PD)

$x_d(t)$ = Transmitted signal by the data transmitting WLED sources (hotspot)

$x_{na}(t)$ = Transmitted signal (noise) by the ambient light sources

$h(t)$ = Impulse response of the channel

For a given n^{th} source (S_n) and receiver R_{ij} placed at point P_{ij} , the impulse response of IM/DD communication channel is given by^(137,138)

$$h_{nij}(t) = \sum_{k=0}^M h^k(t, S_n, R_{ij}) \quad (3.2)$$

M = order of inter reflection

It has been studied earlier that, apart from the direct response, the contribution of higher order reflection in overall channel response is significantly small⁽¹³⁹⁾. The direct gain of the VLC channel is expressed by⁽³⁹⁾,

$$H(0) = \frac{(m+1)A}{2\pi d^2} \cos^m(\varphi) \cos(\theta) \text{ when, } 0 \leq \theta \leq \psi_C \quad (3.3)$$

Where, ψ_C represents FOV of the receiver, A is the physical area of a photo-diode, d is the distance between optical source (S_n) and receiving point (P_{ij}), m denotes Lambertian index, φ represents the angle between the light emission direction and the light source normal direction, θ is the incidence angle of radiation. The value of the channel gain $H(0)$ is zero when the incidence angle is greater than the FOV of the receiver

In case of 1st reflection channel DC gain is represented as⁽³⁹⁾

$$dH_{ref}(0) = \frac{(m+1)A}{2\pi^2 d_1^2 d_2^2} \rho dA_{wall} \cos^m(\varphi) \cos \alpha \cos \beta \cos(\theta) \text{ when, } 0 \leq \theta \leq \psi_C \quad (3.4)$$

where d_1 is the distance between optical source and a reflection point, d_2 represents the distance between the reflection point and receiving point (P_{ij}), ρ denotes the reflection coefficient, dA_{wall} expresses emission area of indirect source, φ is the radiation angle of reflection points, α expresses the incidence angle of reflection point, β denotes radiation angle of the receiver, and θ is the incidence angle of the receiver.

Now, received optical power due to data transmitting LED sources $P_{r,data}$ and ambient light sources $P_{r,na}$ have been computed incoherently by means of direct gain and reflection channel gain. It is given by,

$$P_{r,data} = \sum_{data \text{ sources}} \{P_{t,data}H(0) + \int_{wall} P_{t,data}dH_{ref}(0)\} \quad (3.5)$$

$$P_{r,na} = \sum_{ambient \text{ light sources}} \{P_{t,na}H(0) + \int_{wall} P_{t,na}dH_{ref}(0)\} \quad (3.6)$$

Where, $P_{t,data}$ is the transmitted power by the data transmitting LED sources and $P_{t,na}$ is the transmitted power by the ambient light sources.

Horizontal Illuminance at point P_{ij} for a specified n^{th} source (S_n) is given by,⁽¹⁴⁰⁾

$$E_0 = I(0) \cos^m(\phi_0) \cos(\theta) / d^2 \quad (3.7)$$

3.3.2 TRANSMITTER DESIGN

Figure 3.3 shows the main block diagram of the transmitter utilized in the proposed VLC system. Here, ON-OFF Keying (OOK) modulation technique has been used to send data at 100 Mb/s through visible light beam. Initially an infinite stream of binary data is broken into packets/dataframes of length 100.

The output of FEC encoder is directly fed to the line coder to acquire a data pattern with constant signal power. Manchester coding technique has been chosen in this work to facilitate the line coding operation. Because of its level insensitive, self-clocking characteristics this line coding method is widely accepted in the communication field. This encoder is realized with a number of logic gates, clock generator and a signal adder. The frequency of the clock generator used in the Manchester encoder is set to double of the incoming bit stream.

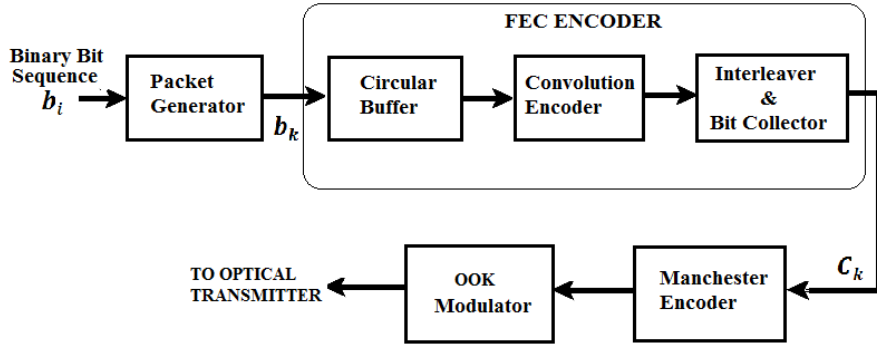


Figure 3.3: Block diagram of the proposed FEC-equipped data transmitter.

3.3.3 RECEIVER ARCHITECTURE

The receiver architecture of the proposed VLC system is shown in Figure 3.4. The front end of the receiving unit comprises with a photodiode followed by a TIA. The generated photocurrent is proportional to the incident optical power, while trans-impedance configuration is used to convert the current in the corresponding voltage format. BPW34 photodiode is considered as a front end of the receiver. This fast response PIN photodiode has a radiant sensitive area of 7.5 mm^2 with $\text{NEP } 4 \times 10^{-14} \text{ W/Hz}^{1/2}$. The received signal by the photo-detector is an algebraic sum of received signals due to four data transmitter (DL) and ambient light noise generators (L). Moreover, thermal noise and shot noise contributes to the receiving front end. These noises are treated as the internal noise ($n_{int}(t)$) of the receiver and can be estimated as

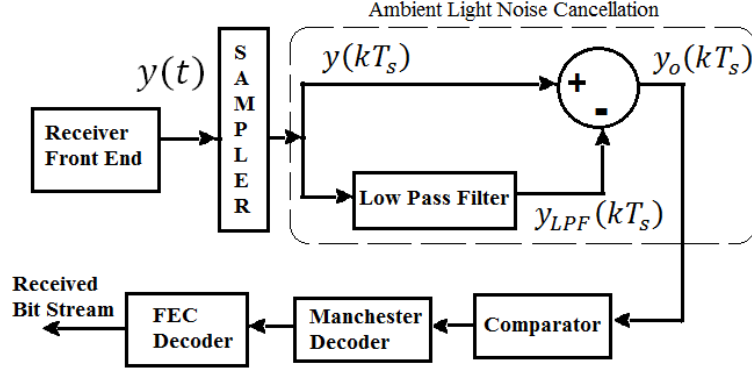


Figure 3.4: Receiver block diagram of the proposed VLC system

Table 3.2: Receiver Specification

Parameter (Unit)	Description	Value
$q(e)$	Charge of electron	1.6
$I_{bg}(nA)$	Background current	30
I_2	Noise bandwidth factor	0.562
$\gamma(A/W)$	Detector responsivity	0.53
$B(MHz)$	Equivalent Noise Bandwidth	100
F_n	Noise figure of TIA	0.2
$R_L(\Omega)$	Load resistance	50
$K_B(J/K)$	Boltzman's constant	1.38
$\psi_C(degree)$	Receiver's field of view	65

additive white Gaussian noise (AWGN)⁽¹⁴¹⁾. The variance of the total noise and interference is given as,

$$N_{total} = \sigma_{shot}^2 + \sigma_{thermal}^2 + \gamma^2 P_{r,na} \quad (3.8)$$

The shot noise (σ_{shot}^2) and thermal noise ($\sigma_{thermal}^2$) variances are given as⁽³⁹⁾

$$\sigma_{shot}^2 = 2q\gamma (P_{r,data} + P_{r,na}) B + 2qI_{bg}I_2B \quad (3.9)$$

$$\sigma_{thermal}^2 = 4 \left(\frac{K_B T}{R_L} \right) F_n B \quad (3.10)$$

The signal to interference plus noise ratio of the receiver is given by,

$$SINR = \frac{\gamma^2 P_{r,data}}{N_{total}} \quad (3.11)$$

Explanation of receiver's parameters and its values used in the simulation are listed in Table 3.2.

The sampled output of the photodetector $[y(kT_s)]$ is fed to the FIR low pass filter as per the configuration shown in Figure 3.4. In order to allow only low-frequency ambient light

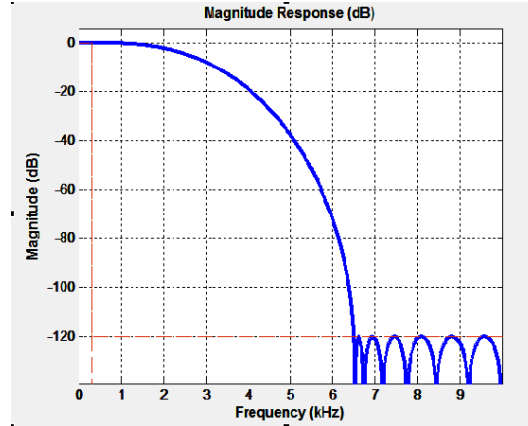


Figure 3.5: Magnitude response of FIR filter (Low pass) used in receiver

noise and block the transmitted high-frequency signal the cut of frequency of the filter at parallel path is set at 2 kHz. The magnitude response of the LPF is shown in Figure 3.5. If the ideal filter characteristics is considered with a sharp cutting edge then there should not be any ambient noise component at the output. This is given by,

$$y(kT_s) = y_d(kT_s) + y_{na}(kT_s) + n_{int}(t) \quad (3.12)$$

$$y_{LPF}(kT_s) = y_{na}(kT_s) + \tilde{n}_{int}(kT_s) \quad (3.13)$$

$$y_o(kT_s) = y_d(kT_s) + n_0(kT_s) \quad (3.14)$$

where,

$$n_0(kT_s) = n_{int}(kT_s) - \tilde{n}_{int}(kT_s) \quad (3.15)$$

3.4 FORWARD ERROR CORRECTION

The Forward Error Correction (FEC) in the designed system includes an FEC encoder within the transmitter. This encoder receives information bits, adds calculated redundant symbols, and generates encoded data at an increased bit rate. In pursuance of forward error correction, channel coding of incoming continuous stream of bits has been done using (171,133) Tail Biting Convolutional Code which is one of the recommended NASA planetary standard codes^(142,143).

3.4.1 TAIL BITING CONVOLUTION CODE

A tail-biting convolution code is a type of error-correcting code used in digital communication systems. It is called "tail-biting" because the encoder's feedback loop is terminated after a fixed number of input symbols, instead of being allowed to run indefinitely. This makes the encoder more compact and easier to implement but also requires special decoding algorithms. The encoding process of a tail-biting convolution code involves multiplying the input sequence

with a set of generator polynomials, which generates a longer output sequence. The encoder is designed to transmit both the input sequence and the generator polynomials to the decoder, which uses them to reconstruct the original input sequence and correct any errors that may have occurred during transmission.

In this design, the convolution encoder with constraint length seven is first initialized by inputting the last 6 information bits of the packet with the help of a circular buffer and the corresponding output symbols generated by the convolution encoder is ignored. Hereafter, the remaining 94 data bits are encoded and transmitted, followed by the first 6 bits. As a consequence, the starting state of the encoder remains the same as its ending state. It is also ensured that the entire packet has been readily available at the encoder before the first symbol is transmitted.

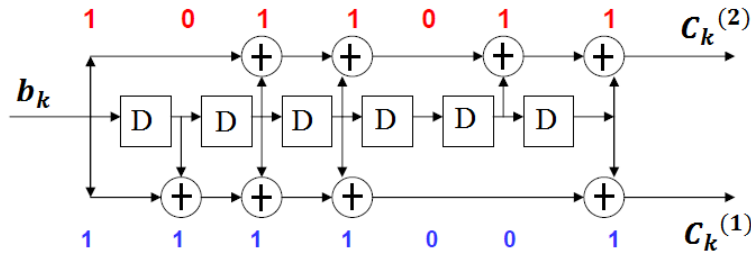


Figure 3.6: Block diagram of the convolution encoder

Figure 3.6 shows the block diagram of the convolution encoder used in this work. Incoming packet data (b_k) is passed through six sharing memory elements and produces two output streams, given by⁽¹⁴⁴⁾

$$C_k^{(1)} = b_k + b_{k-1} + b_{k-2} + b_{k-3} + b_{k-6} \quad (3.16)$$

$$C_k^{(2)} = b_k + b_{k-2} + b_{k-3} + b_{k-5} + b_{k-6} \quad (3.17)$$

In order to generate the encoded output stream (C_k) these two streams are interleaved together.

3.4.2 VITERBI DECODER

In present study, to decode the tail-biting convolution encoded sequence, the Viterbi decoding algorithm has been used at receiving end. This decoder works by comparing the received sequence of symbols with all possible paths through the trellis diagram of the convolution code. The decoder computes a metric for each path, which is the sum of the Euclidean distances between the received symbols and the expected symbols for that path. The path with the lowest metric is chosen as the most likely decoded sequence.

Maximum likelihood technique has been employed in this decoding algorithm to estimate the transmitted bit sequence^(145,146,147). In section 3.4.1 it has been mentioned that the initial

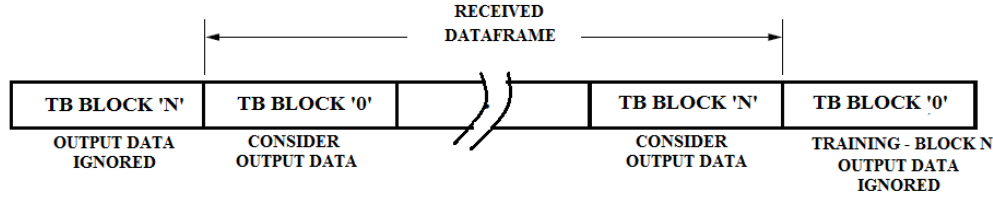


Figure 3.7: Decoding technique for Tail Biting Convolution code

and final state of the tail-biting trellis structure remains the same. This approach enables the Viterbi algorithm to maintain consistency with the end of a block by cyclically repeating the received codeword. Consequently, the model duplicates the received codeword and processes this data through the Viterbi decoder, performing the traceback from the optimal state after the repeated data set. In this proposed study direct traceback with a traceback depth of 40 has been adopted. In a Viterbi decoder starting state plays an important role for trellis construction. In our design, the last TB is considered primarily to obtain the correct state for TB Block 0. At that time output data is simply overlooked. Now the process continues starting from TB Block '0' to TB Block 'N'. Finally, TB Block '0' is inserted again to provide a training sequence for decoding of last traceback block. This technique is clearly shown in Figure 3.7.

3.5 RESULTS

In this section, joint communication and illumination performance of the proposed system has been evaluated using MATLAB and DIALux respectively.

3.5.1 ILLUMINATION PERFORMANCE

DIALux simulation in terms of average horizontal illuminance and overall uniformity. An average horizontal illuminance of 363 Lux with uniformity of 0.841 has been achieved using the parameter listed in Table 3.1. This result complies with the lighting requirement of an office environment as per ISO as specified in previous section. Figure 3.8 shows the distribution of simulated horizontal illuminance on the working plane. From the distribution, it can be observed that the corners of the room receive the lowest illuminance of 305 Lux while the center receives the maximum illuminance of 391 Lux.

Maximum received optical power has been observed in between the middle and corner positions of the room. The explanation behind these two different findings lies in the luminaire layout-the DLs and the Ls referred to Figure 3.1. Both direct and reflected optical power distribution are computed using equations 3.3, 3.4 and 3.5 and are shown in Figure 3.9 and Figure 3.10.

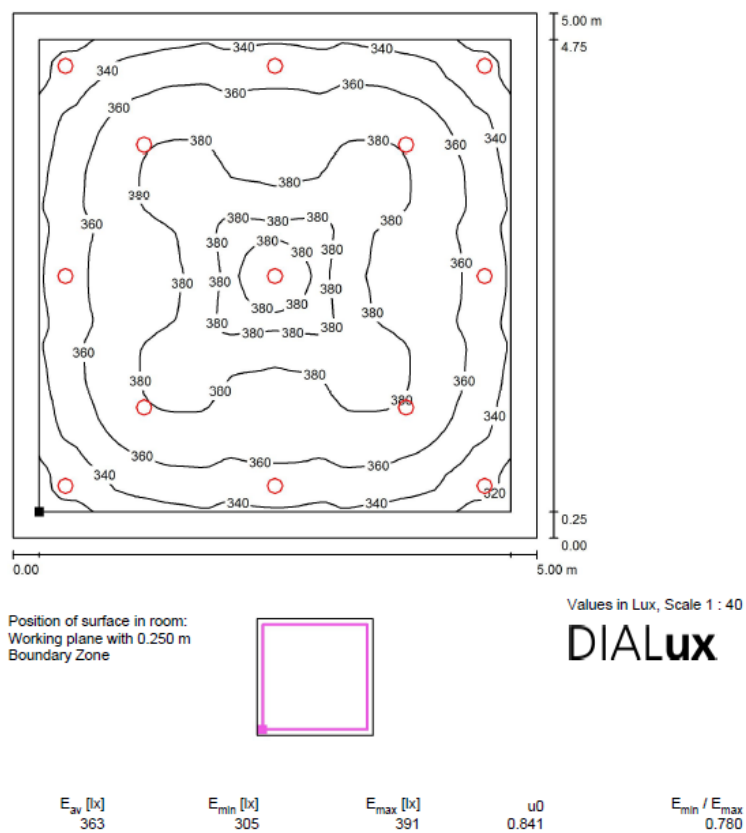


Figure 3.8: Distribution of horizontal illuminance over the working plane, $z=0.8m$

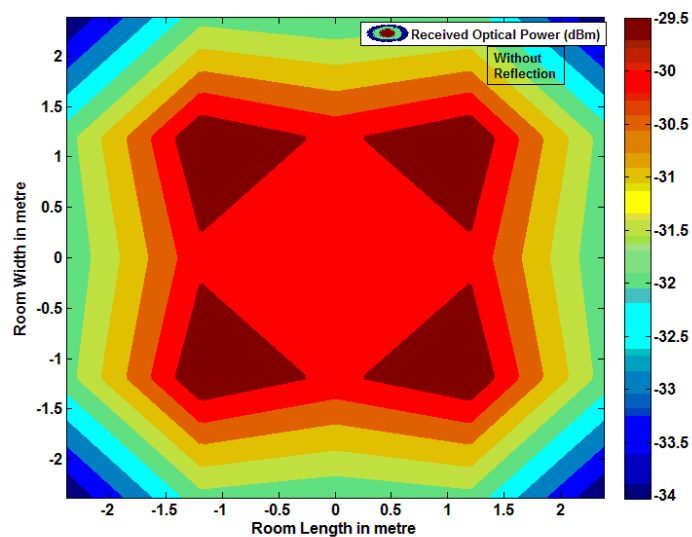


Figure 3.9: Distribution of optical received power: direct component, $z=0.8m$

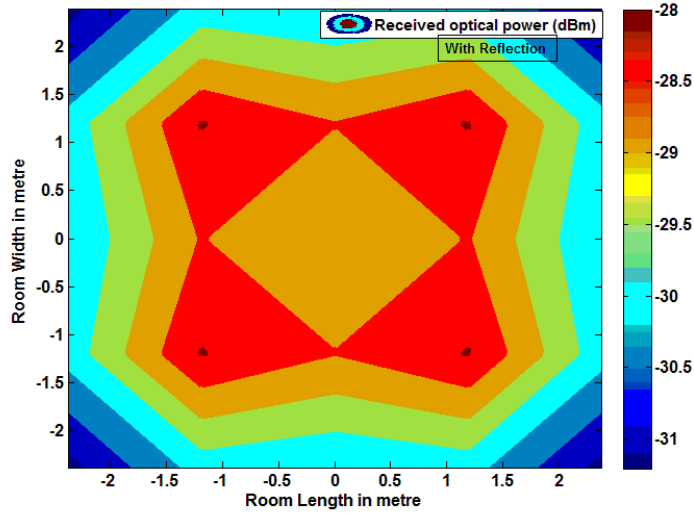


Figure 3.10: Distribution of optical received power: direct with reflected component, $z=0.8\text{m}$

3.5.2 COMMUNICATION PERFORMANCE

From the communication point of view, as the reflected component of optical power reduces noise due to intersymbol interference is gradually reduced. Result shows, -31.293 dBm average optical received power considering only direct component. 6% increment in average optical received power can be observed if the reflected component is taken into account. This result is advantageous from a communication perspective. However, greater uniformity in horizontal illuminance demands higher reflected share. In spite of very little reflected component, excellent overall uniformity (0.841) is achieved. This is only possible due to the luminaire arrangement shown in Figure 3.1 where two different types of illuminant are considered and placed accordingly.

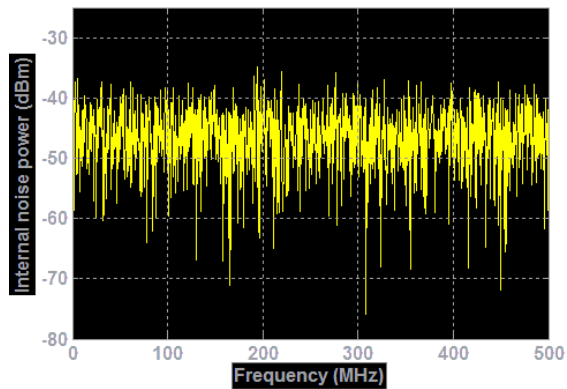


Figure 3.11: Power spectrum of internal noise of photodetector

In order to determine the signal to interference plus noise power ratio, received power at different grid points due to ambient light sources are determined using Equation 6. In gen-

eral noise power at receiver is incorporated in form of thermal noise and shot noise. These noises, considered as the internal noise of photodetector, are almost remain same irrespective of the receiver location. The power spectrum of simulated internal noise is shown in Figure 3.11. Apart from this internal noise, the ambient light noise is highly dependent on luminaire arrangement, room geometry and receiver location. In our system design, luminaries are arranged in such ways that signal to interference plus noise ratio, given by equation 13, does not fluctuate over a wide range. Result shown in Figure 3.12 clearly suggests that **SINR** ranges from -3.08 dB to 1.205 dB. In order to verify the validity of the proposed scheme, it is compared with existing research outcome. In⁽¹²⁸⁾ Pham et al. achieved **SINR** ranging from -0.8 dB to -7 dB for same room dimension. From this standpoint, results obtained by the proposed VLC system exhibit better consistency with comparatively smaller deviation.

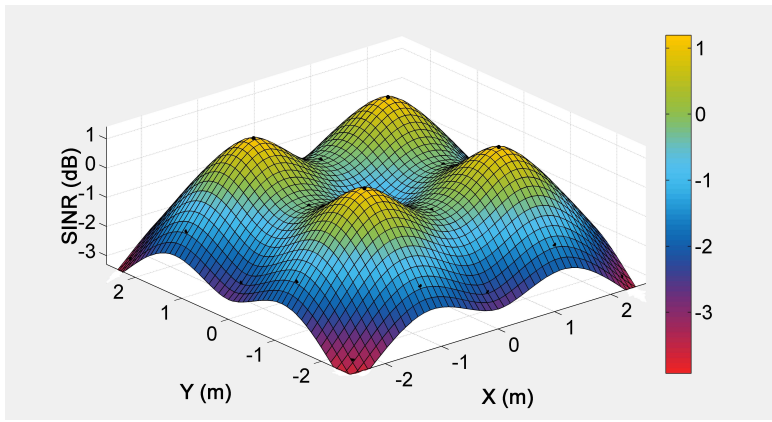


Figure 3.12: Distribution of SINR at different location inside the room, $z=0.8\text{m}$

The transmitted binary bit sequence and received data after demodulation are compared in Figure 3.13. Even though an exact match of the transmitted and received waveform is observed for some sample data, still there exists some error in the transmitted and received bit pattern when a very long stream of data is taken under observation.

In spite of having negative **SINR** (in dB), excellent BER has been achieved by using the proposed receiver architecture with FEC. It has been observed that the maximum ambient light interference frequency is very low (less than 2 KHz). So, a substantial amount of noise originating due to ambient light source has been removed by noise cancellation block using low pass filter. With the help of MATLAB simulation BER has been computed for spatial **SINR**, obtained at different receiving locations inside the room. Figure 3.14 shows BER performance of the proposed scheme. It shows significant improvement in BER with a forward error correction scheme compared to receiver architecture without forward error correction. The BER of the designed system (with forward error correction) can be represented as a function of **SINR** and it can be obtained using the cubic curve fitting method given as,

$$BER_{FEC} = Ax^3 + Bx^2 + Cx + D \quad (3.18)$$

where,
 $x = \text{SINR in dB}$

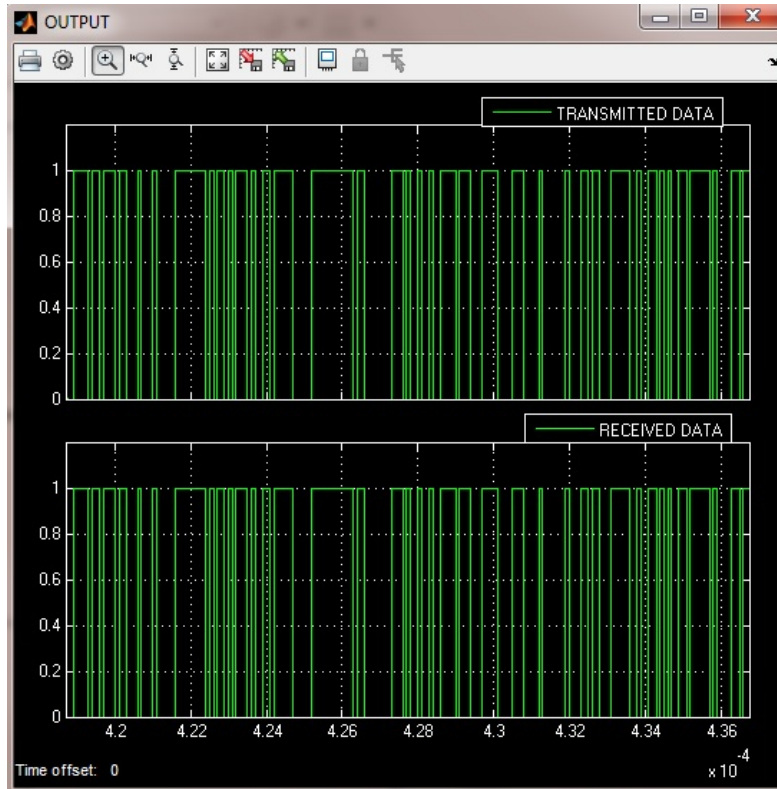


Figure 3.13: Transmitted and Received waveform for sample random binary data

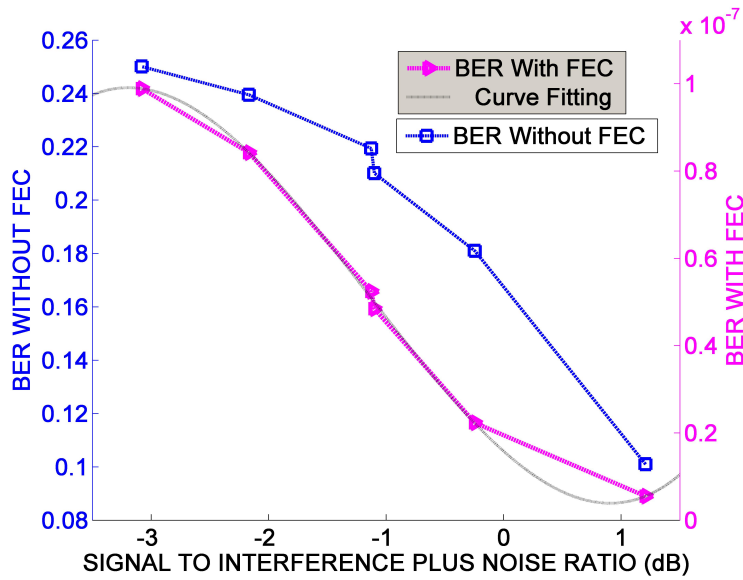


Figure 3.14: Variation of BER with SINR (dB)

$$A = 2.8 \times 10^{-9}, B = 9.5 \times 10^{-9}, C = -2.4 \times 10^{-8}, D = 1.6 \times 10^{-8}$$

From the distribution of BER shown in Figure 3.15 it can be noticed that maximum BER (9.89×10^{-8}) has been recorded at corner of the room while minimum BER (5.514×10^{-9})

has been obtained at four grid points just below the data transmitting optical source. However, in average BER lies in the order of 10^{-8} across the room.

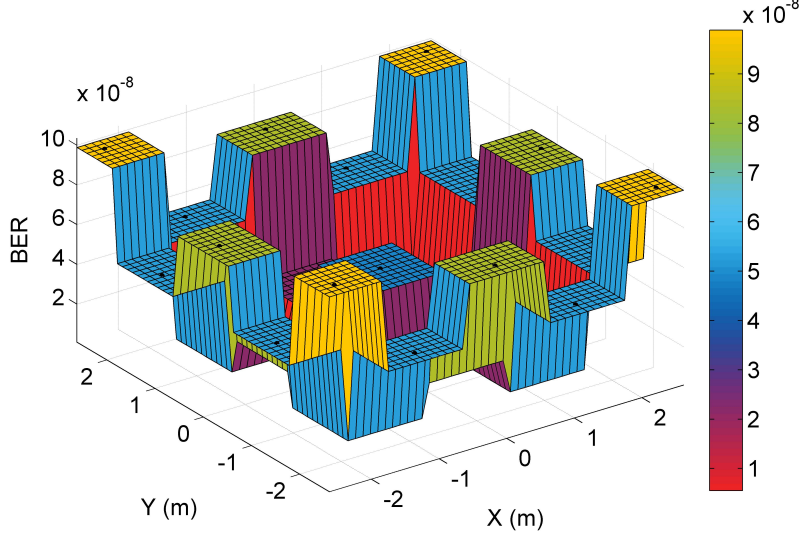


Figure 3.15: Obtained BER at different location inside the room, $z=0.8\text{m}$

3.6 A SPECIAL CASE: DESIGN WITH OFFICE ENVIRONMENT AND INFRASTRUCTURE

The ambient light interference mitigation strategy discussed so far is now adopted for a more realistic office environment with chairs, tables, and cubicles. Commercially available luminaires are selected for lighting and data transmission purposes. In section 3.6.1 the office geometry and luminaire specifications have been described. Section 3.6.2 deals with the joint communication and illumination performances considering the ambient light factor.

3.6.1 OFFICE GEOMETRY AND DESIGN PARAMETERS

The office room, measuring $7\text{m} \times 6\text{m} \times 3\text{m}$, is divided into six small cubicles, as illustrated in Figure 3.16. The corridor within the room is 1.6m wide, and each task area within a cubicle measures 1.5m by 0.85m . Each cubicle is equipped with a separate AP with zero CCI. The WLED installed at each AP can transmit data through intensity modulation and meet the primary lighting needs of the task area. Additionally, Compact Fluorescent Lamps (CFL) are installed throughout the office to ensure good uniformity and the necessary horizontal illuminance across the entire indoor environment. As there is no CCI inside the cubicles (clearly mentioned), a receiver with wide FOV can easily support the system. However, in this specific study, 120-degree FOV is considered for simulation. The intensity distributions of both light sources (LED and CFL) are depicted in Figure 3.17.

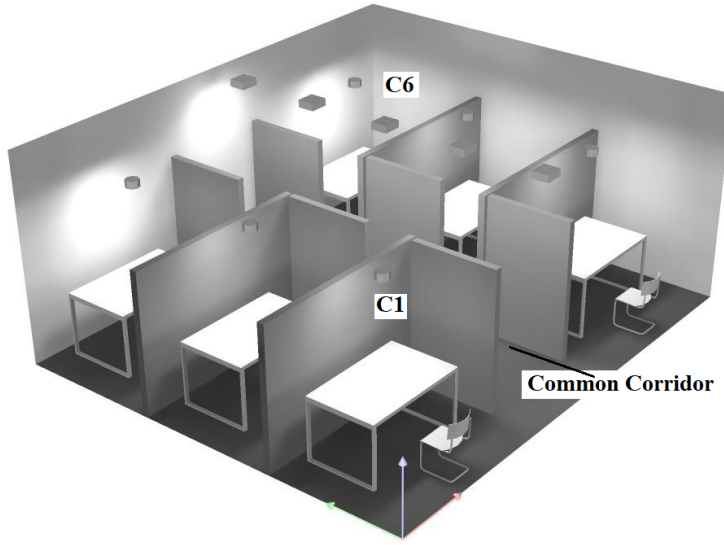


Figure 3.16: Li-Fi enabled LED lighting system in office cubicle (3-D view)

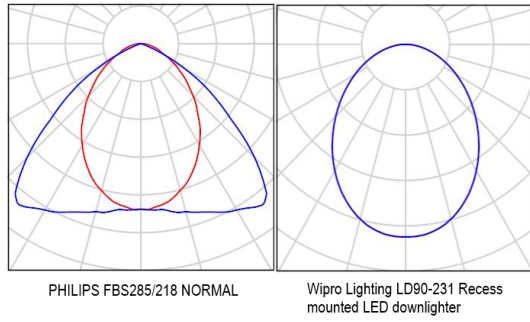


Figure 3.17: Intensity distribution of the optical sources

3.6.2 SYSTEM PERFORMANCE

A DiaLux simulation was conducted for the entire office space, considering the contributions of both the optical transmitter and ambient light. Five CFLs, primarily installed to illuminate the common corridor, also enhance the lighting within the task areas inside all cubicles. The results, presented in Table 3.3, indicate satisfactory lighting performance across all task areas and corridors in terms of horizontal illuminance and overall uniformity. Due to the symmetrical design of the room and the arrangement of luminaires, almost identical illuminance distribution was achieved in all opposite-facing cubicles.

The simulated results indicate that the ambient light source's contribution over the task area inside the cubicle ranges from 41 to 109 Lux. As the ambient light increases over the task area, the **SINR** gradually decreases from 5.94 dB to 0.96 dB. Although, satisfactory BER in the order of 10^{-8} can be obtained over the communication floor (over the table at each cubicle). The variation of BER and **SINR** with an increase in ambient illuminance is depicted in Figure 3.18.

Table 3.3: Lighting performance over different task area

Task Area	Avg. horizontal illuminance (Lux)	Overall Uniformity
Left Lower (C ₁)	311	0.73
Left Middle (C ₂)	338	0.76
Left Upper (C ₃)	314	0.74
Right Lower (C ₄)	311	0.73
Right Middle (C ₅)	338	0.76
Right Upper (C ₆)	314	0.74
Common Corridor	260	0.77

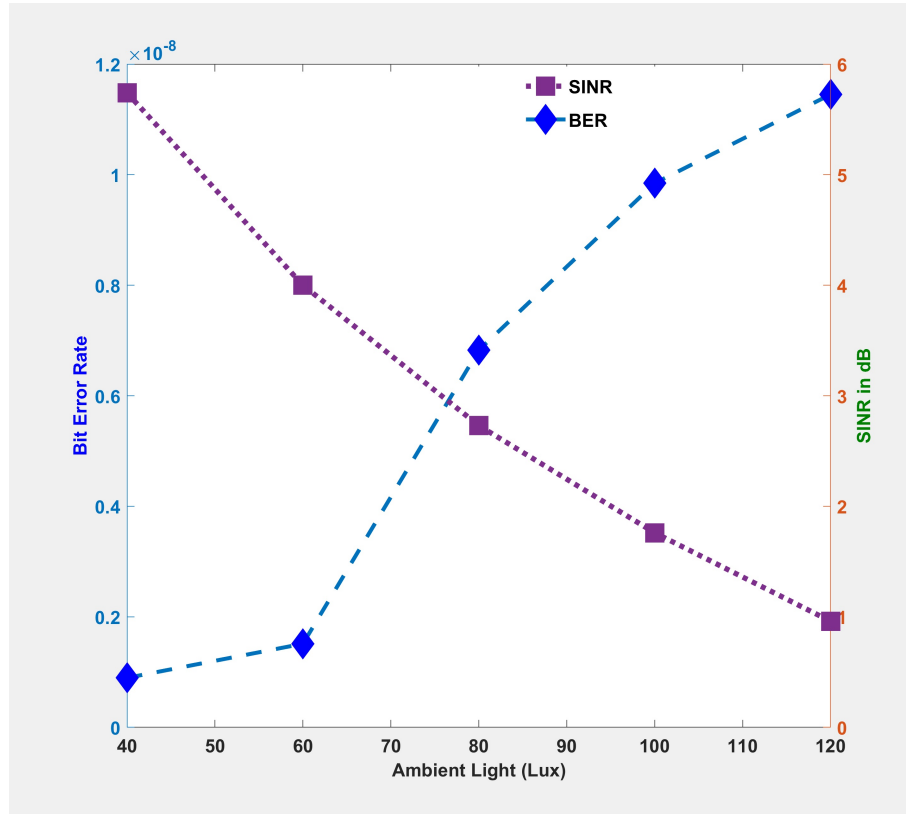


Figure 3.18: BER & SINR at different Ambient Light Intensity

3.7 SUMMARY

This chapter considers an indoor visible light communication system within a room with quality lighting provision, as per the ISO standard, in terms of two lighting design parameters viz. average illuminance and uniformity of illuminance over the horizontal working plane. All of the ceiling-mounted luminaires act as illuminator (light source) responsible to create desired lighting ambience within the indoor space, while some of the luminaires act as both the data transmitter as well as illuminator. Now at the time of data reception by the photo-detector, the illuminators used only for illumination purposes create noise commonly known as ambient light noise. In this work, novel receiver architecture with FEC is proposed to get

back the transmitted packet data at a data rate of 100 Mbps by rejecting ambient light noise. To achieve forward error correction, the receiver's decoding section uses a Viterbi decoder, while the transmitter's encoding section employs a tail-biting convolutional encoder. Results obtained using simulations show satisfactory BER ranging from 10^{-8} to 3×10^{-9} in the presence of -26.19 dBm average ambient light interference and 363 Lux average horizontal illuminance with 0.841 uniformity. Results reveal that the proposed VLC system can detect erroneous reception of packet data and correct it accordingly at a moderate BER even if ambient light noise is significant along with internal noise.

3.8 RESEARCH OUTPUT

The findings from this chapter are reported in the following research publications:

- **Chatterjee, S., & Roy, B. (2020).** An approach to ensure joint illumination & communication performance of a forward error-corrected indoor visible light communication (VLC) system in presence of ambient light interference. *Journal of Optical Communications*.
DOI: doi.org/10.1515/joc-2019-0212
- **Chatterjee, S., & Roy, B. (2020).** Design, development and practical realization of a VLC supportive indoor lighting system. *Light & Engineering*, 28(3).
DOI: doi.org/10.33383/2019-048

“Only a philosopher’s mind grows wings, since its memory always keeps it as close as possible to those realities by being close to which the gods are divine.”

Plato

4

Daylight Integrated Indoor VLC System

IN CHAPTER 3, ambient light interference mitigation technique has been discussed. However, the ambient light from the sun can be purposefully integrated with artificial light sources to reduce energy consumption, especially for lighting purposes. This chapter deals with a dimmable VLC-supportive lighting system. Based on the block diagram of our proposed system (see section 4.2) the brief system design with the practical circuit is presented in section 4.3. The overall transmitter design involving data enabled LED driver, dimming control mechanism and OOK modulator have been discussed in sections 4.3.1, 4.3.2 and 4.3.3 respectively. Detail design of the receiving unit and the associated noise of the proposed system are outlined in section 4.4. In section 4.5 illumination and communication performances of the designed system has been evaluated. Finally, in section 4.6 the importance and relevance of the work have been discussed.

4.1 INTRODUCTION

In sustainable building designs, daylight is considered as an alternative free source of light to artificial lighting. So, in the case of indoor VLC application available daylight can be integrated with the artificial source to conserve energy and make the system more energy-efficient⁽¹⁴⁸⁾. So far, a step up in the energy efficiency of the existing VLC system has been achieved by controlling the brightness of the optical source using several data transmission and power allocation schemes^(149,150). PAM and PWM are widely adopted techniques for dimming support in an indoor VLC system⁽¹⁵¹⁾. To maximize the energy efficiency of the multi-color LED-based VLC systems an optical power allocation scheme is formulated in⁽¹⁴⁹⁾. Din et al. proposed a brightness control and sub-carrier L-ary pulse position modulation (SC-L-PPM) scheme that proficiently minimizes the energy consumption of a VLC system⁽¹⁵⁰⁾. In this paper, it has been claimed that the system satisfies users’ lighting and communication requirements. How-

ever, none of the above-mentioned researches^(149,150) specifies the inherent perceived flicker of the systems. This issue of flicker puts a serious question on the implication of the system from the lighting perspective. In contrast to the existing energy-efficient techniques proposed in earlier works, automated dimmable VLC system can be adopted where illumination level would be maintained based on ambient daylight⁽¹⁵²⁾. Integration of ambient daylight with the artificial light source is a very well-known practice for lighting engineers. On the other hand, it has been clearly demonstrated by the researchers that degradation in system performance due to ambient sunlight is another key area of concern^(153,154).

4.2 SYSTEM DESIGN

This chapter considers a practical VLC-supportive lighting system in an office cubicle as shown in Figure 4.1. The LED luminaire which also works as a transmitter is placed at a 1-meter height over the working plane. As per the international standard⁽¹³³⁾, for a commercial indoor environment, the required minimum average indoor illuminance on the working plane is 300 Lux. During the daytime, substantial energy can be saved by integrating diffused daylight with this system. The proportion of daylight is varied depending upon room geometry and sky condition. In this study, the measured average diffused daylight over the working plane is 0 lux to 110 lux. As the experimentation is done in the interior portion of a building direct daylight component is unavailable. So, the diffused daylight value is in the lower range. However, the goal is to utilize the full range of available daylight to design the subsequent segment and achieve the required lux level. This integrated daylight serves as a potential source of noise considering our system from a communication perspective. So, the goal of the project is to implement and evaluate the performances of a prototype system which is capable of transmitting the data with minimum error even in the presence of ambient daylight noise and providing sufficient illuminance on the working plane at the expense of minimum energy. Flicker is one of the important performance metrics in a VLC system. IEC 61000-3-3⁽¹⁵⁵⁾ suggests short-term flicker severity should have a maximum limit of 1. In this work, the short-term flicker severity at the time of data transmission through the designed VLC system has also been measured.

4.2.1 OVERALL BLOCK DIAGRAM

The optical wireless communication scenario is dependent on the modulation characteristics of the transmitter and the detection characteristics of the receiver in an indoor environment. A generalized block diagram of our proposed system is illustrated in Figure 4.2. The system comprises mainly two units- transmitter and receiver. The transmitter section encompasses a dimming control mechanism for energy-efficient illumination purposes along with a modulator for data transmission.

In order to achieve the required illumination level with daylight integrated artificial light source, Luxeon Rebel ES LED module as shown in Figure 4.3 is used⁽¹⁵⁶⁾. This module consists of seven LXML PWN₂ LEDs (CCT: 4100K). Out of these seven LEDs six LEDs have been used in a series configuration to design the luminaire. This luminaire contributes 200-300 lux over the task area depending upon ambient daylight. When the ambient daylight is

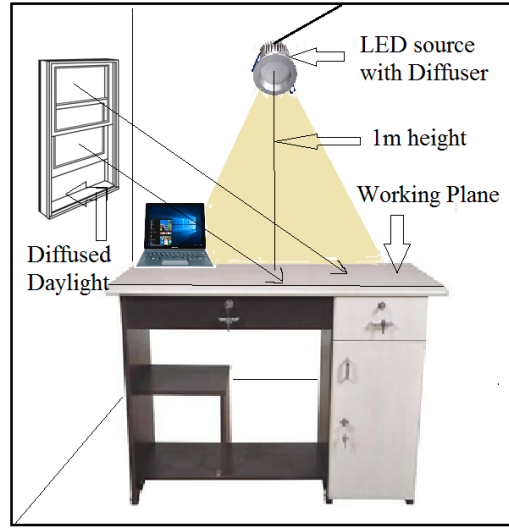


Figure 4.1: VLC supportive indoor lighting scheme

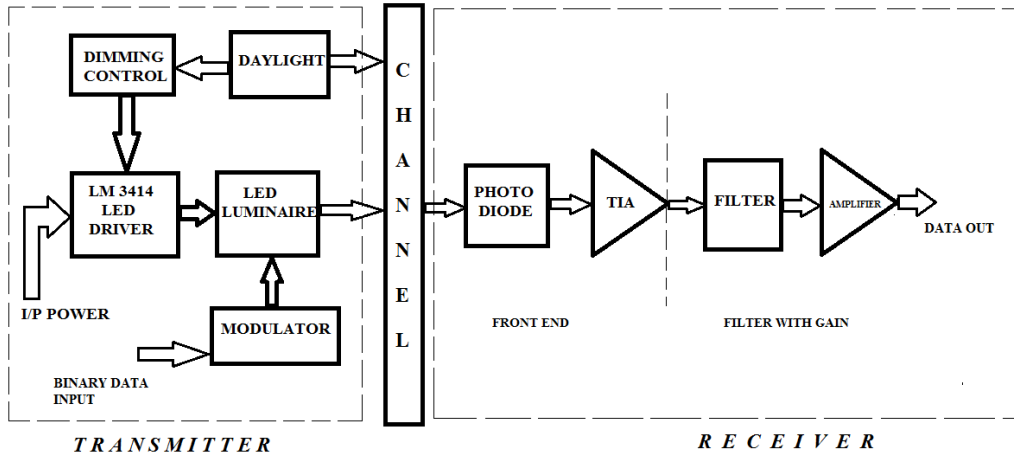


Figure 4.2: Generalized block diagram of the proposed system

at maximum, the artificial light source contributes 200 lux and the additional 100 lux is supported by daylight.

4.2.2 MATHEMATICAL FRAMEWORK FOR DIMMING CONTROL MECHANISM

According to the CIE technical report⁽¹⁵⁵⁾, the design of the transmitter needs careful consideration of eye safety. So, to counter with the discomfort glare, a diffuser has been used over the LED panel for uniform light distribution. Apart from the Lambertian scattering it also absorbs light flux which in turn reduces the transmitted optical power.

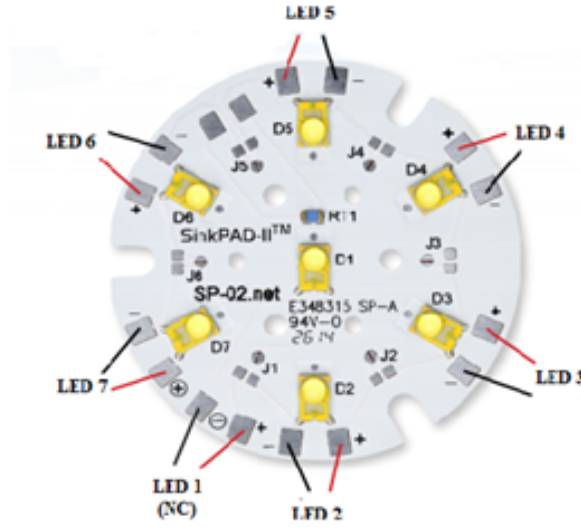


Figure 4.3: LUXEON LED Module used for designing optical source

The light output (ϕ_{LED}) from a single LED at constant LED current (I_{LED}) is given by⁽³⁹⁾,

$$\phi_{LED|I_{LED}} = 683 \times k_v \int V(\lambda) f_e(\lambda) |_{I_{LED}} d\lambda \quad (4.1)$$

where, k_v =Visibility index

$V(\lambda)$ =Spectral luminous efficacy function for photopic vision

$f_e(\lambda)$ =Relative spectral power distribution of LED

The $V(\lambda)$ function is defined by the numerical values at 1 nm intervals given in ISO 23539 standard⁽¹⁵⁷⁾. In this case, the integration in Equation (4.1) usually takes the form of numerical summation over the visible spectrum and given as,

$$\phi_{LED|I_{LED}} = 683 \times k_v \sum_{\lambda=380}^{780} V(\lambda) f_e(\lambda) |_{I_{LED}} \quad (4.2)$$

Now, the light output of a single LED at different LED current is expressed by,

$$\phi_{LED|I_{LED}} = \psi_R \times 683 \times k_v \sum_{\lambda=380}^{780} V(\lambda) f_e(\lambda) |_{I_{LED}=700mA} \quad (4.3)$$

The relative output factor (ψ_R) of LXML PWN2 LED is modeled as:

$$u(I_{LED}) = .001 I_{LED} + 0.054 \quad (4.4)$$

The luminous flux of the designed luminaire ϕ_{LUM} is given by,

$$\phi_{LUM} = 683 \times (.001I_{LED} + 0.054)k_v \sum_{\lambda=380}^{780} V(\lambda)f_c(\lambda)|_{I_{LED}=700mA} \times LLF \times N_L \quad (4.5)$$

where, LLF = Light loss factor of diffuser

N_L = No of LED in array

Substituting I_{LED} in terms of external bias current $I_{EXT}^{(158)}$ of the sensor (briefly described in Section 4.3),

$$\phi_{LUM} = 683 \left[.001 \left\{ \left(\frac{1.255}{R_{IADJ}} - I_{EXT} \right) 249 \times 10^3 \right\} + 0.054 \right] k_v \sum_{\lambda=380}^{780} V(\lambda)f_c(\lambda)|_{I_{LED}=700mA} \times LLF \times N_L \quad (4.6)$$

In this design, external bias current (I_{EXT} in ampere) is a function of ambient daylight (E_{DL} in Lux) given by,

$$I_{EXT} = (0.779E_{DL} - 0.733) \times 10^{-6} \quad (4.7)$$

$$\text{when, } \begin{matrix} 10 \leq E_{DL} \leq 100 \\ 0 \quad \text{otherwise} \end{matrix}$$

The horizontal illuminance \bar{E} over the working plane is expressed by⁽¹³⁴⁾,

$$\bar{E} = \frac{\phi_{LUM} \times COU}{A} \quad (4.8)$$

COU = Coefficient of utilization, A = Area of the working plane

4.3 OPTICAL DIMMABLE TRANSMITTER

To achieve energy-efficient illumination followed by data transmission through intensity modulation, a daylight integrated data-transmitter is designed using IC₃₄₁₄. This LED driver IC is also capable of driving the source at rated current as per the requirement. Theoretical derivation using the lumen method⁽¹³⁴⁾ exhibits that the driving current of LED should be around 550 mA when daylight is not available. However, in case of maximum available daylight, the required driving current dips to 350 mA to achieve 300 lux average illuminance over the working plane hereby realizing an energy-efficient system.

4.3.1 INTEGRATED DATA ENABLED LED DRIVER

The circuit diagram of the proposed transmitter with dimming control and OOK modulation is shown in Figure 4.4. The heart of the designed transmitter is IC LM₃₄₁₄. It is used as a LED driver that contains a clock generator to generate constant internal switching frequency for the

device. An external resistor R_{FS} determines the switching frequency in the range of 250 kHz to 1 MHz. The internal switching frequency of the LM3414 is governed by Equation 4.9⁽¹⁵⁸⁾.

$$f_{sw} = \frac{20 \times 10^6}{R_{FS}} \quad (4.9)$$

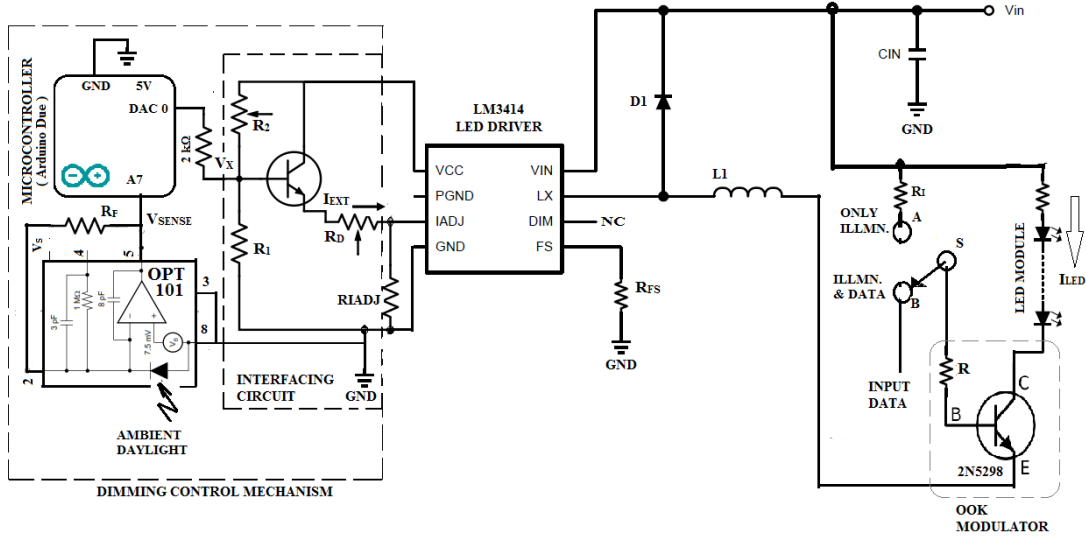


Figure 4.4: Overall circuit diagram of transmitter involving dimming control and OOK modulator

The minimum inductance of the inductor (L_1) is decided by the defined average LED current and allowable inductor current ripple. It can be expressed in terms of input voltage and internal switching frequency given by:⁽¹⁵⁸⁾

$$L_{MIN} = \frac{V_{IN} - V_{LED}}{1.2I_{LED}} \times \frac{V_{LED}}{V_{IN}} \times \frac{1}{f_{SW}} \quad (4.10)$$

Parameters used to design the transmitter section are summarized in Table 4.1.

4.3.2 DIMMING CONTROL MECHANISM

In order to save energy during the daytime dimming control mechanism is adopted using photodiode sensor OPT101, Atmel SAM3X8E microcontroller (Arduino Platform) and an interfacing circuit. The interfacing circuit shown in Figure 4.4 generates the external bias current I_{EXT} depending upon its input voltage V_X which is fed from the DAC pin of the microcontroller platform. When the current I_{EXT} is applied to the IADJ terminal of LM3414 the reduction of the output LED current takes place which is expressed by⁽¹⁵⁸⁾

$$I_{LED} = \left[\left(\frac{1.255}{R_{IADJ}} - I_{EXT} \right) \times 2490 \times 10^3 \right] \quad (4.11)$$

when, $I_{EXT} < 1.255/R_{IADJ}$

Table 4.1: Design Parameters of Transmitter

Description	Symbol	Value
Input Voltage (DC)	V_{IN}	24V
Forward Voltage drop across LED array	V_{LED}	16.2 V
Average LED Current	I_{LED}	348 mA – 555 mA
Internal Switching Frequency	f_{sw}	800 kHz
Switching frequency-selective resistor	R_{FS}	25 k Ω
LED Current control resistor	R_{LADJ}	5.67 k Ω
Dimming Control Resistor	R_D	3.7 k Ω
External Feedback Resistor of OPT101	R_F	3 M Ω
Min. Value of inductor L1	L_{MIN}	10 μ H
Light Loss Factor (for using diffuser)	LLF	0.75
Downward Light Output Ratio (Luminaire)	$DLOR$	0.8

At zero input voltage (V_X), the external bias current (I_{EXT}), fed by the interfacing circuit is given by,

$$I_{EXT} = \frac{V_{CC} - 1.955 \left(R_1/R_2 + 1 \right)}{R_E \left(R_1/R_2 + 1 \right)} \quad (4.12)$$

In our designed circuit the value of R_1 and R_2 are so chosen that I_{EXT} is almost zero when the input voltage (V_X) of the interfacing circuit is zero. In that situation, no reduction in LED current is observed. The theoretical calculation reveals that the ratio of R_1 and R_2 should be 1.557 for zero external bias current. However, in the practical circuit, the R_1 is taken as 10 k Ω and R_2 is adjusted using a 20 k Ω pot. As the input voltage (V_X) increases, external bias current gradually increases which in turn reduces the LED current. However, the current (I_{RADJ}) through the LED current control resistor (R_{LADJ}) remain almost constant. Figure 4.5 shows the practically obtained transfer characteristics of the interfacing circuit between microcontroller and LM3414 for 550 mA maximum LED current. As suggested in Figure 4.5, the operating range of the interfacing circuit is shown by the lower threshold input voltage (V_a) and upper threshold input voltage (V_b) respectively. So, for the faithful dimming operation, the output voltage of microcontroller has to be mapped in between V_a and V_b .

The ambient daylight acts as input to the photodiode sensor OPT101 and in return it gives voltage output⁽¹⁵⁹⁾. This Integrated Circuit (IC) is a monolithic photodiode with an on-chip trans-impedance amplifier and the internal feedback resistor of the amplifier is 1 M Ω ⁽¹⁵⁹⁾. However, in this work, 3 M Ω feedback resistor is used externally to get higher voltage output. Depending upon the ambient daylight, OPT101 generates a particular voltage (V_{SENSE}) which is fed to the analog input pin of the microcontroller. The microcontroller is programmed in such a way that it constantly monitors the input voltages (V_{SENSE}) and generates required output voltages (V_X) to control the current through the artificial light source (I_{LED}). This voltage is applied to the interfacing circuit through a 2 k Ω resistor. With the increment in ambient daylight, microcontroller fed more input voltage (V_X) to the interfacing circuit and the external bias current (I_{EXT}) increased simultaneously. This, in turn, reduces the LED current (I_{LED}) accordingly. The correspondence between the measured LED current (I_{LED}) and ex-

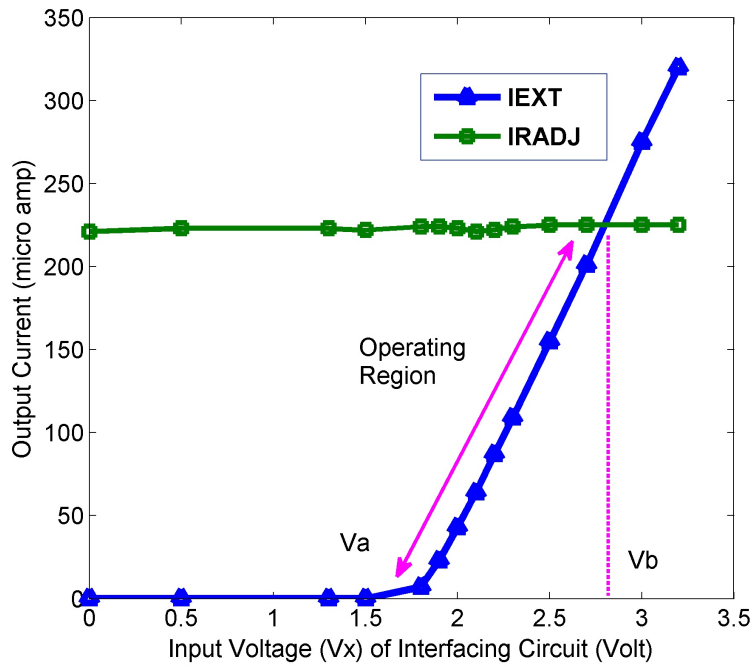


Figure 4.5: Transfer characteristics of the designed interfacing circuit for dimming

ternal bias current (I_{EXT}) is shown in Figure 4.6.

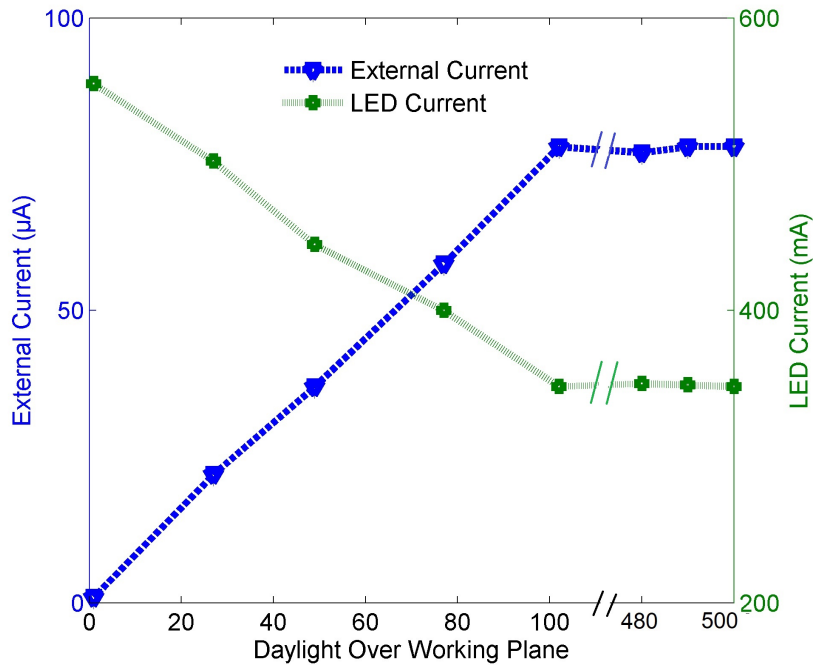


Figure 4.6: Variation of external bias current and LED current with ambient daylight

It has been mentioned earlier that the maximum available diffused daylight over the working plane is around 110 *Lux*. However, the dimming control mechanism of the VLC system is designed for a much wider range so that it can integrate a maximum 500 *Lux* ambient daylight with the artificial light source whenever required. This can be achieved with minor customization in the microcontroller program as per the requirement. In our case, LED current goes down with the increment in ambient daylight up to 100 *Lux* and then saturates. It is clearly shown in Figure 4.6. As the maximum available ambient daylight is not more than 110 *Lux*, the verification of the dimming range is tested by using a separate light source that can provide supplementary horizontal illuminance. Instead of saturation, if the LED current dips further with the improvement in ambient daylight, then received optical power will also reduce and affects in BER performance of the system. Due to this reason, there must be a higher LED current that can complement the amount of daylight integration and BER performance. When $I_{LED} = 800mA$, a maximum 500mA reduction is possible with the designed circuit depending upon the ambient daylight. Thus, the adopted dimming control mechanism provides a higher degree of flexibility over a wide range.

4.3.3 OOK MODULATOR

Binary Amplitude Shift Keying (BASK) or OOK modulation techniques is employed here to transmit digital data using the optical source, i.e. LED array. To achieve the OOK data transmission technique, the transistor 2N5298 is used which acts as a high-speed switching device. The proposed system can be utilized to illuminate the working plane in standalone mode. Alternatively, binary data could also be transmitted through intensity modulation by OOK. For this purpose, a Single Pole Double Throw (SPDT) mechanical switch has been used for appropriate selection. Terminal 'A' corresponds to the only illumination while terminal 'B' supports OOK data transmission through the optical link. The transmitted optical power for data transmission is given by,

$$P_{t,data} = \frac{1}{2} \times \frac{\phi_{LUM}}{683} \quad (4.13)$$

The received useful optical power ($P_{r,data}$) due to data transmitting LED module is given by,

$$P_{r,data} = P_{t,data}H(0) \quad (4.14)$$

Here $P_{t,data}$ is the transmitted optical power and $H(0)$ is the channel gain defined in Chapter 3. In this work, data transmission has been considered inside a small cubicle of area (1.5m × 1.5m) inside an office room. So, the only direct component of transmitted optical power has been taken into account.

4.4 OPTICAL RECEIVER

The optical receiver section is comprised of two major stages. The first stage involves a TIA, constituted by CMOS OPAMPs whose current input is provided by a photodiode. The incident LED illumination along with the daylight excites the diode to get the TIA input current.

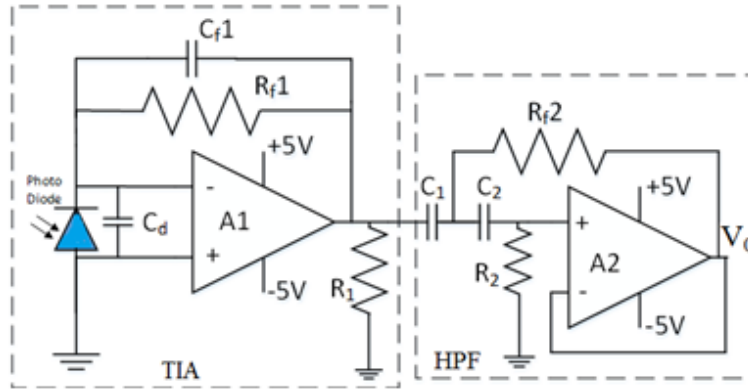


Figure 4.7: Circuit diagram of Optical Receiver

The second stage is a high-pass Butterworth filter with additional gain. The detailed circuit diagram of the receiver section is shown in Figure 4.7. The photodiode⁽¹⁶⁰⁾ acts as an optical to electrical (O/E) signal interface.

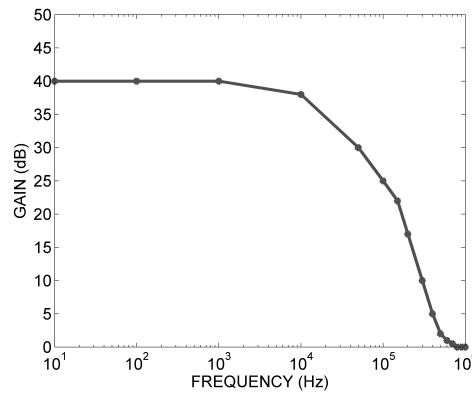


Figure 4.8: AC transfer characteristics of TIA

simultaneously transmitted using an external switching circuit at 100 kHz. Both these frequencies have some obvious effect on the receiver. However, rejection of unwanted high frequency is required for faithful reception of the data pulse. This is obtained by an appropriate bandwidth selection of TIA. AC transfer characteristic of the designed TIA filter is shown in Figure 4.8. The second stage has been designed to provide additional gain and bypass the disturbance due to the low-frequency component of ambient daylight. Design values of all the components of the receiver section are outlined in Table 4.2.

4.4.1 SHOT NOISE

Shot noise is a type of noise that occurs in any optical receiver, including VLC receivers. It is caused by the statistical fluctuations in the number of photons detected by the receiver^(161,33). As shown in Figure 4.7, light is converted into an electrical signal by a photodiode. When a photon strikes the photodiode, it generates an electron-hole pair, which can be measured

Table 4.2: Component values of designed optical receiver

Component	Value
Photodiode (PD)	VISHAY BPW ₃₄
OpAmp (A ₁)	OPA725
OpAmp (A ₂)	OPA2241
Resistor (R ₁)	1k
Resistor (R ₂)	5.5k
Resistor (R _{f1})	10k
Resistor (R _{f2})	3k
Capacitor (C ₁)	150nF
Capacitor (C ₂)	130nF
Capacitor (C _d)	10nF
Capacitor (C _{f1})	500pF

in terms of current or voltage. However, due to the random nature of photon emission and detection, the number of photons detected in a given time interval can fluctuate, leading to shot noise.

Shot noise can limit the sensitivity of the optical receiver and increase the BER. To reduce the effect of shot noise, one can increase the received optical power of the transmitted signal, by using a larger photodiode with higher responsivity, or reduce the bandwidth of the receiver⁽¹⁶²⁾. However, reducing the bandwidth will restrict the data capacity and data speed. So, reducing the bandwidth is not always a good option especially where high-speed data transmission and reception are required. However, using advanced signal processing techniques such as error correction codes and equalization can help mitigate the effects of shot noise and improve the receiver's performance.

The shot noise is dependent with received optical power (P_r) and its variance is given by^(39,163,164)

$$\sigma_{shot}^2 = 2q\gamma P_{r,data}B + 2qI_{bg}I_2B \quad (4.15)$$

Where, γ = responsivity of PD (0.54 A/W), B = Bandwidth of TIA (100 MHz), I_{bg} = background current due to daylight (30 nA), I_2 = noise bandwidth factor (0.562)

4.4.2 THERMAL NOISE

Thermal noise or Johnson-Nyquist Noise occurs in each and every material which is conducting in nature. So, it is obvious this noise will affect VLC detector as well. Thermal fluctuation of electrons is the main cause of this noise. It depends mainly on the equivalent resistance of the circuit and the temperature associated with it. The electrons always move with a steady motion, but often then collide with neighboring atoms or molecules of the material. As a result very small current flows for each and every free flight of an electron. However, the summation of all these minute current is zero considering a long time interval. The thermal noise voltage is a function of frequency and is characterized by a spectrum. However, as this noise has a zero time average, the power spectrum is specified for each frequency interval and the spectral density ($S_T(f)$) is constant for a long frequency interval. Due to this reason, the ther-

mal noise is called as a ‘white’ noise. The thermal noise follows Gaussian distribution with zero mean and variance.

The total current considering thermal noise is:

$$I_{total} = I_p + i_s(t) + i_T(t) \quad (4.16)$$

here I_p is the average current, $i_s(t)$ is the current due to shot noise and $i_T(t)$ is the current for thermal noise

Mathematically, $i_T(t)$ is modeled as a stationary Gaussian random process with a spectral density that is frequency independent up to 1 THz (nearly white noise) and is given by

$$S_T(f) = \frac{2k_B T}{R_L} \quad (4.17)$$

From the auto-correlation function of $i_T(t)$ the noise variance can be calculated by setting the scanning parameter to zero value, expressed as:

$$\sigma_T^2 = \left(\frac{4k_B T}{R_L} \right) F_n B \quad (4.18)$$

Thermal noise can also be estimated from the NEP of the photodiode, given by

$$\sigma_{thermal}^2 = NEP \sqrt{B} \quad (4.19)$$

4.5 SYSTEM PERFORMANCE

The daylight-integrated VLC system incorporated in this chapter deals with two major sub-areas namely only illumination on the working plane and transmission of data through intensity modulation of the illuminated source (LED). In order to estimate the illumination performance of the designed system, thrust has given on three aspects namely average horizontal illuminance, short-term flicker severity, and energy efficiency of the source in the presence of daylight. On the other hand, the quality of the received data in terms of waveform retrieval has been taken care of mostly by the appropriate design of the TIA and high pass filter. The SNR distribution over the working plane and BER of our proposed system have also been computed to evaluate the communication performance of the designed VLC system.

4.5.1 AVERAGE HORIZONTAL ILLUMINANCE

In order to determine the average horizontal illuminance, the entire working plane (1.5 m × 1.5 m) is first divided into arrays of 5 × 5 = 25 grid points for grid-specific lux data collection purposes. A lux-meter is placed at each grid point and the corresponding illuminance value is recorded. This recorded illuminance incorporates two components. Apart from the LED light source, diffused daylight inside the room also contributes to the measured lux value. The average illuminance \bar{E} is the arithmetic mean of the illuminance values measured at each grid point and

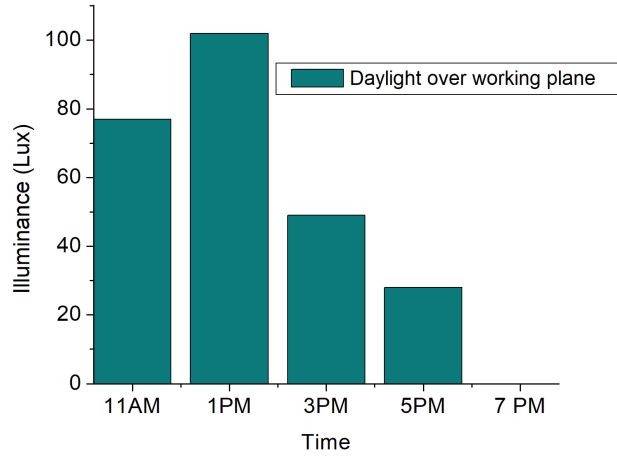


Figure 4.9: Variation of ambient daylight during different time in a day

expressed as:

$$\bar{E} = \frac{1}{25} \sum_{i=1}^{25} E_i \quad (4.20)$$

where, \bar{E} = average Illuminance and E_i = Measured illuminance at the i^{th} grid point.

The sole contribution of the diffused daylight has also been measured at different daylight conditions from 11 AM to 7 PM. During this measurement, the LED source has been kept off. Figure 4.9 shows the variation of this ambient daylight throughout the day.

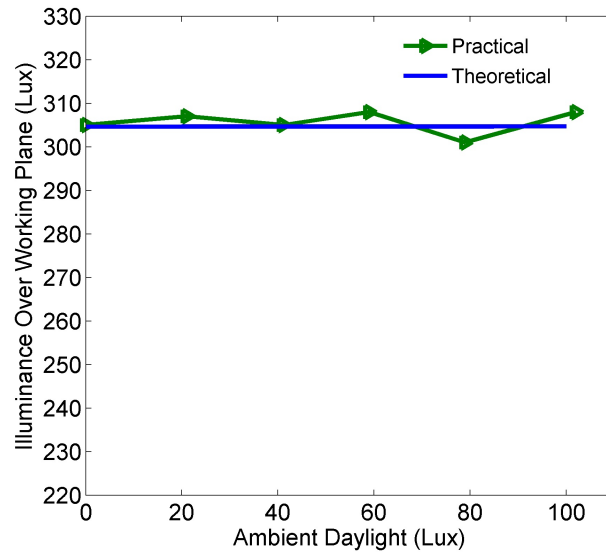


Figure 4.10: Obtained Average horizontal illuminance incorporating dimming control

Satisfactory uniform average illuminance around 300 lux has been observed by incorpo-

rating the dimming control mechanism and is shown in Figure 4.10. This result complies with ISO recommendation and exhibits close matching with theoretically obtained results derived from the mathematical model discussed in section 4.2.2.

4.5.2 SHORT TERM FLICKER SEVERITY

Short term flicker severity is another important performance metric for quality illumination design. It has been pointed out by Saadi et al. that flickering is one of the challenging issues in the VLC system and can cause grave detrimental physiological disorders in humans⁽¹⁶⁵⁾. The International Electrotechnical Commission (IEC) also mentioned the threshold of irritability due to change of luminance of the artificial light source⁽¹⁵⁵⁾. So, consideration of flicker severity at the time of data transmission has immense importance to evaluate the lighting performance of a VLC system.

In this work, the LI-210R photometric sensor is used to figure out the short-term flicker severity by measuring the light variation for a specified duration. This sensor has the same spectral sensitivity as a CIE standard observer⁽¹⁶⁶⁾. The specified sensor is connected with the Agilent 34970A data acquisition system to monitor the light intensity over a period of time T . The measured data in the form of a time-domain signal is recorded and the cumulative probability of discrete signal level l is computed. The cumulative probability $p(l)$ that a signal level l is exceeded during a period T is defined as $p(l) = T_l/T$ ⁽¹⁶⁷⁾.

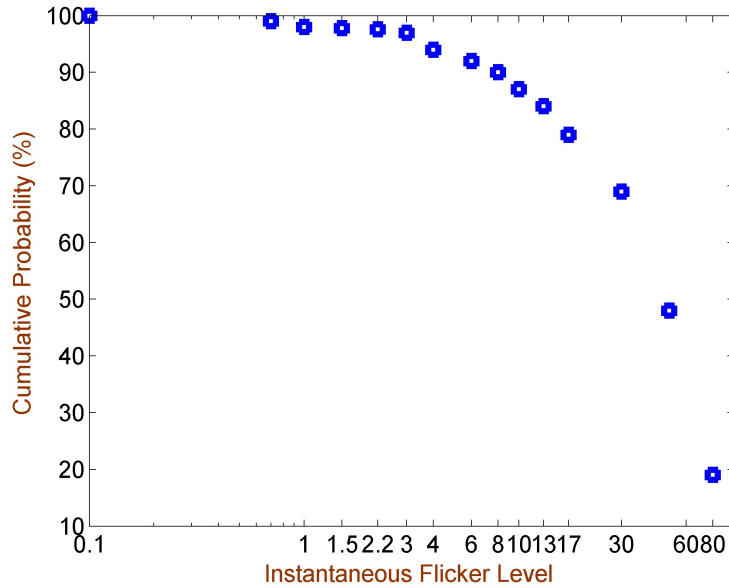


Figure 4.11: Cumulative Probability Function of the signal for 10 min observation time

Here, T_l is the total time when the signal level is no less than l . The cumulative probability function (CPF) curve is obtained from the readings of the data acquisition system over the 10 min interval as suggested by the IEC. The short term flicker severity index (P_{ST}) for OOK

modulation is calculated according to the formula, given as⁽¹⁶⁷⁾.

$$P_{ST} = 0.1\sqrt{(3.14P_{0.1} + 5.25P_1 + 6.57P_3 + 28P_{10} + 8P_{50})} \quad (4.21)$$

where, P_{x_i} = CPF curve level is exceeded for x_i % of the observation period.

$$P_1 = \frac{(P_{0.7} + P_{0.1} + P_{1.5})}{3} \quad (4.22)$$

$$P_3 = \frac{(P_{2.2} + P_3 + P_4)}{3} \quad (4.23)$$

$$P_{10} = \frac{(P_6 + P_8 + P_{10} + P_{13} + P_{17})}{5} \quad (4.24)$$

$$P_{50} = \frac{(P_{30} + P_{50} + P_{80})}{3} \quad (4.25)$$

Figure 4.11 exhibits experimentally obtained values of $P(x_i)$ at the time of data transmission in the presence of maximum ambient daylight. From the figure, it is evident that the average intensity level is more than 50% for half of the observation period. As the profile of this curve becomes flatter the flicker severity gradually increases. However, it is possible to determine the exact flicker severity index from the obtained values of P_{x_i} using Equation 4.21. The calculated short-term flicker severity is 0.67 which lies within the threshold limit as specified by IEC⁽¹⁵⁵⁾.

4.5.3 ENERGY EFFICIENCY

As explained earlier energy-saving opportunity by integrating available daylight is the key feature of our designed VLC system. In the absence of ambient daylight over the working plane, 555 mA current is fed to drive the artificial light source for achieving the required average horizontal illuminance. With the improvement in ambient daylight, a substantial decrement in LED current takes place automatically. However, horizontal illuminance and communication performance remain almost unchanged over the period. To evaluate the energy efficiency of the system, LED current is measured at different daylight conditions throughout the day.

$$\%EnergySavings = ((P_0 - P_{VAR})/P_0) * 100 \quad (4.26)$$

Where, P_0 = LED power consumption to achieve required horizontal illuminance without any daylight contribution and P_{VAR} = LED power consumption considering daylight contribution. In this work energy savings has been calculated at five different test time with two hours interval. Test time 5 (at 7 PM) signifies zero daylight availability whereas test time 2 (at 1 PM) implies maximum available daylight over the working plane. Apart from the LED current, ambient daylight and corresponding average illuminance are also noted down at five test time. Results shown in Figure 4.12 exhibit 37.29% reduction in consumed energy at test time 2 when extreme ambient daylight is available over the task area. This result also ensures the

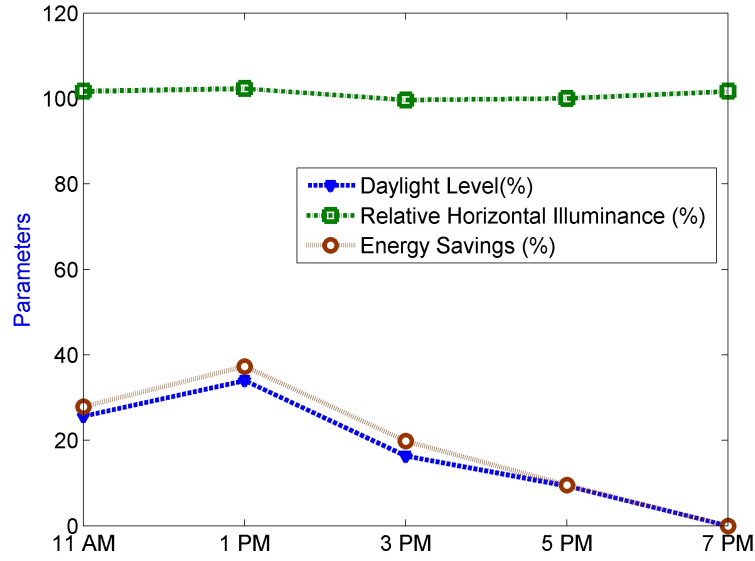


Figure 4.12: Relative Horizontal Illuminance & Energy Savings at different test time

desired constant relative average illuminance over the working plane at five different daylight conditions.

4.5.4 SIGNAL TO NOISE RATIO

The maximum daylight condition is chosen strategically to evaluate the communication performance of the proposed system. At maximum available ambient daylight condition, LED current dips at the lowest value which in turn minimizes the received optical power. This is obvious that increments in transmitted and received optical power provide a better signal-to-noise ratio and improved communication performance.

The experimentation has been done by mounting the LED luminaire at a height of 1 m above the horizontal working plane and modulating the intensity of the optical source with the help of incoming binary data stream. This on-off keying modulation is done by the OOK modulator of the transmitter section as described in section 4.3.3. The noise associated with the designed receiver section has been computed with the help of Equations 15 and 16. As the shot noise is related to the received optical power, it varies at different grid points on the working plane. On the contrary, the thermal noise remains unchanged irrespective of receiver location. The distribution of the signal-to-noise ratio (in dB) over the working plane at maximum daylight condition (at 1 PM) is shown in Figure 4.13.

4.5.5 BER PERFORMANCE

In order to judge the waveform retrieval capability of the receiving unit of our developed system, a square wave of 0.5 duty cycle is generated using a function generator and connected to the data input of our proposed optical transmitter

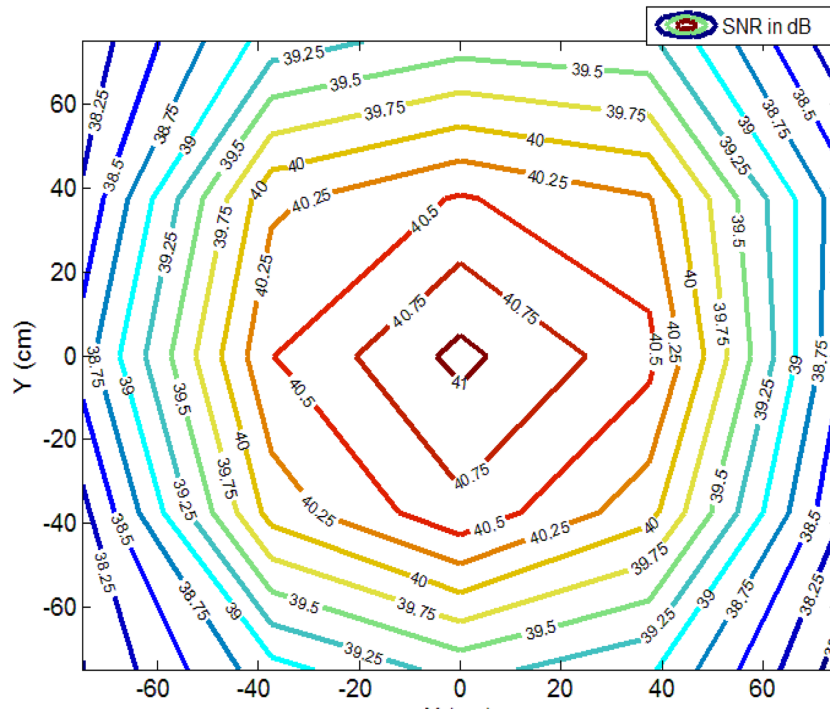


Figure 4.13: Signal to noise ratio over the task area (at 1 PM)

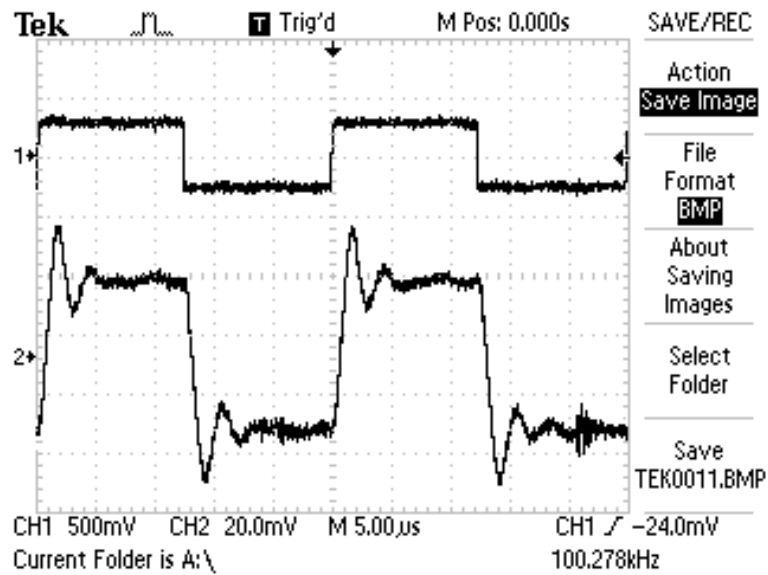


Figure 4.14: Transmitted and received waveform at 100 kHz frequency

Now the intensity-modulated data is received by the photodiode followed by TIA and high pass filter. Figure 4.14 shows the transmitted and received waveform pattern at 100 kHz frequency in the presence of maximum available ambient daylight. The result shows the proper reception of transmitted waveform in the presence of ambient daylight noise. To evaluate the BER of the designed system theoretical approach has been taken in this work.

The BER of the OOK modulated system is a function of the SNR and is given by:

$$BER = Q\sqrt{SNR} \quad (4.27)$$

Where,

$$Q(x) = \frac{1}{\sqrt{2\pi}} \int_x^{\infty} e^{-y^2/2} dy \quad (4.28)$$

The BER performance of the designed system, computed at each grid point is depicted in Figure 4.15. The result shows satisfactory BER, which lies in the range of 10^{-10} over the entire task area.

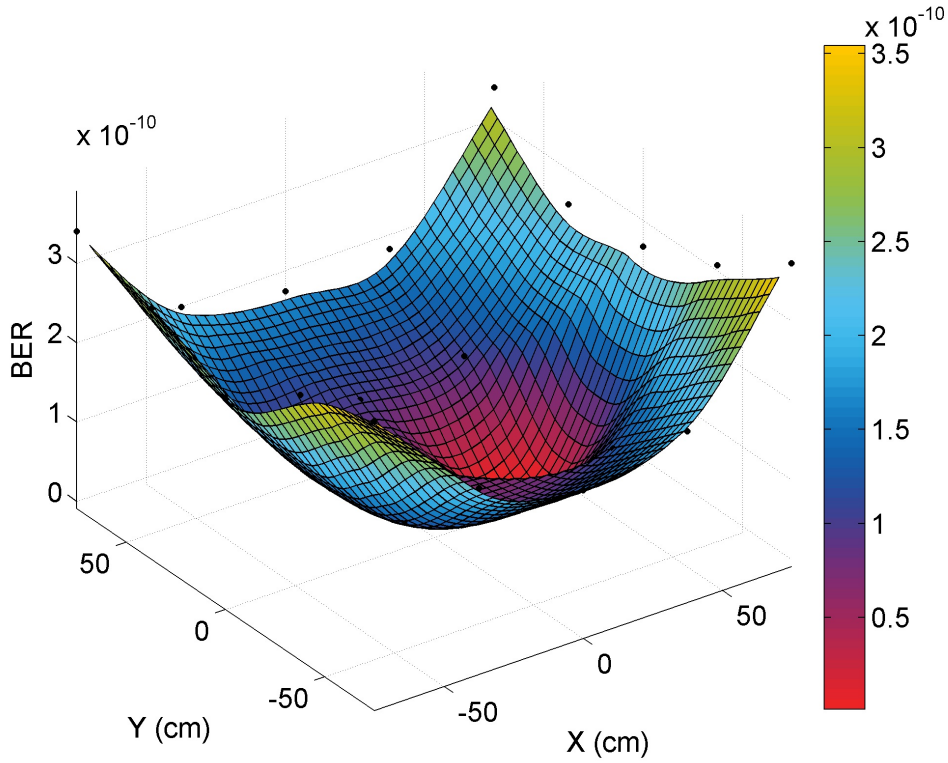


Figure 4.15: Distribution of Bit Error Rate over the task area

4.6 DISCUSSION

It has been discussed earlier that BER is a function of the SNR and as the ambient daylight increases the contribution of artificial light sources reduces accordingly to maintain almost constant horizontal illuminance. This has a direct effect on received useful optical power over the task area. The received useful optical power and SNR decrease with increasing daylight. Conversely, power saving is maximum when ambient daylight is utmost. So, in order to save the

input power, scarification of average BER is evident which is depicted in Figure 4.16. However, this increment in BER is trivial and the average BER in the order of 10^{-10} is obtained at different test time throughout the day

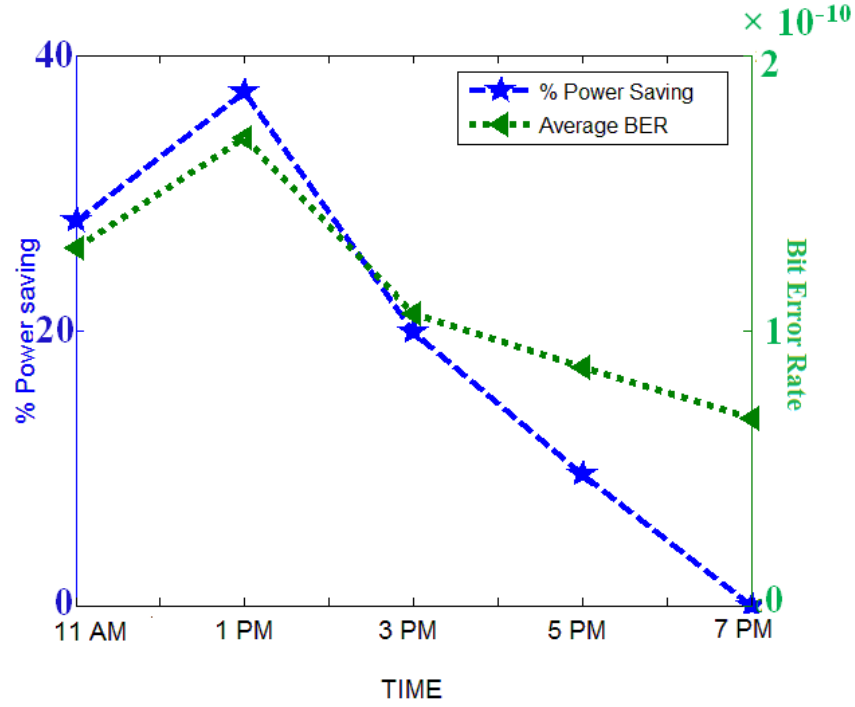


Figure 4.16: Percentage power-saving and BER performance at different test time

As illustrated in sections 4.5.1 and 4.5.2, the average horizontal illuminance and the short-term flicker severity index of the proposed system meet international standards. So, the proposed system exhibits satisfactory performance both from lighting and communication points of view and simultaneously saves a considerable amount of energy by integrating available ambient daylight. The wide-range dimming mechanism adopted in this work has the provision to integrate ambient daylight up to 500 Lux depending upon the daylight availability and system requirement.

4.7 SUMMARY

To implement the daylight-integrated VLC system, a low-cost data-enabled LED driver circuit has been initially designed using IC LM3414. Depending upon the ambient daylight the transmitter can also control the LED current through an integrated dimming control mechanism. As the available daylight increases LED current goes down accordingly, however con-

stant horizontal illuminance is retained over the task area. It is based on the fact that the transmitter is also flexible to use as a standalone light source whenever data transmission is not required. The communication performance of our proposed system has also been evaluated experimentally in the presence of daylight. This work addresses a hardware design-oriented approach to establish exhaustive lighting performances of **VLC** system in terms of horizontal illuminance and short-term flicker as per standard. The energy savings have been calculated at different daylight conditions. The result shows a satisfactory BER in the order of 10^{-10} in the presence of ambient daylight which in turn saves a maximum of 37.29% energy. Also, the obtained average horizontal illuminance and perceived flicker meet international standards.

The major contribution of this chapter is summarized as follows,

- Simple prototype of a daylight-integrated indoor **VLC** system is proposed to save a considerable amount of energy and subsequently validate its illumination and communication performances as per the international guidelines.
- Short-term flicker severity index is experimentally evaluated and the result is compared with the threshold level as specified by the International Electrotechnical Commission (IEC-61000-3-3).

4.8 RESEARCH OUTPUT

The findings from this chapter are reported in the following research publication:

- **Chatterjee, S., & Sabui, D. (2020).** Daylight integrated indoor VLC architecture: an energy-efficient solution. *Transactions on Emerging Telecommunications Technologies*, 31(9), e3800.
DOI: doi.org/10.1002/ett.3800

“No communication technology has ever disappeared, but instead becomes increasingly less important as the technological horizon widens.”

Arthur C Clarke

5

Optimal Transmitter Configuration & Receiver FOV

THIS CHAPTER thoroughly addressed the effect of installing luminaires with diverse transmitter configurations and finally proposed the best-compromised solution to obtain the optimal channel allocation scheme under illumination constraints. One of the most important findings that emerge from this chapter is the proposed methodology to improve **SINR** performance by accomplishing lighting recommendations. The influence of HPBW on **CCI** in a multi-cell **VLC** network is initially discussed in Section 5.1. Section 5.2 deals with the system model where a mathematical framework of luminous intensity distribution and average spatial **SINR** have been established for a given luminaire deployment and receiver FOV. The proposed methodology to determine optimal transmitter configuration and receiver FOV are introduced in Section 5.3. This section also outlined the impacts of altering HPBW over communication and lighting performance metrics. The MCDM optimization algorithm and the obtained results with discussion are presented respectively in Section 5.4 & 5.5. Eventually, in Section 5.6 the relevance of the study is summarised.

5.1 INTRODUCTION

A multi-cell **VLC** network is a system that comprises multiple **VLC** base stations or access points, each serving a specific coverage area or cell. These base stations use visible light as a medium to transmit data to **VLC**-enabled devices. The network enables simultaneous communication between multiple cells, employing techniques such as interference management, handover support, network management, and scalability to optimize performance and coverage. It provides extended coverage, capacity, and connectivity options compared to a single-cell **VLC** system. The intensity distribution of each optical source is an important parameter that can control the interference from the surrounding sources and the overall uniformity of

lighting design. The intensity distribution of a light beam is typically described by its beam profile, which can have various shapes such as Gaussian, flat-top, Lambertian, super-Gaussian etc. Throughout this study, a Lambertian beam radiator with a specific angular spread is considered. In Lambertian radiator, the intensity distribution follows Lambert's cosine law, which means the intensity gradually decreases as the viewing angle deviates from the surface normal.

5.1.1 HPBW AND CCI

The concept of half-power beam width is typically associated with the radiation pattern of an antenna or an optical source such as a WLED. In general, luminaires provide a means to control the direction, intensity, and distribution of light. They help to shape the light emitted from the light source and direct it to specific areas or objects, allowing for effective illumination and highlighting of desired spaces or elements. To quantify the directionality of a light source, the HPBW is used. Thus, it is an important parameter to compute the channel gain of the VLC system.

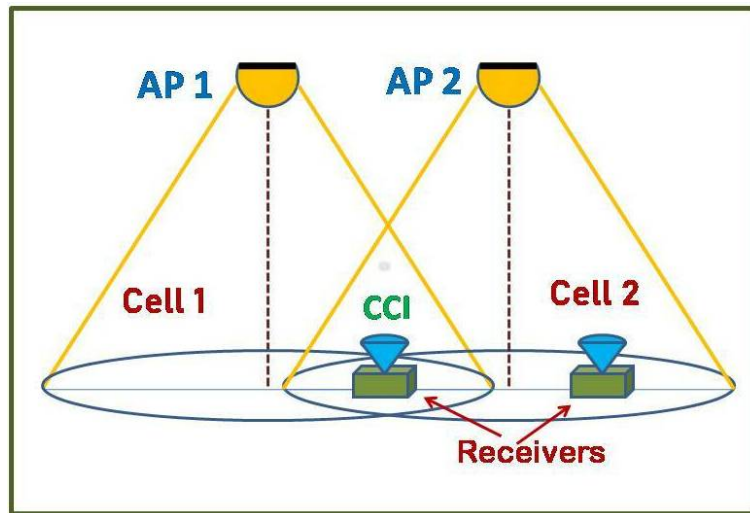


Figure 5.1: Schematic representation of CCI

In the case of a light source, the half-power beam width refers to the angular extent of the beam where the power density is at least half of the maximum power density at the center of the beam. For example, if the maximum power density of an LED beam is located at its center, the half-power beam width would be the angle at which the power density drops to half its maximum value. Thus CCI is strongly dependent on HPBW of all the APs. The schematic description of CCI is given in Figure 5.1. The reduction in HPBW of APs always decreases the interference signal power from the adjacent APs.

5.1.2 RESEARCH GAP

For any wireless communication system, channel allocation schemes are based on the insight of the physically separated transmitters to reduce co-channel interferences⁽¹⁶⁸⁾. However, in

the case of a multi-cell VLC system, the transmitter's configuration ($Tx_{\alpha_H}^{A_i}$) and optimal selection of the receiver's FOV are the two important aspects for efficient utilization of downlink optical channels. In general, $Tx_{\alpha_H}^{A_i}$ of a VLC system is described by the combination of spatial luminaire deployment arrangement (A_i) and HPBW (α_H) of the deployed luminaire. The useful optical signal power (P_{sig}) over the CF largely depends on this HPBW which determines the radiating flux distribution over the coverage area as well⁽¹⁶⁹⁾. The HPBW can also be considered as twice the semi-angle of the Li-Fi AP or data transmitter. So, the VLC channel gain is highly dependent on HPBW or semi-angle ($\gamma_{1/2}$) at half power. Usually, the downlink multi-cell VLC channel suffers from two major interferences (CCI and ISI) which limit the SINR and overall throughput of the system. ISI is caused by multipath reflection & CCI occurs when multiple adjacent transmitters run with the same optical frequency^(170,104). In this chapter, the joint effect of these two interferences over the CF is regarded as total interference (P_{intf}). With the reduction in separation distance of neighboring AP (d_s) and increment in α_H , the correlation between surrounding co-channels progressively increases which in turn augments the total interference in terms of CCI and ISI. On the contrary, U_O increases with reduced d_s and higher HPBW. Due to this lighting limitation, most contemporary studies on MIMO/MISO VLC systems maintain the transmitter's semi-angle at a higher range of 60° to 80° ^(13,171,172,173,174,175). Nevertheless, choosing a non-optimal semi-angle result in subpar channel allocation and low SINR.

So far, several researches have been carried out to improve SINR performance by modifying receiver architecture. On the other hand, maximum utilization of the allocated channel through proper channel estimation is an important aspect for improved system performance. Recently, a novel channel estimation approach is reported based on Bayesian CS algorithm⁽¹⁷⁶⁾. Highly uncorrelated VLC-MIMO (multiple-input multiple-output) channel matrices have been achieved by using different angular diversity receiving techniques where several photodiodes (PDs) are used as front-end of the receiver^(177,88,90). At the expense of receiver complexity and cost, this technique can eradicate CCI from the neighboring AP and reduce ISI caused by multipath reflection. Additionally, efforts have been made to minimize ISI in the downlink VLC channel using the OFDM technique⁽¹⁷⁵⁾. Another study⁽¹⁷⁸⁾ achieved high spectral efficiency by combining asymmetrically clipped optical OFDM with OOK modulation schemes. Despite these advancements in improving communication performance, research has largely focused on the receiver unit or modulation properties, leaving the transmitter section relatively unexplored.

Moreover, modification in transmitter geometry and configuration strategy has no conflict with receiving architecture and modulation schemes. Both can be accomplished together to allocate optimal channels without sacrificing the recommended lighting criteria. This creates an opportunity for a detailed study of optimal channel allocation by selecting proper transmitter and receiver parameters to facilitate joint communication and illumination performance.

Despite the best possible literature survey, hardly any composite study has been noticed regarding the optimal channel allocation from the lighting and communication aspects together. Very recently Saxena et. al reported a novel optimization approach of transmitter semi-angle considering received optical power and degree of non-uniformity as objective pa-

rameters inside a square room where only the contribution due to the direct component of the optical source is considered and zero wall reflectance has been taken⁽¹⁷⁹⁾. However, in a practical scenario, the reflected share of the received optical flux can't be neglected and this issue needs to be carefully addressed. As the optimization is performed only on the transmitter side this approach can be treated as a sub-optimal solution to improve the performance of a multi-cell indoor VLC system. In⁽¹⁸⁰⁾, an optimally designed semi-angle with the appropriate LED arrangement was investigated to improve various communication performances. The significance of LED lamp arrangement to reduce SNR fluctuation has also been reported in another work⁽¹³¹⁾. Despite some contributions from the communication point of view the lighting design parameters and interference mitigation factors are not scrupulously considered in aforesaid studies. Moreover, a marginal improvement in **SINR** performance can be observed considering low-cost single-PD receiver architecture.

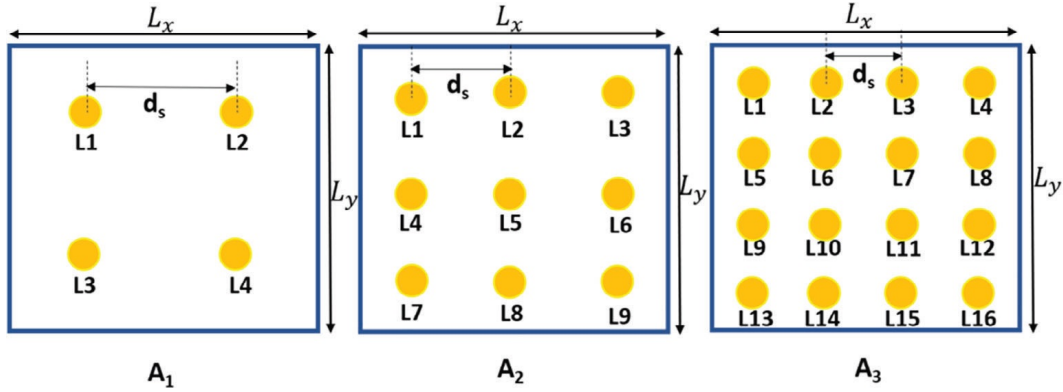


Figure 5.2: Plan view of luminaire deployment arrangements

5.2 SYSTEM MODEL

5.2.1 ROOM GEOMETRY AND LUMINAIRE CONFIGURATION

A square-shaped test room is considered for the purpose with dimension $5\text{ m} \times 5\text{ m}$. The height of the test room is taken as 3 m . As per the ISO, an indoor environment, for example, any typical office room, requires a minimum of 300 Lux average illuminance (E_{avg}) and 0.7 overall uniformity (U_0) on the working plane to carry out visual activities⁽¹³³⁾. Considering these lighting requirements, ceiling-mounted WLED down-lighter with three different luminaire arrangements (A_1, A_2, A_3) are considered for the experimentation. The plan views of the test room with these three luminaire arrangements are shown in Figure 5.2. The entire working plane is subdivided into N_t numbers of equal cells and luminaires are placed at 2.15 m above the center of each cell. The height of the working plane/communication floor is 0.8 m above the floor^(181,182). As the number of luminaires increases from A_1 to A_3 , SHR decreases accordingly. The lumen delivered by each of the three types of luminaires (ϕ_L) gradually decreases proportionately to keep the total installed lumen output of the three arrangements constant. The objective is to investigate the optimal transmitter configuration to achieve the best pos-

Table 5.1: Parameters used for different luminaire deployment arrangements

Parameters	A_1	A_2	A_3
Total No of luminaires	4	9	16
Separation distance	2.15	1.66m	1.25m
Space to Height Ratio	1.16	0.7753	0.5814
Lumen package of each luminaire	2880 Lumen	1280 Lumen	720 Lumen
Wattage of each luminaire	26.55 Watt	11.8 Watt	6.64 Watt
Range of HPBW	20-120	20-120	20-120
Optical Power of luminaire	4.22 Watt	1.88 Watt	1.055 Watt
Total optical power	16.9 Watt	16.9 Watt	16.9 Watt

sible communication and lighting performance together. The parameters used for different luminaire arrangements inside the indoor environment are listed in Table 5.1.

5.2.2 LUMINOUS INTENSITY DISTRIBUTION

Average horizontal illuminance and overall uniformity of light distribution over the horizontal working plane/CF for different luminaire configurations are computed using the lighting design software DiaLux. To perform each simulation, the luminous intensity distribution of optical source has to be provided in a standardized IES (Illuminating Engineering Society) photometric format known as IES file (.ies file). This Section illustrates the mathematical framework to compute the intensity distribution of luminaires with different HPBWs and wattages. In photometry, luminous intensity of an optical source can be described by measuring radiated directional light propagation and is defined as:

$$I = \frac{d\phi}{d\Omega} \quad (5.1)$$

Where, $d\phi$ is the luminous flux propagated within the solid angle $d\Omega$ from the source towards a particular direction. The radiated light from an indoor WLED downlighter with a diffuse emitter can be modeled using a generalized Lambertian emitter where the spatial intensity distribution of the optical sources is axially symmetric and hence depends only on the vertical angle of emission. The intensity along a direction is directly proportional with the cosine of the vertical emission angle γ , concerning the direction of maximum intensity (I_N) and is given as:

$$I(\gamma) = I_N \cos^m \gamma \quad (5.2)$$

Here, ‘m’, the Lambertian order or mode number, decides the HPBW or the semi angle of a luminaire/transmitter of the optical source. For the most commonly used Lambertian emitter, the value of ‘m’ is 1 and the corresponding HPBW or the semi-angle are 120 degree and 60 degree respectively. The photometric file for a light source of specific semi-angle $\gamma_{1/2}$ is generated with the luminous intensity model, represented by eq. 5.2 in accordance with IESNA:LM-63-2002⁽¹⁸³⁾. In this experiment, IES files are generated for luminaires with a range of HPBW: 20 to 120 degrees. For a given value of HPBW or semi-angle, the value of ‘m’

can be obtained as:

$$m = \frac{-\log 0.5}{\log \cos\left(\frac{\alpha_H}{2}\right)} = \frac{-\log 0.5}{\log \cos\left(\gamma_{1/2}\right)} \quad (5.3)$$

The value of maximum intensity I_N can be obtained from the mathematical equation 5.4, formulated on the physical basis that the entire emitted flux (φ_L) from an indoor WLED downlight is confined within 2π solid angle.

$$\varphi_L = \int_0^{\pi/2} 2\pi I(\gamma) \sin \gamma d\gamma \quad (5.4)$$

Further equation 5.4 can be modified by replacing $I(\gamma)$ from equation 5.2 to obtain the maximum luminous intensity I_N of a light source as given by:

$$I_N = \frac{\varphi_L}{2\pi} \frac{1}{\int_0^{\pi/2} \cos^m(\gamma) \sin \gamma d\gamma} \quad (5.5)$$

5.2.3 AVERAGE SPATIAL SINR

The estimation of the received signal power and its distribution over the CF is illustrated by a channel model depicted in Figure 5.3. An NLOS channel model has been considered where both the direct and the reflected components of the transmitted power have been taken into account to estimate the strength of the desired signal and interferences. For a given i^{th} source and receiver placed at point P_j , DC channel gain depends on transmitter and receiver parameters and is given by^(184,39),

$$H_{LOS}^{ij} = f_{ij}(S_i, R_j) = \frac{m+1}{2\pi} \cos^m(\phi_{ij}) d\Omega T_s(\theta_{ij}) \text{rect}\left(\frac{\theta_{ij}}{\psi_c}\right) \quad (5.6)$$

Here the source is defined by its position (v_{Si}), orientation (\hat{n}_{Si}) and the Lambertian order or mode number (m). It is given as:

$$S_i = \{v_{Si}, \hat{n}_{Si}, m\} \quad (5.7)$$

where,

$$v_{Si} = \text{Position vector of source} = [X_{Si}, Y_{Si}, Z_{Si}] \quad (5.8)$$

Similarly, the receiver R_j at position P_j is represented using four parameters and expressed by:

$$R_j = \{v_{Rj}, \hat{n}_{Rj}, A_R, \psi_c\} \quad (5.9)$$

The subtended solid angle of receiver differential area is written as:

$$d\Omega = \frac{\cos(\theta_{ij})g_c(\theta_{ij})A_R}{d^2} \quad (5.13)$$

$g_c(\theta_{ij})$ is the gain of the optical concentrator that depends on lens index (n_c) as:

$$\begin{aligned} g_c(\theta_{ij}) &= \frac{n_c^2}{\sin^2 \psi_c} \text{ for } \theta_{ij} \leq \psi_c \\ &= 0 \quad \text{for } \theta_{ij} > \psi_c \end{aligned} \quad (5.14)$$

The function $\left[\text{rect} \left(\frac{\theta_{ij}}{\psi_c} \right) \right]$ is defined as:

$$\begin{aligned} \text{rect} \left(\frac{\theta_{ij}}{\psi_c} \right) &= 1 \quad \text{for } \theta_{ij} \leq \psi_c \\ &= 0 \quad \text{for } \theta_{ij} \geq \psi_c \end{aligned} \quad (5.15)$$

The received optical power due to LoS channel is expressed as:

$$P_{LOS}^{ij} = H_{LOS}^{ij} \times P_{ti} \quad (5.16)$$

Where, P_{ti} is the transmitted optical power from source.

To determine the NLOS channel gain H_{NLOS}^{ij} the reflected components from four side walls of the room are considered in this work. Each wall is subdivided into 240 numbers of similar grids and the center of each grid is considered as an auxiliary point source. The emissivity of each source is calculated by the product of received power at that point and the reflectance (δ) of the wall. Due to multipath reflection, the NLOS channel is responsible for intersymbol interference. The received optical power at j^{th} point (due to the i^{th} source) that leads to ISI is given by:

$$P_{NLOS}^{ij} = \sum_{ref} H_{NLOS}^{ij} \times P_{ti} = P_{ISI}^{ij} \quad (5.17)$$

As SSS scheme suggests, it has been considered that i^{th} AP provides the highest received signal power at j^{th} point over CF. Thus the desired signal strength and interference (in optical domain) are formulated as:

$$P_{sig}^{ij} = P_{LOS}^{ij} \quad (5.18)$$

and

$$P_{intf}^{ij} = P_{ISI}^{ij} + P_{CCI}^{ij} \quad (5.19)$$

here,

$$P_{CCI}^{ij} = \sum_{k \neq i} H_{Li-Fi}^{kj} \times P_{tk} \quad (5.20)$$

Table 5.2: Simulation parameters for VLC receiver

Parameter	Description	Value
A_R	Physical Area of PD	1 cm ²
R_{PD}	Responsivity of PD	0.53 A/W
$T_S(\theta_{ij})$	Transmission coefficient of the optical filter	1
n_c	Lens Index	1.47
n_g	Total test points over CF	400
δ	Reflectance of wall	0.7
η_{Li-Fi}	Noise Power Spectral Density	$10^{-21} \text{ A}^2/\text{Hz}$
B_{Li-Fi}	Modulation bandwidth of LED	40 MHz

and

$$H_{Li-Fi}^{kj} = H_{LOS}^{kj} + H_{NLOS}^{kj} \quad (5.21)$$

Now, the average useful signal power and interference over the CF are computed by:

$$\bar{P}_{sig} = \frac{1}{N_g} \sum_i \sum_j P_{sig}^{ij} \quad (5.22)$$

$$\bar{P}_{intf} = \frac{1}{N_g} \sum_i \sum_j P_{intf}^{ij} \quad (5.23)$$

Where N_g is the total number of test points over the CF. The **SINR** of the useful signal received at j^{th} test point is written as:

$$SINR_{Li-Fi}^{ij} = 10 \log \left[\frac{(R_{pd} P_{sig}^{ij})^2}{\eta_{Li-Fi} B_{Li-Fi} + (R_{pd} P_{intf}^{ij})^2} \right] \quad (5.24)$$

The average **SINR** over the CF is determined as:

$$\overline{SINR}_{Li-Fi} = \frac{1}{N_g} \sum_j SINR_{Li-Fi}^{ij} \quad (5.25)$$

The simulation parameters are listed in Table 5.2.

5.3 PROPOSED METHODOLOGY

In an indoor environment, luminaires are generally used to achieve the desired average horizontal illuminance with good uniformity over a horizontal working plane. The light loss due to the reflection at walls can be restricted by installing a luminaire with shallow beam-width. Improved average horizontal illuminance can be achieved with this type of luminaire but at the cost of uniformity of light distribution. On the contrary, the overall uniformity can be improved by selecting luminaires of wide HPBW/semi-angle. Therefore, the selection of HPBW

plays a critical role in indoor lighting design⁽¹⁸⁵⁾. Before physical installation, it is a common practice for lighting engineers to choose suitable HPBW and spatial luminaire arrangement by simulating the lighting environments using lighting design software. In addition to lighting requirements, when these luminaires are also used as communication links, the received optical power over the CF profoundly depends on semi-angle of the transmitter, its deployment strategy and FOV of the receiver. The optimal selections of transmitter configuration and receiver's FOV are always beneficial to improve the system performance.

In this work, to transmit the data among users, signal strength strategy has been adopted. This mechanism simply picks out the AP that delivers the maximum received optical power⁽¹⁸⁶⁾. Only the LOS path from the selected AP has been taken to estimate the desired received signal strength. The ISI is composed of the signal received from selected AP through NLOS paths while the signal received from the rest of the APs acts as CCI. The deployment arrangement (A_i) and HPBW (α_H) of luminaire used only for the lighting purpose may not always be fruitful from the communication perspective while designing a multi-cell indoor VLC system. In that case, the channel allocation can be carried out by selecting HPBW in such a way that it can provide maximum desired optical power with reduced interference signal accomplishing recommended minimum lighting requirements. However, the selection is not very straightforward considering all the above-mentioned communication and lighting parameters simultaneously which engenders a constrained MCDM problem. An exhaustive study has been done to demonstrate the dependency of two lighting parameters (E_{avg} , U_0) and two communication parameters over HPBW of luminaires. The workflow diagram shown in Figure 5.4 describes the proposed methodology to determine the required parameters of the transmitter and receiver to obtain optimal channel allocation.

Depending upon the luminaire deployment and the transmitted power of individual luminaire (P_{ti}), three luminaire arrangements (A_1 , A_2 , A_3) are taken up for the experimentation process. However, the total transmitted optical power remains unchanged in all cases. These luminaire arrangements are concisely illustrated in Section 5.2.1. Initially, any one arrangement is selected and the arrangement-centric optimized FOV angle (ψ_{opt}) of the receiver is computed so that the spatial coverage probability P_{cov}^{CF} over the CF is greater than a threshold limit. This optimal value of the FOV angle can effectively control a substantial amount of CCI and ISI. In order to compute SINR coverage probability downlink channel gain and the corresponding value of average signal and interference power have to be determined considering unity Lambertian order. This FOV optimization process is briefly explained in Section 5.4. Now, for each A_i , HPBW is varied from 20 to 120 degrees with 5-degree intervals. For a specific beam-width and FOV, the VLC channel model is given in Section 5.2. Utilizing the obtained channel gain for each HPBW, average useful signal power (\bar{P}_{sig}) and average interference (\bar{P}_{intf}) over the CF are computed using MATLAB simulation while the lighting parameters (E_{avg} , U_0) are determined using the DiaLux lighting simulation tool. The required IES (Illuminating Engineering Society) file for a particular transmitter configuration is generated using the luminous intensity distribution model illustrated in Section 5.2.2. The same process is repeated until a set of four parameters are obtained for each HPBW at a 5° interval. When complete results of all three luminaire arrangements are available, the set of Pareto optimal solutions are determined keeping in view of the minimum lighting requirement as specified

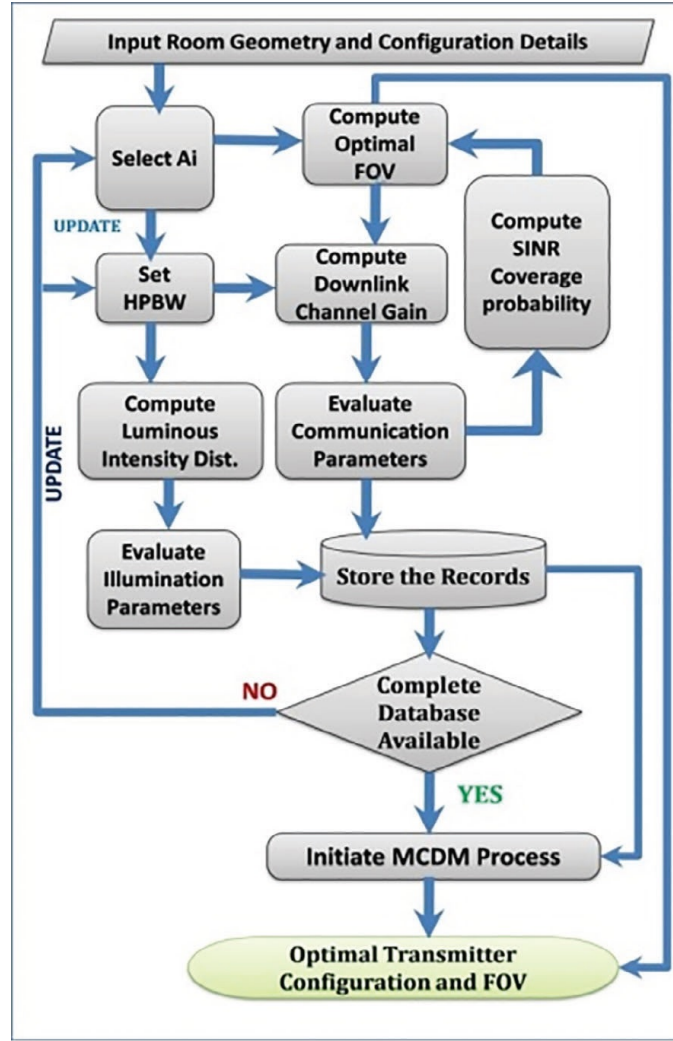


Figure 5.4: Proposed methodology to determine optimal transmitter configuration and receiver's FOV

by ISO⁽¹³³⁾. This set (S_{Tx}) of Pareto optimal solutions formulate the database for an MCDM problem and optimization is done subsequently using the TOPSIS algorithm which is illustrated in Section 5.4. This TOPSIS algorithm select best-compromised solution of transmitter configuration in terms of deployed luminaire arrangement and HPBW. Depending upon the specific luminaire arrangement, optimal FOV of the receiver is obtained from the earlier stage. Eventually, the required design parameters are obtained that ensure improved **SINR** and comply with lighting requirements.

5.3.1 SELECTION OF OPTIMAL FOV

To improve the average **SINR** of the system with any transmitter configuration, total interference (P_{intf}^{ij}) has to be decreased. LOS signals coming from undesired AP are the major source of interference signal power. It has been observed that the LOS signal comes from more than one transmitter when the receiver FOV is not optimized. It has been assumed that PD is always

placed at a test point in a vertically upward direction to receive the transmitted data. With the reduction in the FOV angle of the PD, the total interference can be slashed in most of the test points over the CF⁽¹⁸⁷⁾. However, the reduction of FOV in an uncontrolled way may lead to zero signal strength at several test points. This manifests an optimization problem to improve **SINR** over the CF with extensive spatial coverage. The objective is to find the minimum FOV angle (Ψ_{opt}) for each luminaire arrangement \mathcal{A}_i that ensures at least one LOS connection with a target **SINR** and spatial coverage probability over the CF. In wireless communication, the coverage probability is described as the probability P_{cov}^{CF} with which the **SINR** of a distinctive user achieves a target threshold $SINR_{th}$. In this work, the threshold value of **SINR** is set at zero dB and the FOV angle is optimized to achieve the coverage probability of greater than 0.95 over the CF. The objective function of this constrained optimization problem is formulated as:

$$\begin{aligned} \psi_{opt} &= \min_j \min_i \theta_{ij}(S_i, R_j) \\ \text{Subject to:} \\ 0 &\leq X_{Rj} \leq L_x \forall j, \\ 0 &\leq Y_{Rj} \leq L_y \forall j, \\ Z_{Rj} &= h_{CF}, m = 1, \theta_{ij} \in \psi_c \forall i, j \\ i &\in \{1, 2, \dots, N_t\}, j \in \{1, 2, \dots, N_g\} \end{aligned} \quad (5.26)$$

This optimization process is carried out in this study for all three luminaire arrangements separately where the spatial coverage probability over the CF is determined as:

$$(P_{cov}^{CF}) = \frac{N_{threshold}}{N_g} \quad (5.27)$$

$N_{threshold}$ is the number of test points where **SINR** is greater than zero dB while n_g represents the total number of test points considered over CF. Irrespective of the transmitter's HPBW, P_{cov}^{CF} increases with a higher FOV angle. Figure 5.5 depicts the optimized FOV angle (ψ_{opt}) for three luminaire deployment schemes ($\mathcal{A}_1, \mathcal{A}_2, \mathcal{A}_3$). With the increment in the total number of luminaire N_t , the value of (ψ_{opt}) gradually decreases. So the optimal value of FOV is maximum for 2×2 arrangement and minimum for 4×4 arrangement.

5.3.2 EFFECT OF ALTERING HPBW

With the alteration in HPBW of optical links, the communication and illumination performances of the system are changed considerably. This section illustrates the impact of varying HPBW for a specific luminaire arrangement with the respective optimal FOV angle (ψ_{opt}). The experimentation is done analytically by varying HPBW from 20° to 120° considering the mathematical abstraction described in Section 5.2. For an explicit configuration and FOV, system responses are evaluated in terms of four performance-indicating parameters at different HPBW with 5° interval.

Figure 5.6 shows the effect of altering the transmitter's HPBW on communication per-

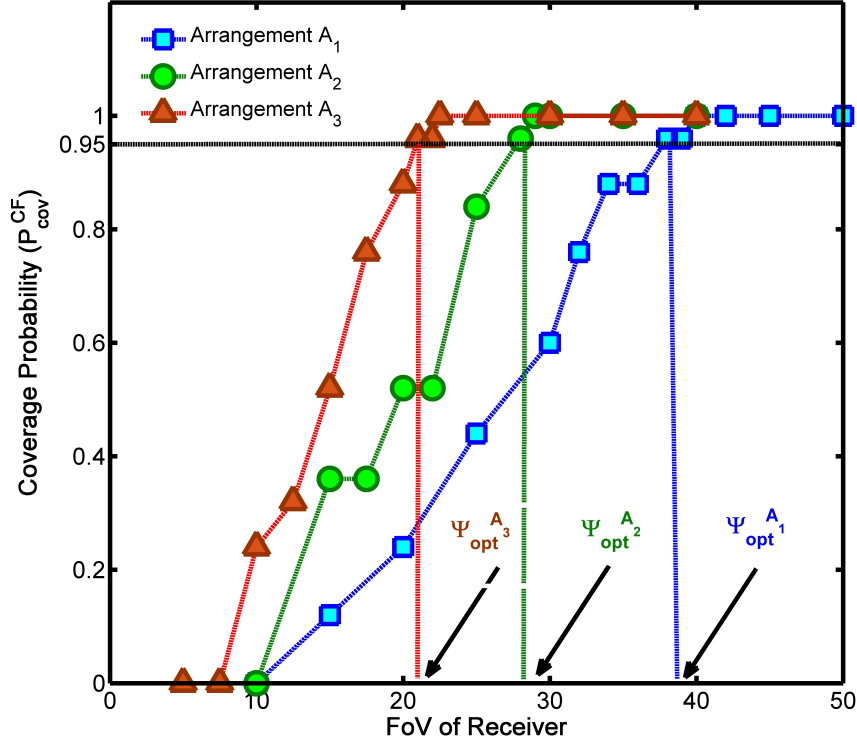


Figure 5.5: Relational dependency between spatial coverage probability and receiver's FOV

formance. As mentioned earlier, this performance is shaped by two parameters: a) Average useful signal power on CF (\bar{P}_{sig}) (b) Mean signal interference (\bar{P}_{intf}). The variations of (\bar{P}_{sig}) and \bar{P}_{intf} with HPBW are explored for all three luminaire arrangements. For 2×2 luminaire arrangement (A_1) the FOV is set at 39° while the optimal FOV for other two deployment schemes (A_2, A_3) are 28° and 22.5° respectively. Results suggest that as the directivity is get reduced with the increment in HPBW, the modulated light flux becomes more diffused. This, in turn, reduces the \bar{P}_{sig} value over the CF. On the other hand, the mean signal interference (\bar{P}_{intf}) gradually increases and attains a peak value before it rolls down. However, the slope of rolling down is very small compared to the rising slope. The rolling slope is highly dependent on the reflectance of the wall. Results suggest that the correlations between the communication parameters and HPBW are true irrespective of luminaire deployment (A_i) and receiver's FOV. In contrast to communication metrics, lighting parameters are not at all dependent on FOV and the effect of varying HPBW is depicted in Figure 5.7. The average horizontal illuminance drastically curtailed at higher HPBW while U_O gets better with the enhancement in α_H . In a common lighting scenario, down-lighters with higher HPBW (120° and above) are used in indoor space to improve the overall uniformity. However, this selection is not suitable for a multi-cell VLC system as CCI may predominantly be increased, resulting in poor SINR performance.

The inherent conflicting nature of this VLC system-performance metric is a serious obli-

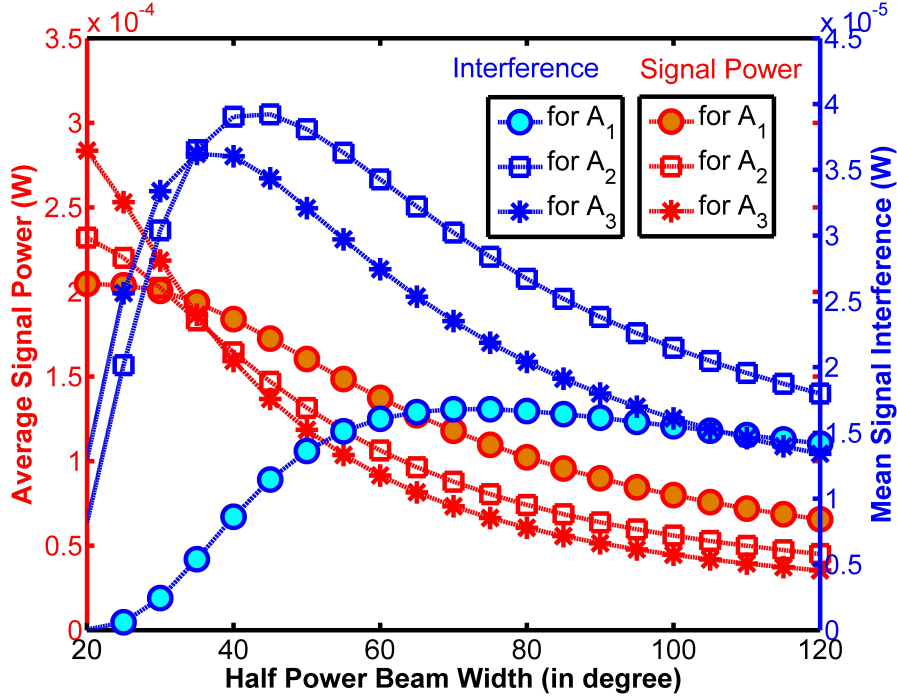


Figure 5.6: Variation of communication performance metrics with transmitter's HPBW

gation for picking the best alternatives (optimal solution) among a finite set of transmitter configurations. To confront this conflicting state of affairs, a set of Pareto optimal solutions are initially screened by imposing lighting constraints. Finally, an integrated approach of the Analytic Hierarchy Process (AHP) and *technique for order preference by similarity to ideal solution* (TOPSIS) has been applied to determine the best-compromised solution, briefly illustrated in Section 5.4.

5.4 MCDM UNDER LIGHTING CONSTRAINTS

From the obtained results illustrated in Section 5.3, it has been observed that when the transmitter's HPBW is set at the lower side the combined effect of CCI and ISI are significantly marginal. However, a lower value of transmitter semi-angle leads to very poor illumination performance, especially in terms of overall uniformity. This striking difference in illuminance around the task area gives rise to visual discomfort and glare. As per the IEEE 802.15.7-2018 standard, the communication performance has to be augmented without sacrificing existing illumination service⁽⁶¹⁾. Thus, for all three luminaire deployment strategies, a specific range of HPBW is considered to find the best solution where lighting performance complies with ISO standard. The minimum requirement of horizontal illuminance for indoor is 300 lux with 0.7 overall uniformity. Considering these lighting constraints, a set of (S_{Tx}) 25 distinguish transmitter configurations is obtained encompassing all three luminaire deployment arrangement. Out of total 25 alternatives, six configurations are obtained from arrangement A_1 where the minimum HPBW of the transmitter is 95° . In the case of arrangement A_2 and A_3 , nine and

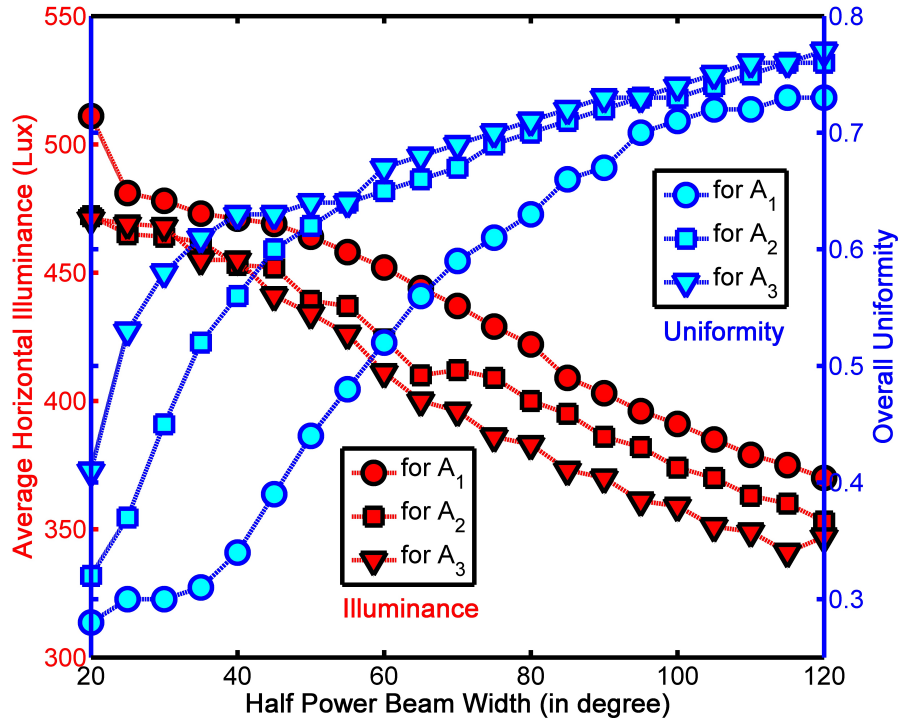


Figure 5.7: Effect of varying HPBW on lighting parameters

ten configurations are selected respectively that follow minimum lighting criteria. These 25 solutions are non-inferior and admissible in nature and all four performance indicators cannot be simultaneously improved. Thus it forms a Pareto optimal front.

The prime goal of MCDM is to support decision-makers (DM) with an aid that helps to select the best compromise Pareto solution under several conflicting criteria. Among different MCDM approaches “technique for order preference by similarity to ideal solution” (TOPSIS) was found to be more proficient due to its simple computational complexity and it has been used in this study.

In this problem, a set of transmitter configurations (*alternatives*) ($T_c = \{T_{ci}, i = 1, 2, \dots, m\}$) have to be compared to a set of performance metrics (*criteria*) ($C = \{C_j, j = 1, 2, \dots, n\}$). Thus the *decision matrix*; (D) which consist of *alternatives* and *criteria*, can be represented as:

$$D = \begin{pmatrix} d_{11} & \dots & d_{1n} \\ \vdots & \ddots & \vdots \\ d_{m1} & \dots & d_{mn} \end{pmatrix} \quad (5.28)$$

Here, indicates the rating of viable alternatives. The criteria are classified into two categories: benefit criteria (J_B) and cost criteria (J_C). The cost criteria suggest the superiority of lower value while benefit criteria are valid for a higher value. \bar{P}_{sig} , E_{avg} and U_O are considered as benefit criteria and \bar{P}_{intf} comes under cost criteria. Out of four distinguishing criteria,

the importance of any criteria depends on DM's subjective preference as well as the objective characteristics of the criteria themselves⁽¹⁸⁸⁾.

The current optimization problem is addressed by considering the Analytical Hierarchy Process (AHP) that gives a numerical weight through ordering criteria. Considering every element of the decision matrix (D), the generated weights are evaluated by the pairwise attribute comparison method⁽¹⁸⁹⁾. The total number of comparison (O_N) is given by:

$$O_N = \frac{n(n-1)}{2} \quad (5.29)$$

5.4.1 CLOSENESS COEFFICIENT

The execution steps to determine the closeness coefficient are summarized below:

Step-1: To compare all conflicting and heterogeneous criteria (C_j) the decision matrix (D) is transformed into a dimensionless normalized decision matrix:

$$R = [r_{ij}]_{m \times n}$$

The normalized value r_{ij} is given by:

$$r_{ij} = \frac{d_{ij}}{\sqrt{\sum_1^m d_{ij}^2}}; \forall i = 1, 2, \dots, m \& j = 1, 2, \dots, n \quad (5.30)$$

Step-2: The normalized decision matrix (R) is multiplied by its associated weight (W) to obtain the weighted normalized decision matrix P,

$$P = [p_{ij}]_{m \times n} \text{ where } p_{ij} = w_i \times r_{ij} \forall i = 1, 2, \dots, m \& j = 1, 2, \dots, n \quad (5.31)$$

Step-3: The positive (best) ideal solution (A^+) and negative (worst) ideal solution (A^-) are identified as:

$$A^+ = (p_1^+, p_2^+, \dots, p_m^+); A^- = (p_1^-, p_2^-, \dots, p_m^-) \quad (5.32)$$

Here, $p_j^+ = \text{Max}(p_{ij})$ when $C_j \in J_B$ and $\text{Min}(p_{ij})$ when $C_j \in J_C$, $i = 1, 2, \dots, m$
 $p_j^- = \text{Min}(p_{ij})$ when $C_j \in J_B$ and $\text{Max}(p_{ij})$ when $C_j \in J_C$, $i = 1, 2, \dots, m$

Step-4: The Euclidean distances from the best and worst solution are obtained as:

$$S_i^+ = \sqrt{\sum_j (p_j^+ - p_{ij})^2} \quad (5.33)$$

$$S_i^- = \sqrt{\sum_j (p_j^- - p_{ij})^2} \quad (5.34)$$

Step-5: The relative proximity to the positive ideal solution is obtained through a well-

Table 5.3: Normalized Relative Weight (AHP)

	\bar{P}_{sig}	\bar{P}_{intf}	E_{avg}	U_O
\bar{P}_{sig}	0.363	0.363	0.375	0.333
\bar{P}_{intf}	0.363	0.363	0.375	0.333
E_{avg}	0.181	0.181	0.186	0.250
U_O	0.093	0.093	0.064	0.084
<i>Sum</i>	1.000	1.000	1.000	1.000

defined Closeness Coefficient ξ_i

$$\xi_i = \frac{s_i^-}{s_i^+ + s_i^-} \quad (5.35)$$

The transmitter configuration $Tx_{\alpha_H}^{A_i}$ corresponding to the maximum ξ_i is considered as the best alternative.

5.5 RESULTS

As mentioned in the previous Section, the decision matrix is generated considering a Pareto optimal set of 25 transmitter configurations that encompasses all three luminaire arrangements. Here the computed results of \bar{P}_{sig} , \bar{P}_{intf} , E_{avg} & U_O are considered as criteria and corresponding transmitter configuration as alternatives. Subsequently, TOPSIS optimizations are performed employing AHP based weighting method where DM's observation is taken into account to determine the weight. The consistency of the derived weight using the AHP method is further verified by comparing it with Satty's Random Consistency Index⁽¹⁹⁰⁾. Result shows a satisfactory and accepted Consistency Index (CI) of 0.087 as per the method proposed in⁽¹⁹¹⁾. Normalized relative weight, associated with pairwise criterion is shown in Table 5.3 and used to calculate the principal Eigen vector for subsequent TOPSIS optimization.

5.5.1 BEST TRANSMITTER CONFIGURATION

To determine the best-compromised $Tx_{\alpha_H}^{A_i}$, closeness coefficients (ξ_i) are calculated and depicted in Figure 5.8. In comparison with arrangements A_2 and A_3 , A_1 luminaire arrangement exhibits better results. Overall maximum closeness coefficient of 0.8511 is obtained at 95° HPBW with a 2×2 deployment scheme. However, the best result for 3×3 & 4×4 arrangements are observed at HPBW of 80° & 75° respectively. Figure 5.9 shows the system responses in terms of four performance indicating metrics where best transmitter configurations are selected from respective luminaire arrangements with the help of corresponding closeness coefficient. Transmitter configuration related with overall maximum closeness coefficient (95° HPBW & 2×2 arrangement) exhibits better communication performance compared to the other two arrangement in terms of average signal power and interference. However, average horizontal illuminance is marginally smaller while the achieved overall uniformity accomplishes identical results. Under these circumstances, the transmitter configura-

tion with $95^\circ \alpha_H / 47.5^\circ \gamma_{1/2}$ & 2×2 luminaire arrangement can be holistically considered as the best-compromised transmitter configuration that can provide optimal channel allocation to maximize **SINR** performance.

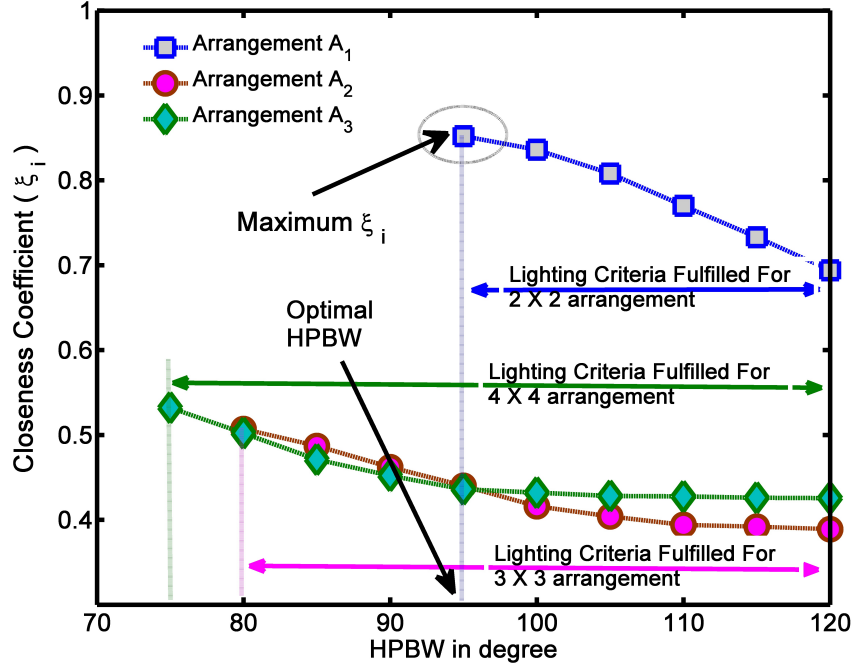


Figure 5.8: Closeness-Coefficients for different transmitter configuration

5.5.2 SINR DISTRIBUTION

It has to be noted that, a simple receiver with a single-PD is considered throughout this study to compute and compare the **SINR** over the CF for different schemes. As mentioned before the transmitter configuration and the FOV is set at its optimal value in the present study. However, non-optimal transmitter and receiver configuration have been used in most state of the art researches^(169,170,104,13,171) on **VLC** where transmitter HPBW is kept at a higher value. Figure 5.10 shows the **SINR** distribution of a typical non-optimal case with a 70° semi-angle.

Considering the optimal semi-angle specified in⁽¹⁷⁶⁾ comparatively better **SINR** performance is obtained over the CF as depicted in Figure 5.11. Despite the trivial improvement in minimum and average **SINR**, neither the receiver FOV is optimized nor the illumination aspect is taken into account by the study⁽¹⁷⁶⁾. So, this result can be considered as a sub-optimal solution of channel allocation. Compared to this existing sub-optimal solution, the proposed transmitter configuration along with its optimal FOV can provide significant improvement in **SINR** with a coverage probability of 96 percent. The **SINR** distribution of the proposed scheme is shown in Figure 5.12. With a maximum **SINR** of around 60.17 dB and an average **SINR** of 36.13 dB, the proposed configuration simply outperforms the existing scheme.

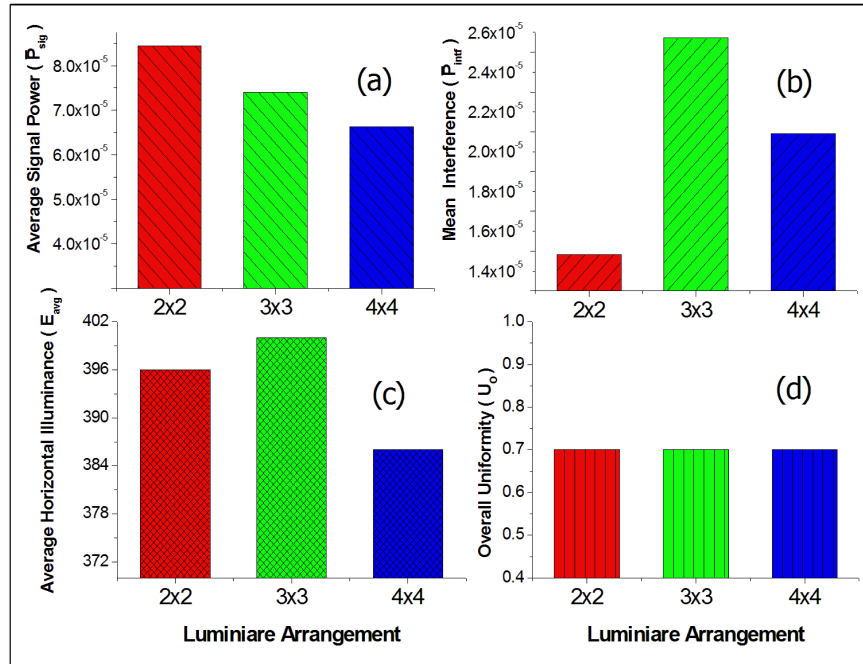


Figure 5.9: Performance indicating metrics at best transmitter configurations of different luminaire arrangements

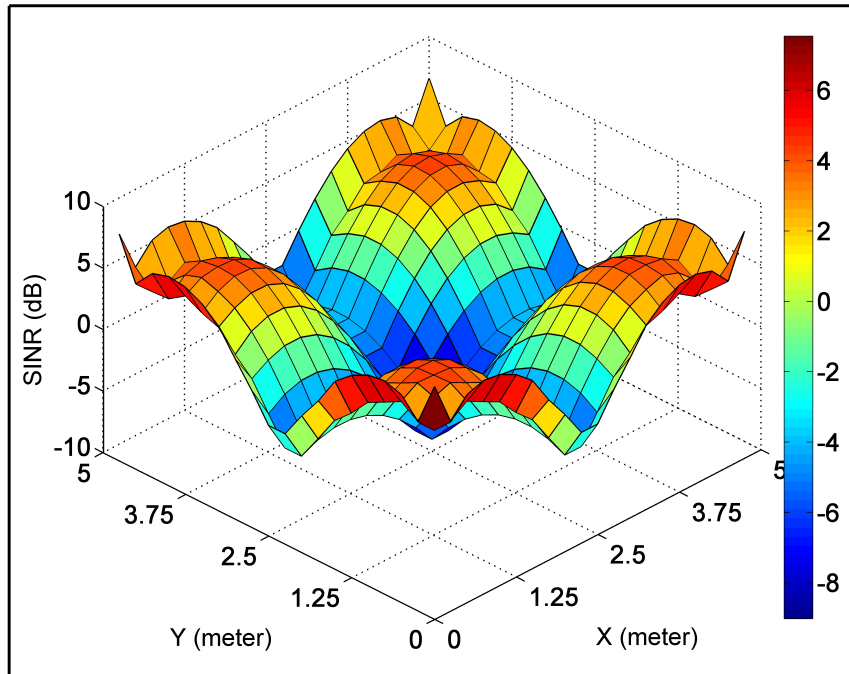


Figure 5.10: SINR distribution without any optimization in transmitter configuration and FOV (Non-optimal scheme)

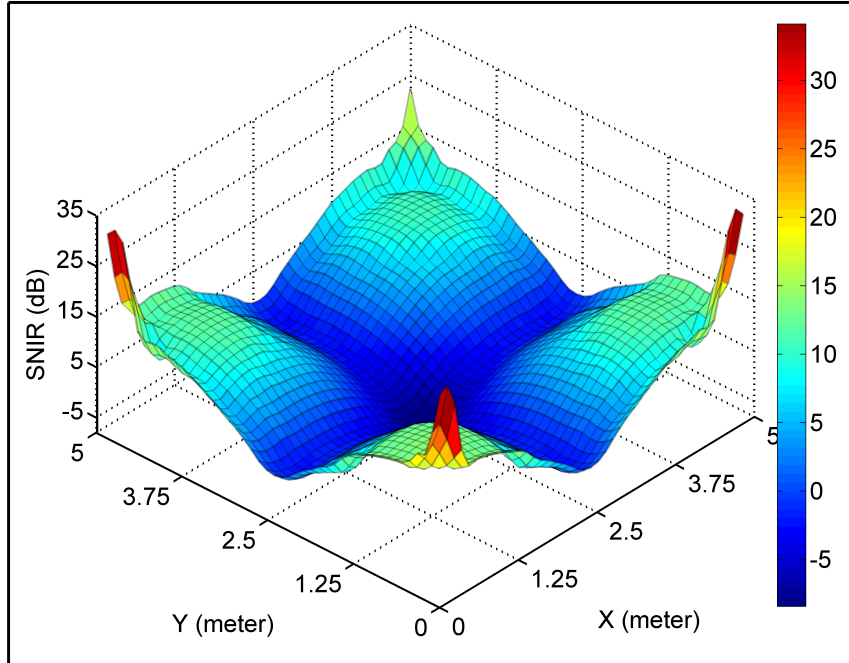


Figure 5.11: SINR distribution with only optimal transmitter semi-angle (sub-optimal scheme)

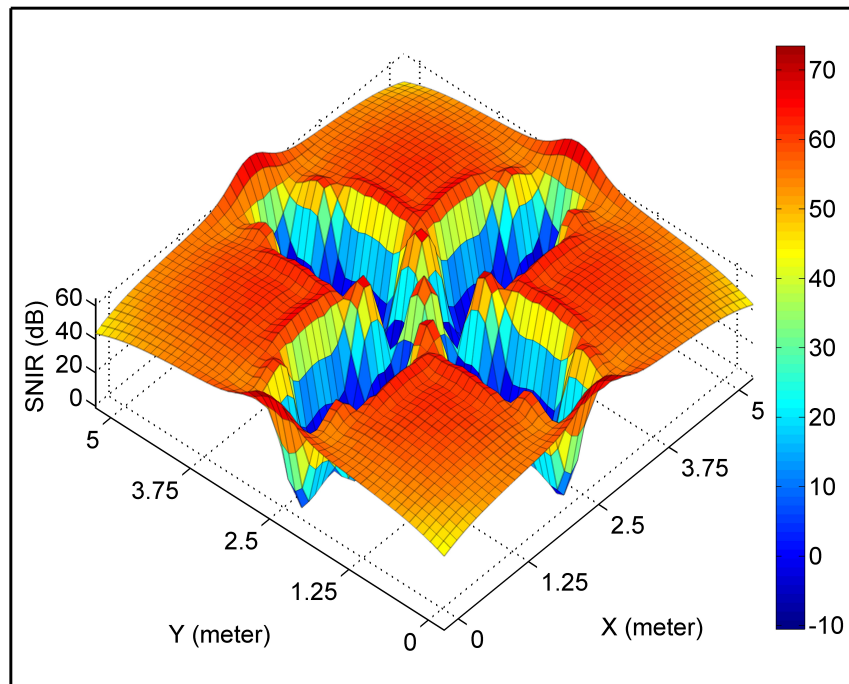


Figure 5.12: SINR distribution of the proposed scheme with optimal transmitter configuration & receiver's FOV

5.5.3 VALIDATION AND COMPARISON

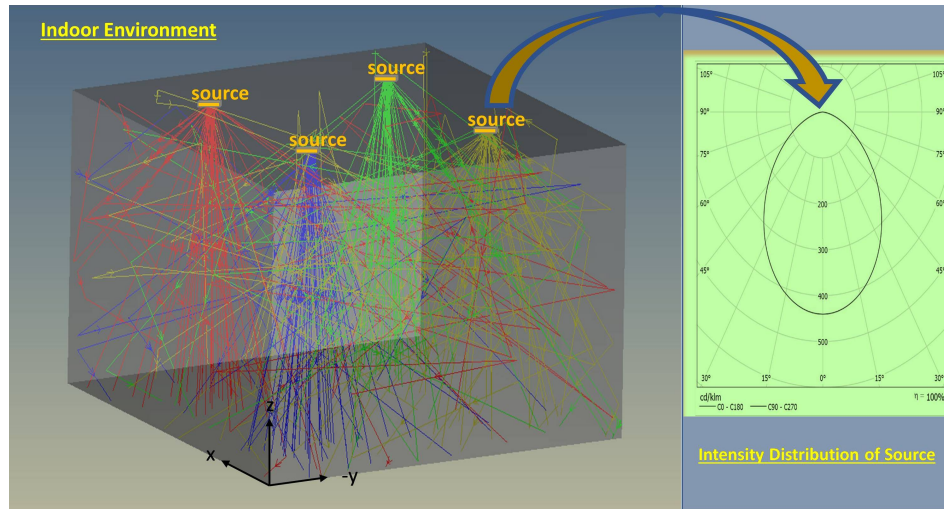


Figure 5.13: Monte-Carlo ray tracing (Zemax) with optimal transmitter configuration

In order to validate the analytically obtained result, a three dimensional indoor environment is simulated with optimal transmitter configuration and room geometry specification using a commercial optical software, Zemax. The non-sequential platform of Zemax offers an accurate Monte-Carlo based ray tracing description. IES files of 95° HPBW is integrated to contrive the optimal source description inside the indoor environment. This is shown in Figure 5.13. The receiver's radial field is restricted to 39° by selecting appropriate radius of curvature and lens-thickness through lens data editor. Subsequently, the receiver, designed in sequential mode is imported in 3-D environment for ray tracing.

Figure 5.14 indicates composite representation of proposed optimal scheme, both analytical (using mathematical model) and simulated (using ray tracing-Zemax) results at different room positions. The sub-optimal and non-optimal scenarios are also incorporated in same figure. Less than 10% deviation have been observed between the analytical and simulated results. However, more importantly both the results are far better in comparison with existing solutions.

The gross comparative result, depicted in Figure 5.15, indicates a noteworthy improvement (27.35 dB) in average **SINR** at the expense of marginal decrement (0.04) of overall uniformity of illuminance. However, the obtained horizontal illuminance (345 lux) and its uniformity (0.70) comply with ISO recommendation. The distribution of the horizontal illuminance is shown in Figure 5.16. So, the proposed optimal channel allocation strategy illustrated in this work can be readily used to specify the HPBW of the optical luminaire that can serve joint communication and illumination purpose.

5.6 SUMMARY

For enhanced illumination and communication performance in a multi-cell indoor **VLC** system, the choice of transmitter configuration and the receiver's FOV are crucial factors. This

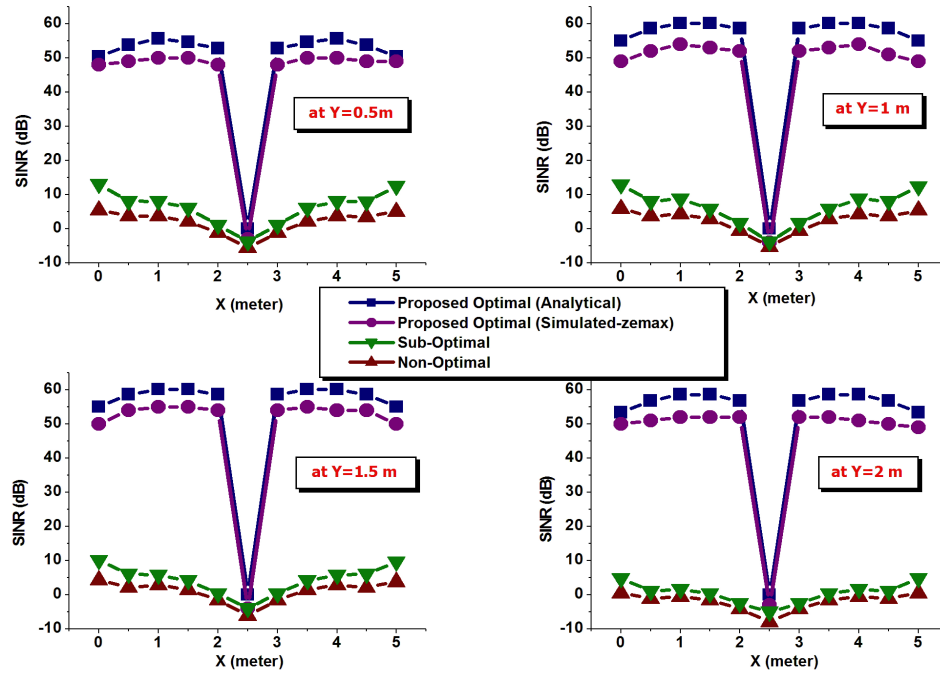


Figure 5.14: SINR performance at different room positions along the x-axis

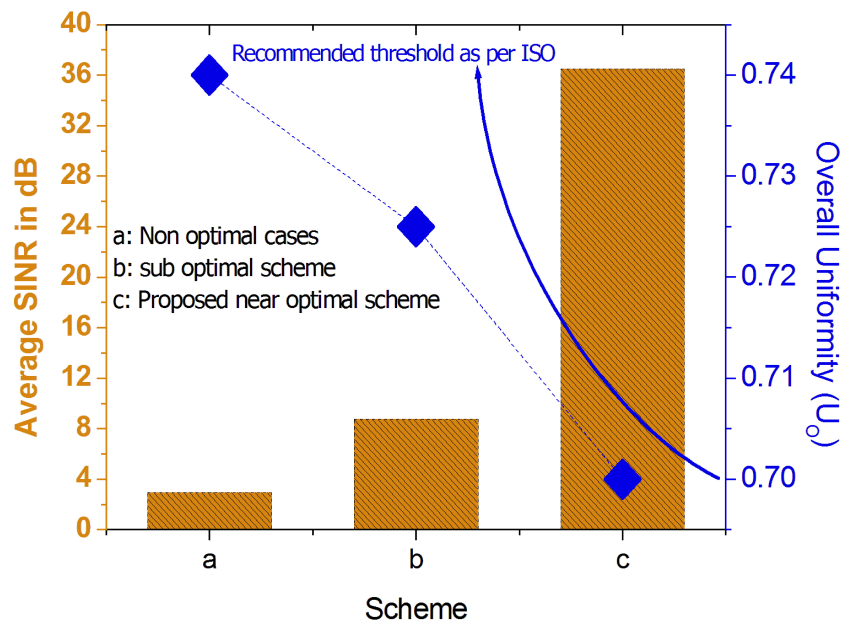


Figure 5.15: Comparative results of average SINR and overall uniformity

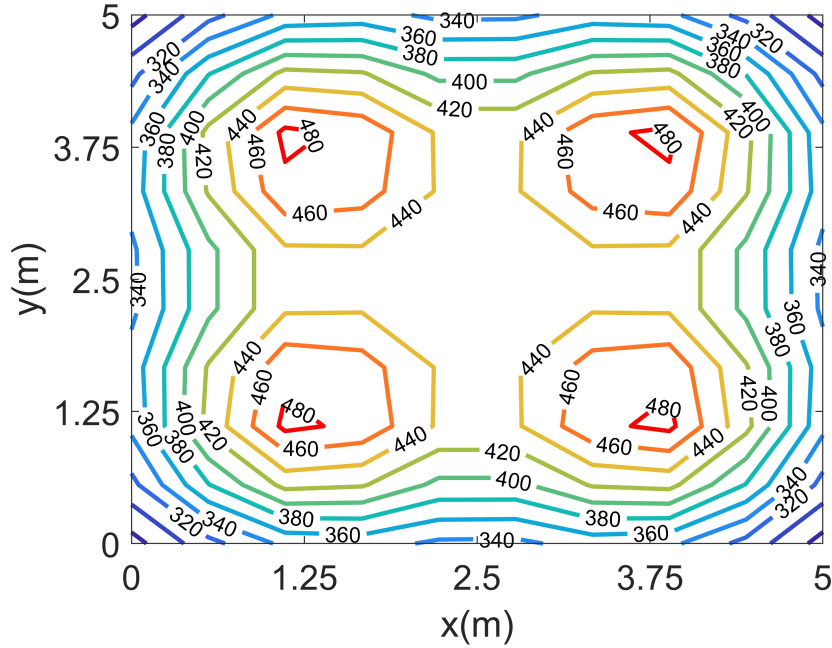


Figure 5.16: Distribution of horizontal illuminance (Iso-lux)for optimal transmitter configuration

chapter proposes a design-centric methodology based on MCDM to determine the optimal transmitter configuration and receiver FOV within lighting constraints. These optimal parameter selections are instrumental to obtain a highly uncorrelated channel, thus significantly mitigating both **CCI** from the neighboring transmitter and ISI due to multipath reflection. The implication for the optimum selection is explored using two communication ($\bar{P}_{sig}, \bar{P}_{intf}$) and two lighting (E_{avg}, U_o) performance indicating metrics.

The salient contributions of this study are summarized as follows:

- Considering simple single-PD receiver architecture, the design algorithm proposed in this work exhibits significantly improved **SINR** performance by assigning an optimal downlink channel. The proposed method can be readily utilized for the design of any multi-cell indoor **VLC** system to achieve joint illumination and communication performance.
- The proposed solution undergoes zero real-time computational complexity to mitigate **CCI** and ISI.
- Significance for concurrent adoption of the optimal transmitter configuration and the receiver's FOV are explored to obtain a highly uncorrelated channel. Using the TOPSIS algorithm the optimal configuration is determined to enhance communication performance under lighting constraints.
- **SINR** performance at different room positions, obtained through analytical study are also compared with simulated results using a ray-tracing optical tool.
- In contrast to the present state-of-the-art **VLC** system with a single-PD receiver the proposed design exhibit 24 dB improvements in average **SINR**. At the same time, 345 lux with 0.7 overall uniformity is obtained that complies with the ISO recommendations.

5.7 RESEARCH OUTPUT

The findings from this chapter are reported in the following research publication:

- **Chatterjee, S., Sabui, D., Khan, G. S., & Roy, B. (2021).** Signal to interference plus noise ratio improvement of a multi-cell indoor visible light communication system through optimal parameter selection complying lighting constraints. *Transactions on Emerging Telecommunications Technologies*, 32(10), e4291.
DOI: doi.org/10.1002/ett.4291

“ Nobody ever figures out what life is all about, and it doesn’t matter. Explore the world. Nearly everything is really interesting if you go into it deeply enough.”

Richard P. Feynman

6

Adopting Receiver Diversity Techniques

IN CHAPTERS 3, 4, and 5 a simple photodiode receiver with a symmetric FOV is employed for system design. However, in a multi-cell VLC system where multiple APs are closely deployed, mitigating CCI proves to be extremely challenging with a simple PD receiver. Consequently, the SINR performance of the system is consistently restricted within a certain limit. Additionally, there is a concern about spatial SINR fluctuations. To address these challenges, diversity in some form can be introduced to reduce channel correlation between adjacent spatial points. In this chapter, various diversity techniques are showcased, aiming at enhancing communication performance in a multi-cell VLC system. The relevance of this chapter from a lighting perspective, as covered in Chapters 3, 4, and 5, is clearly outlined in sub-section 6.1.1.

6.1 INTRODUCTION

Despite the presence of a substantial optical bandwidth of 400 THz, the electrical bandwidth of the VLC system, with a single transmitter, is confined to several megahertz. This limitation arises from the comparatively low switching speed at the transmitter and the low cut-off frequency of the TIA at the receiving end. Consequently, to enhance data rates, the adoption of MIMO strategy becomes an obvious option, especially in indoor scenarios where more than one WLEDs are used for illumination purposes^(192,193). In spite of the numerous potential advantages and excellent spectral efficiency of MIMO, the channel matrices become highly correlated in a multi-cell indoor VLC system⁽¹⁹⁴⁾. Various efforts have been made to enhance system reliability by mitigating channel correlation. For instance, in⁽¹⁷²⁾, the combination of space-frequency block code (SFBC) with frequency-switched transmit diversity (FSTD) has been explored to alleviate CCI. Another approach involves the introduction of a link-blocked (LB) receiver to achieve robust channel performance⁽¹⁹⁵⁾, although LB receivers may not be

suitable for high-mobility applications. In this context, the angle diversity receiver (ADR) has emerged as a promising solution to address the challenges associated with inter-channel interference. The concept of utilizing ADR for parallel data transmission was initially introduced in ^(196,197), presenting two distinct design proposals for practical implementation.

6.1.1 IMPORTANCE OF RECEIVER DIVERSITY FROM LIGHTING PERSPECTIVE

In the preceding chapter, it was established that enhancing the **SINR** performance is achievable through the judicious selection of optimal transmitter and receiver configurations. An optimal transmitter configuration encompasses factors such as the HPBW or the semi-angle of the optical sources. A narrower semi-angle for optical sources effectively minimizes the **CCI**, thereby elevating the **SINR**. However, it is crucial to note that a reduced semi-angle can compromise the uniformity of illumination, a consideration that may conflict with lighting standards. To reconcile this, the adoption of diversity techniques in the receiver front-end proves valuable. By incorporating such diversity techniques, significant improvements in **SINR** can be attained, even when utilizing a higher semi-angle for the transmitter. Consequently, prioritizing angle diversity or an enhanced version thereof in the receiving front-end is consistently advantageous from a lighting perspective.

6.2 ANGLE DIVERSITY RECEIVER FOR VLC

The concept of ADR was initially introduced in 1997 by Kahn and Barry⁽⁵⁹⁾ as a solution for infrared wireless communication, aiming to replace the single PD receiver. The same idea can also be utilized in case of **VLC**. Each element in the ADR employs an individual non-imaging concentrator. Among the conventional concentrators, the hemispherical lens and the compound parabolic concentrator stand out. The lens with hemispherical shape provides a broad FOV. On the other hand compound parabolic concentrator achieves a high optical gain because of adopting narrower FOV. In the context of this study, the chosen concentrator for ADRs is the compound parabolic concentrator. However, it's worth noting that the advantage of a smaller FOV comes at the cost of an increased length for the compound parabolic concentrator. Considering the constraints in size and the complexity of implementation on mobile devices, it becomes imperative to limit the number of PDs on each ADR. The fundamental concept behind the ADR design (for **VLC**) involves altering the normal vector of each PD to introduce variation in the incident angles from a given LED. The arrangement of PDs offers numerous possibilities for changing the orientation of these normal vectors. It focuses on optimizing the reception of the optical signal by employing multiple receiving elements oriented in different directions. Each element is equipped with its own non-imaging concentrator. The primary goal is to improve the SNR and **SINR**, crucial metrics in communication systems. The ADR concept for **VLC** focuses on optimizing the reception of the optical signal by employing multiple receiving elements oriented in different directions. Each element is equipped with its own non-imaging concentrator. The primary goal is to improve the SNR and **SINR**, crucial metrics in communication systems. Despite the basic design, the configurations of ADRs remain suboptimal, and as a consequence, the achievable performance improvement has not been fully harnessed. Furthermore, in the context of indoor

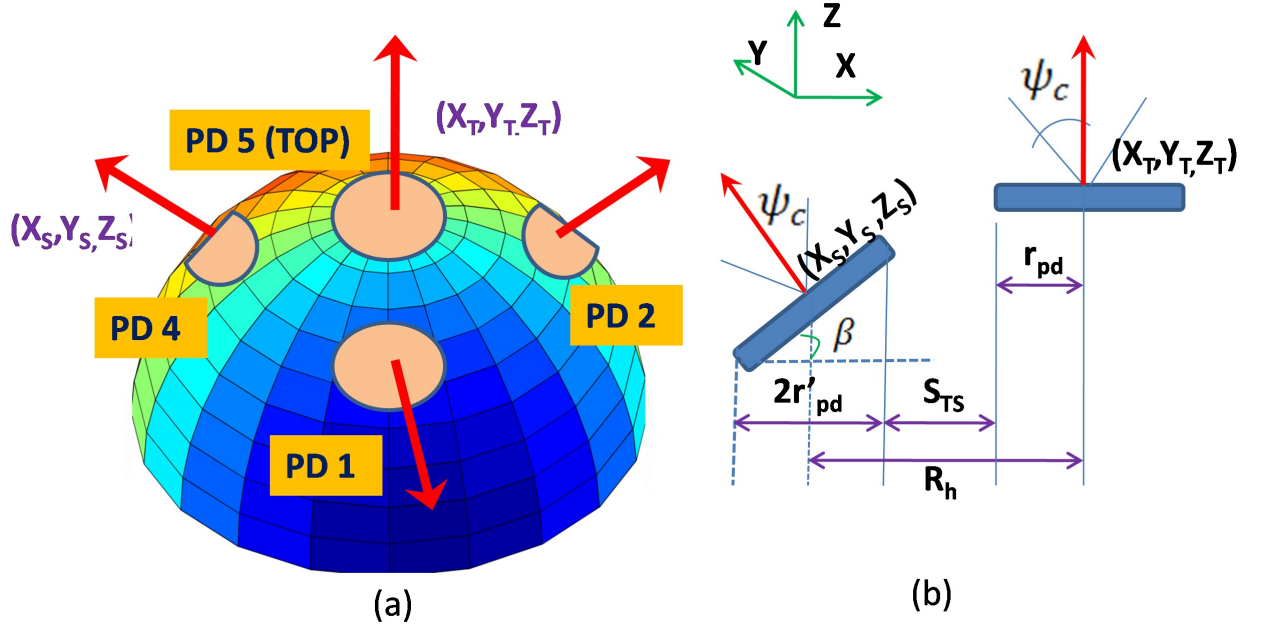


Figure 6.1: Structure of HADR (a) 3-D View (b) Side View.

multi-cell VLC systems, the incorporation of ADRs primarily aims at enhancing the overall system capacity or the area spectral efficiency (ASE). Yet, there is a notable gap in research as the fluctuation of SINR across the receiving plane has not been thoroughly investigated.

6.3 HADR ARCHITECTURE WITH OPTIMAL FOV

In this work, five OSD5E Centric photo-detectors are considered as receiving element. These PDs are pointing towards the different directions of a hemisphere as shown in Figure 6.1(a). However, it is not mandatory to put the receiver on the surface of a hemisphere. Instead, the hemispheric geometry is considered to determine the normal vectors of each PD⁽⁹²⁾. The layout, given in Figure 6.1(a) suggests that the azimuth angle (θ_{az}^j) of the j^{th} side detector is determined as

$$\theta_{az}^j = 360^\circ \times \frac{n}{N_S} + \Theta_{RRA}, n = 0, 1, \dots, N_S - 1 \quad (6.1)$$

Here N_S is the number of side detectors and Θ_{RRA} is the random rotation angle (RRA) of the HADR, which depends on the user's application⁽⁹²⁾. It is clearly discussed in Section 6.3.1.

Four numbers of side detectors (N_S) have been considered in this study. All four PDs obtained the same inclination angle (β) with the X-axis as depicted in Figure 6.1B. However, the top detector (PD₅) makes a 90° inclination angle with X-axis, ie it is parallel with the Z-axis. If the center of the hemisphere is located at (x_b, y_b, z_b) then the co-ordinate of j^{th} side PD

can be represented as:

$$(x_s^j, y_s^j, z_s^j) = (x_b + R_b \cos \theta_{az}^j, y_b + R_b \sin \theta_{az}^j, z_b - r_{pd} \sin \beta) \quad (6.2)$$

Here, R_b is the horizontal distance between the center of the hemisphere and side detectors. It is clearly illustrated in Figure 6.1(b). The radius of the centric photo-detector is taken as r_{pd} and can be obtained from the respective datasheet. The co-ordinate of the top detector is given by,

$$(x_T, y_T, z_T) = (x_b, y_b, z_b + R_b) \quad (6.3)$$

6.3.1 RANDOM ROTATION ANGLE

From Eq. (6.1) and (6.2) it is evident that received optical power is highly dependent on random rotation angle (Θ_{RRA}). The value of RRA is same for all side detectors. When the receiver is positioned at a different location over the CF, Θ_{RRA} is uniformly distributed from 0° to 360° depending upon the user. Due to the symmetric receiver architecture with respect to both the X and Y axis, the range of RRA can be considered from 0° to 90° . Figure 6.2 suggests that the initial azimuth angle of the four side detectors are 0° , 90° , 180° & 270° respectively (shown by blue colour). Now, due to the random placing of the HADR, all the PDs are encountering a circular shift of Θ_{RRA} (represented by yellow colour). This RRA can contribute a substantial **SINR** deviation over the CF.

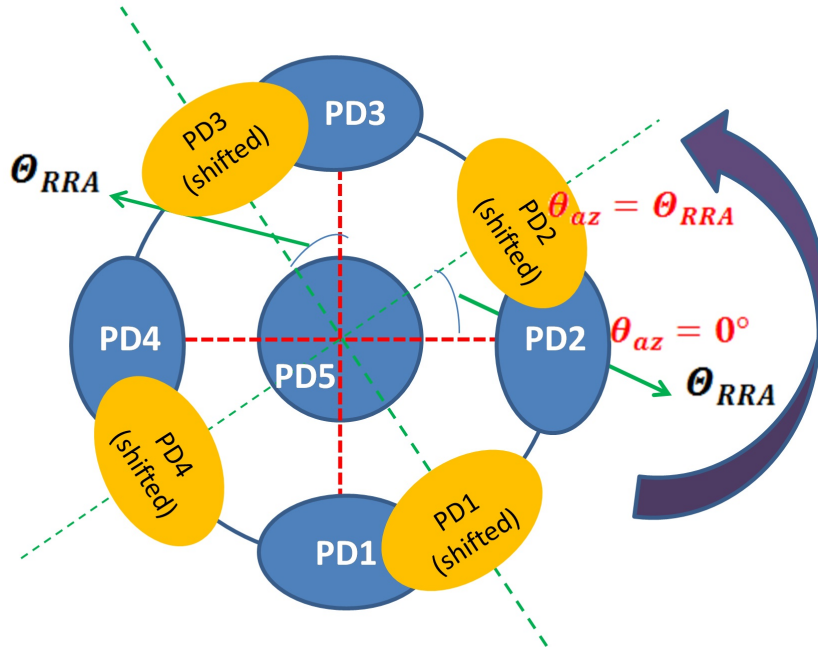


Figure 6.2: Illustration of Random Rotation Angle (Θ_{RRA}).

6.3.2 DESIGN PRINCIPLES

A MIMO (5×4) VLC system is presented in this work where a room with dimension ($L_X \times L_Y \times L_Z$) is equipped with four luminaires for joint communication and illumination purposes.

For a given i^{th} source and j^{th} PD, LOS channel gain depends on transmitter and receiver parameters and is given by:^(184,39)

$$H_{LOS}^{ij} = f_{ij}(S_i, R_j) = \frac{m+1}{2\pi} \cos^m(\varphi_{ij}) d\Omega T_S(\theta_{ij}) \text{rect}\left(\frac{\theta_{ij}}{\Psi_C}\right) \quad (6.4)$$

Here the source (S_i) is defined by its position (v_{si}), orientation (n_{si}) and the Lambertian order or mode number (m) associated with semi-angle (Ψ_{12}). φ_{ij} and θ_{ij} are the angle of irradiance and incidence respectively. Ψ_C is the FOV of the PD. The subtended solid angle by the differential area of receiver is written as:

$$d\Omega = \frac{\cos(\theta_{ij}) g_C(\theta_{ij}) A_R}{d^2} \quad (6.5)$$

A_R is active area of photodetector and $g_C(\theta_{ij})$ is the optical concentrator gain that depends upon lens index (n_c), given as:

$$\begin{aligned} g_c(\theta_{ij}) &= \frac{n_c^2}{\sin^2(\Psi_C)} \quad \text{for } \theta_{ij} \leq \Psi_C \\ &= 0 \quad \text{for } \theta_{ij} > \Psi_C \end{aligned} \quad (6.6)$$

The electrical signal obtained at j^{th} RE, due to i^{th} transmitter is expressed as:

$$S_{elec}^{ij} = \gamma \mu H_{LOS}^{ij} P_{ti} \quad (6.7)$$

To minimize the interference of the VLC attocell network, select best combining scheme (SBC) has been adopted in this study. As the scheme suggests, the received signals from all the PDs are continuously monitored and **SINR** is computed for each PD. However, PD with maximum **SINR** is solely considered as the output of the HADR. A dedicated circuit and a very fast switch are generally used for this processing and selection purpose⁽¹⁹⁸⁾. The **SINR** using the SBC scheme can be computed as

$$SINR_j^{\Re} = \frac{\left(\gamma \mu H_{LOS}^{ij} P_{ti}\right)^2}{\sum_{k=1, k \neq i}^{N_t} \left(\gamma \mu H_{LOS}^{ik} P_{tk}\right)^2 + N_{total}} \quad (6.8)$$

here, j^{th} PD provides maximum **SINR** when the HADR is positioned at \Re^{th} test point over the CF. Considering all 400 test points, spatial **SINR** fluctuation can be determined and represented as

$$SINR_{dev} = [\max(SINR_j^{\Re}) - \min(SINR_j^{\Re})], \forall \Re = 1, 2, \dots, 400 \quad (6.9)$$

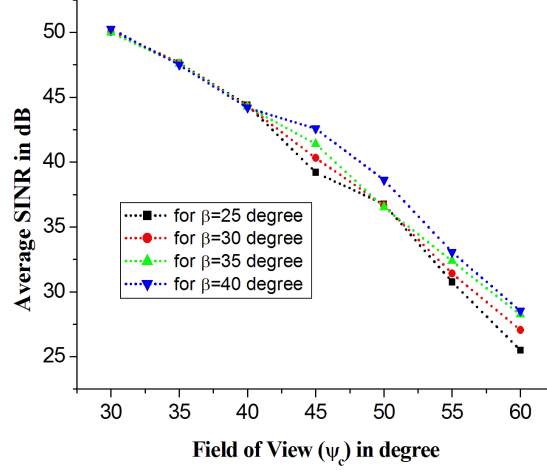


Figure 6.3: Variation of Average SINR with Ψ_C for different values of β .

The spatial average **SINR** is given as

$$SINR_{avg} = \frac{1}{m} \sum_{\mathfrak{R}} SINR_J^{\mathfrak{R}} \quad (6.10)$$

The average **SINR** deviation due to variation in RRA (from 0° to 90°) is expressed as

$$\overline{SINR_{dev}} = \frac{1}{90} \sum_{\Theta_{RRA}=0^\circ}^{90^\circ} SINR_{dev} \quad (6.11)$$

6.3.3 IMPACT OF RRA

From the physical understanding, it is obvious that with the reduction in the FOV angle of the RE, **CCI** should reduce resulting improvement in **SINR**. However, the moto is to investigate the significance of the inclination angle (β) over this improvement in **SINR** due to a reduction in FOV. Figure 6.3 provides the intended results where it can be observed that in case of HADR, **SINR** degrades almost in an identical way with an increase in FOV irrespective of inclination angle.

However, an uncontrolled reduction in FOV may lead to blindness of received signal in some of the positions over the CF. Thus the optimal FOV for our design can be determined

as:

$$\begin{aligned}
\Psi_C^{opt} &= \max_{(x_b, y_b, z_b, \beta)} \theta_{ij}^{\min} \\
\text{subject to :} \\
\theta_{ij}^{\min} &= \min_{i,j} \theta_{ij}(x_b, y_b, z_b, \beta) \\
(x_b, y_b, z_b) &\in f, 10^\circ \leq \beta \leq 45^\circ \\
\Theta_{RA} &= 0^\circ, z_b = h_{CF}, \\
i &\in \{1, 2, \dots, N_t\}, j \in \{1, 2, \dots, N_r\}
\end{aligned} \tag{6.12}$$

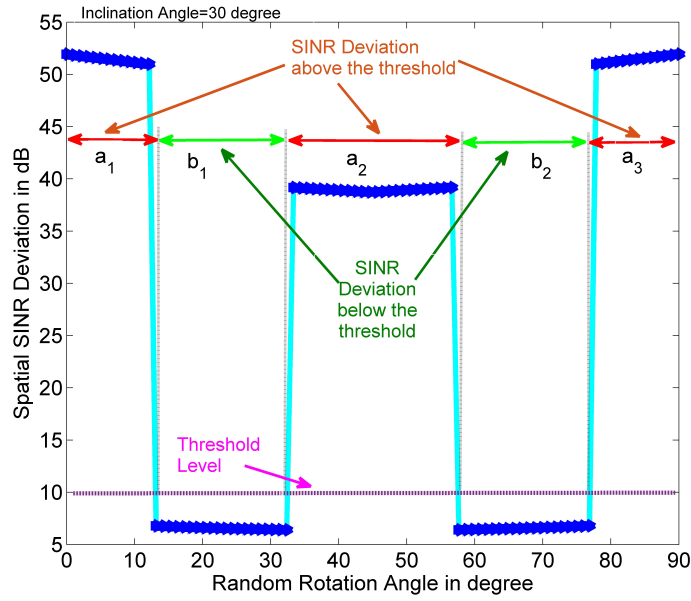


Figure 6.4: Impact of RRA on $SINR_{dev}$ at $\beta = 30^\circ$.

In the previous section, it has been mentioned that Θ_{RA} can be varied randomly in between zero to ninety degrees. Now, its turn to investigate the influence of the inclination angle (β) over the spatial **SINR** deviation considering different Θ_{RA} and fixed Ψ_C^{opt} . One degree interval of RRA is considered to compute the spatial **SINR** deviation. Meanwhile, the inclination angle is also altered at 5° intervals. The simulation parameters are shown in Table 6.1. The optimal field of view Ψ_C^{opt} of 32.93° is obtained using the objective function given in Eq. (16). This optimal value of the FOV angle ensures at least one LOS connectivity between any transmitter and RE of the proposed HADR examined over all the test points (\mathfrak{R}). In earlier research, optimal FOV of any ADR had been determined considering a fixed value of inclination angle (β). However, in this study, a range of viable β (in between 10° to 45°) is taken into account to compute Ψ_C^{opt} . So, it can be also recognized as the upper-bound of the minimum incidence angle when all the test points and inclination angles are taken into account.

This optimization creates an opportunity to investigate the impact of RRA (Θ_{RA}) at different inclination angle. Because, at all inclination angle within the considerable range at least

Table 6.1: HADR performance simulation parameters

Parameters	Value
Room dimension, $(L_X \times L_Y \times L_Z)$	$5m \times 5m \times 3m$
No of WLED transmitter, N_t	4
No of receiving element (PD), N_r	5
Height of the CF, h_{CF}	$0.8m$
Semi angle of the transmitter, $\psi_{1/2}$	60°
Transmitted optical power/transmitter, P_{ti}	$4.22W$
Physical area of PD, A_R	5 mm^2
Lens index, n_c	1.47
Optical to electric conversion efficiency, γ	$0.53A/W$
Transmission coefficient of optical filter, $T_s(\theta)$	1
Gap between top and side detector, S_{TS}	$3mm$
Load resistance, R_L	50Ω
Modulation index, μ	0.3
Noise Bandwidth Factor, I_2	0.562
Modulation Bandwidth, B	$100MHz$
Background current, I_{bg}	$30nA$
Boltzman's Constant, K_B	1.38×10^{-23}

one LOS connection is guaranteed for all test points. Figure 6.4 suggests that the randomness of $\Theta_{RR\Delta}$ can substantially degrade the system mobility by increasing the spatial **SINR** deviation / fluctuation ($SINR_{dev}$).

6.3.4 REDUCING FLUCTUATIONS OF SPATIAL SINR DISTRIBUTION

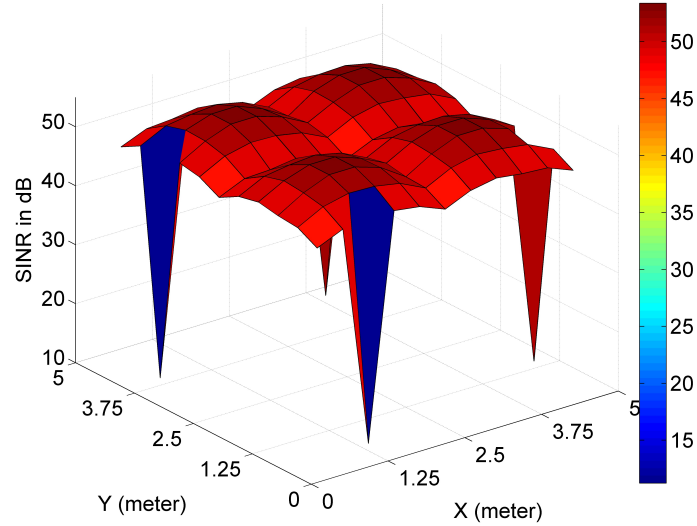


Figure 6.5: SINR distribution over the CF at $\beta = 30^\circ$.

From the spatial **SINR** distribution, shown in Figure 6.5 it has been clearly observed that average **SINR** ($SINR_{avg}$) is in the higher range (48.35 dB). However, the spatial fluctuation

of **SINR** is a reason of concern. It has to be noted that the inclination angle and FOV angle considered for the simulation of Figure 6.4 and Figure 6.5 are the same (30° and 32.93° respectively). Thus, the objective is to select an inclination angle where the possibility to restrict the **SINR** fluctuation within an acceptable threshold limit is comparatively better.

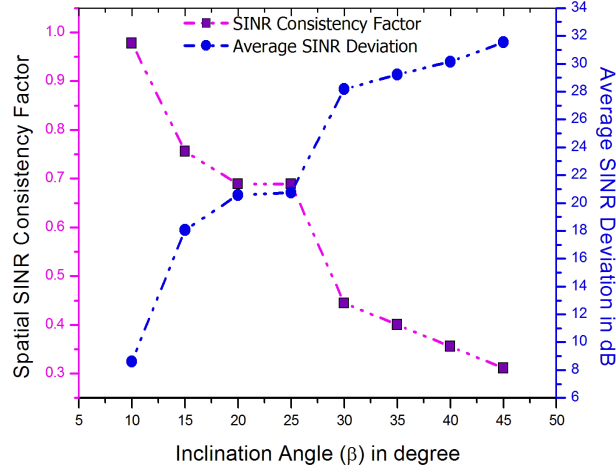


Figure 6.6: Relational dependency of spatial SINR distribution with Inclination angle (β) at optimal FOV.

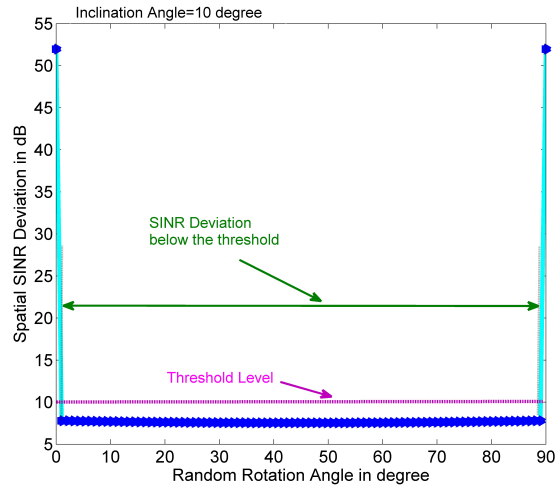


Figure 6.7: Variation of spatial SINR deviation with RRA ($\Psi_C^{opt} = 32.93^\circ, \beta = 10^\circ$).

For this reason, a new parameter termed as “*Spatial SINR Consistency Factor*” has been introduced in this study. It is defined as the probability of getting **SINR** deviation below the threshold limit (TL) when RRA is varied from 0° to 90° . 10 dB threshold level have been considered as shown in Figure 6.4. The spatial **SINR** consistency factor (C_f) is determined as

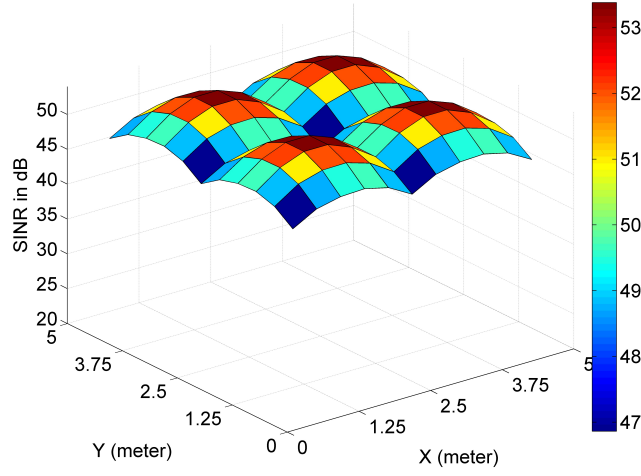


Figure 6.8: SINR distribution over the CF at optimal condition ($\Psi_C^{opt} = 32.93^\circ, \beta = 10^\circ$).

(refer Figure 6.4)

$$C_f = P(SINR_{dev} \leq 10dB) = \frac{\sum_k b_k}{\sum_k b_k + \sum_k a_k} \quad (6.13)$$

here, b_k = range below TL and a_k = range above TL.

The relational dependency of C_f with β (at optimal FOV angle) is depicted in Figure 6.6. Where it can be observed that at lower value of inclination angle, probability of **SINR** fluctuation is lesser. Hence the maximum **SINR** consistency factor ($C_f=0.978$) is obtained at 10° inclination angle. Meanwhile the average **SINR** deviation is also least at the same inclination angle.

The proposed design of HADR with 10° inclination angle and 32.93° optimal FOV can provide excellent communication performance by negating the random error contributed by Θ_{RRA} . Consequently, the average **SINR** deviation is restricted to 8.6087 dB. The distribution of **SINR** deviation at different RRA is shown in Figure 6.7. It can be seen that, the random rotation angle hardly affects the **SINR** fluctuation at the proposed FOV and inclination angle. The spatial **SINR** deviation is almost constant with respect to variation in RRA. So, 10° inclination angle can be considered as an optimal preference to contain spatial **SINR** deviation. Our proposed HADR with this optimal β and Ψ_C^{opt} also delivers outstanding **SINR** at the 400 test points over the CF. This distribution is depicted in Figure 6.8. In comparison with 15.7 dB **SINR** deviation in reference⁽⁸⁸⁾, the proposed system offers 45.17% reduction in average **SINR** deviation. At the same time, 48.81 dB average **SINR** is obtained over the communication floor.

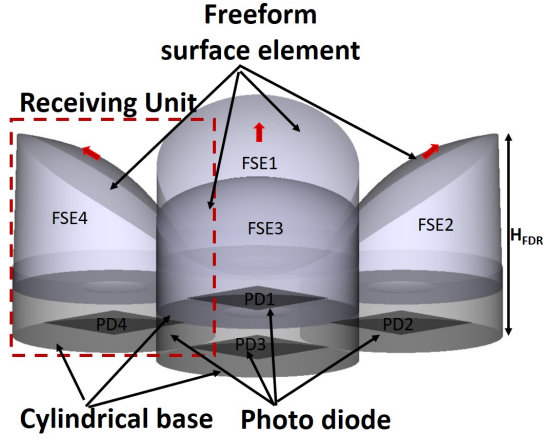


Figure 6.9: FDR Structure with four co-planar RUs

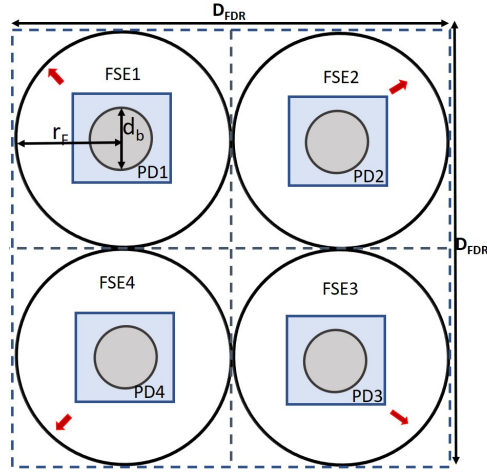


Figure 6.10: Quadruple arrangement of RUs: Top view

6.4 A STEP FORWARD: DESIGN OF IMPROVED ADR WITH FREEFORM SURFACE

Present architecture of ADRs necessitate additional mounting setup for positioning all the PDs in an inclined way. Consequently, this consistently increases the height of the receiver, posing a hindrance to the product's viability in handheld mobile devices. Additionally, there is an ongoing imperative for enhancing the **SINR**, to ensure higher channel capacity and data rates with minimal errors. In association with 'SENSE, IIT Delhi', an initiative is undertaken with twofold objectives: (a) elevating **SINR** and (b) reducing the size of the receiver. With the help of freeform optics an improved version of ADR, called Freeform Diversity Receiver (FDR) has been proposed⁽¹⁹⁹⁾.

6.4.1 FDR GEOMETRY

The freeform diversity receiver based specially tailored optical front-end^(200,201) can be portrayed as a modified and improved version of the angle diversity receiver. In FDR, four identical co-planar receiving units (RU) are placed together in orthogonal orientation with adjacent units as shown in Figure 6.9⁽²⁰¹⁾. Each RU has three parts: a PD chip, a freeform surface element(FSE), and a hollow cylindrical base. As shown in the figure, the position of the PD chip is right at the focal point of the freeform surface element. The quadruple arrangement is shown from the top in Figure 6.10⁽²⁰¹⁾. The highest sag point of each FSE is marked by the red arrow. Unlike the conical FOV of the existing **VLC** receiver, each FSE is rotationally-nonsymmetric and acts as a lens aperture.

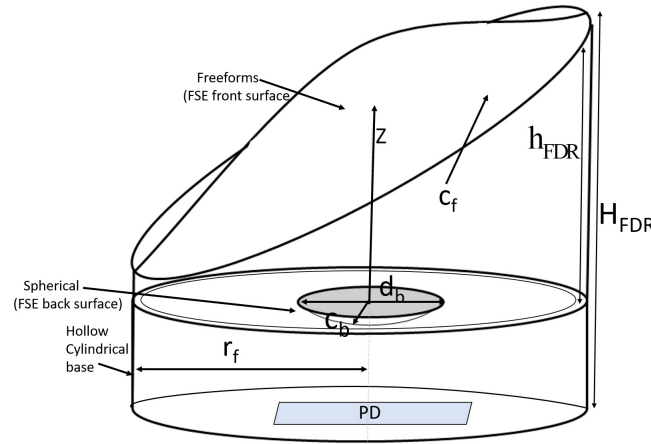


Figure 6.11: Perspective view of RU

The surface slope of all the FSEs is designed in such a way that FDR (four RUs together) can collect optical signals from all the corners of the room with almost zero overlap. With an offset from the optical axis of the lens, each RU offers a quadrilateral FOV. The perspective view of a RU is depicted in Figure 6.11⁽²⁰¹⁾. As shown, the cylindrical base has a semi-diameter r_f . The variable curvature of FSE is denoted by c_f . The thickness (h_{FDR}) of the freeform lens varies with cross-section. However, the maximum height (H_{FDR}) of the lens with base height is considered as the height of the FDR. A smaller circular aperture at the back side of FSE acts as a stop. The designed FSE has a spherical curvature (c_b) at its back side. To obstruct the unwanted flux, the side of FSE and the base of the hollow cylinder are made opaque. The designed parameters are listed in Table 6.2⁽²⁰¹⁾.

6.4.2 IMPROVED SINR PERFORMANCE

To assess the **SINR** performance of the FDR, the indoor multi-cell **VLC** system is arranged in a pre determined environment with dimensions of $5\text{m} \times 5\text{m} \times 3\text{m}$. The CF is positioned at a 0.85 m height. In Figure 6.12a, the **SINR** distribution across the communication floor is depicted⁽²⁰¹⁾, revealing a spatial range from 98 dB to 137 dB . Notably, the average **SINR** value tends to be closer to the higher limit than the lower range, reaching an average **SINR** of 120.5 dB based on 121 uniformly distributed test points over the communication floor. Despite the

Table 6.2: Designed parameters of FSE

Parameter Description	Value
Number of freeform surface elements, N_{FSE}	4
Refractive index (PMMA), n	1.49
Semi diameter, r_f	3.78 mm
FSE height, h_{FDR}	4.76 mm
Front surface clear aperture, d_f	7.56 mm
Freeform front surface radius of curvature, c_f	6.609 mm
Back surface radius of curvature, c_b	6.702 mm
Back surface aperture stop diameter, d_b	2.64 mm
Obtained field-of-view, ψ_F	$28.9^\circ \times 28.9^\circ$

presence of weak signal strength, the proposed design suggest remarkably high **SINR** (achieving 98 dB) at the centre of the room. In Figure 6.12b, a comparison of **SINR** performance along the y -axis for various **VLC** receivers is presented. The figure illustrates that, at each test point along the y -axis, proposed FDR consistently outruns the existing **VLC** receivers. Furthermore, the least **SINR** value noted in this work surpasses the maximum **SINR** reported in other existing studies.

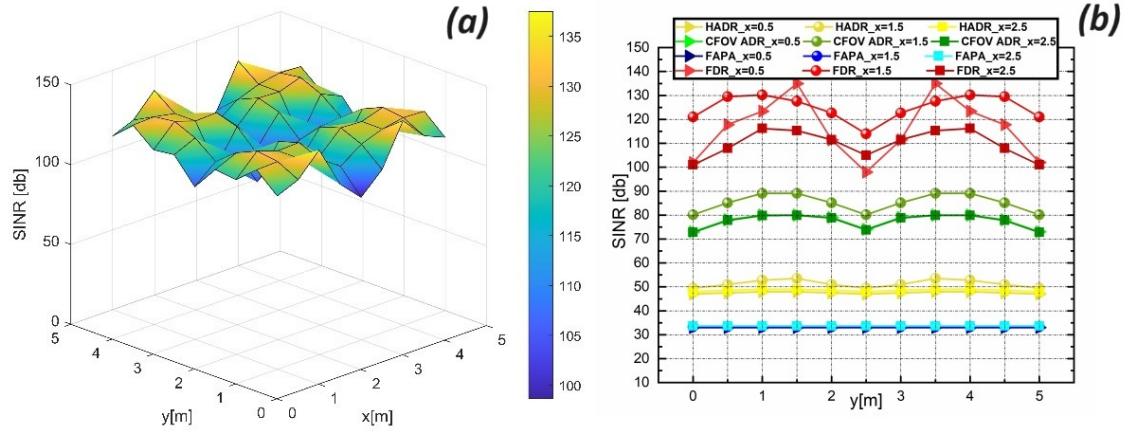


Figure 6.12: (a) Distribution of SINR over CF (using FDR) (b) Comparison of SINR along the y -axis (using different receivers)

6.5 SUMMARY

This chapter focuses on addressing the spatial **SINR** fluctuations in a multi-cell MIMO-VLC system, particularly when employing a hemispheric angular diversity receiver for the reception. These fluctuations arise from the random rotation angles introduced by end-users. A comprehensive optimization of the receiver's FOV and inclination angle is conducted to con-

fine **SINR** variations within a significant threshold. The SBC scheme is implemented to select the relevant MIMO system channel during reception. Additionally, an enhanced iteration of the ADR is devised, incorporating a freeform surface. This novel receiver, termed the Freeform Diversity Receiver (FDR), boasts a more compact size and demonstrates improved **SINR** performance. The development of the FDR is a joint effort in conjunction with SENSE, IIT Delhi and the outcome was reported in reference^(201,200,199). Although I am a contributor and co-author of those reported studies, still these works are not claimed as contributions to this thesis. However, mentioning this work is imperative as the FDR is basically an improved version of ADR and I have further carried forward this work which is reported in the next chapter.

6.6 RESEARCH OUTPUT

The findings from this chapter are reported in the following research publication:

- **Chatterjee, S.& Roy, B.** (2021). Multi-parameter optimization of a hemispheric angle diversity receiver to reduce SINR fluctuation for an indoor MIMO-VLC system. *4th Biennial International Conference on Nascent Technologies in Engineering (ICNTE)* (pp. 1-6) IEEE.
DOI: doi.org/10.1109/ICNTE51185.2021.9487694

“Most people believe the mind to be a mirror, more or less accurately reflecting the world outside them, not realizing on the contrary that the mind is itself the principal element of creation.”

Rabindranath Tagore

7

Moving Towards Hybrid Li-Fi Wi-Fi System

THE SIXTH chapter explores the showcased architecture of a hemispheric ADR and its enhanced version, the Freeform Diversity Receiver. This chapter is dedicated to the exploration of the LiFi channel model, utilizing the FDR and investigating its potential application in a hybrid LiFi-WiFi network (HLWNet) for multiple users. Section 7.2 provides the system model of the HLWNet system, offering an overview of its key components. The subsequent Section 7.3 highlights the effective user throughput under various resource allocation methods. Moving forward, Section 7.4 delves into different network parameters influencing user experience and data service quality. The intricacies of the random waypoint mobility model and scenario formulation are addressed in Section 7.5. For a more in-depth understanding, Section 7.6 meticulously presents detailed results accompanied by pertinent explanations.

7.1 INTRODUCTION

The potential of the **Li-Fi** network is poised to unfold, tapping into a frequency spectrum that is 2600 times larger, enabling enhanced cell densification in the forthcoming 6G networks^(202,104). It's important to note that while **Li-Fi** offers promising advancements, higher-tier RF technologies such as Wi-Fi are not expected to be displaced. Instead, **Li-Fi** is envisioned to complement and collaborate with Wi-Fi, introducing a new layer of network heterogeneity for improved overall performance.

Despite its numerous benefits, this technology may face certain challenges. (a) Co-channel interference (CCI) can arise from signal reception from multiple access points (AP) in a multiple-input multiple-output (MIMO) or multiple-input single-output (MISO) framework. (b) Light path blockage poses a significant disruption to **Li-Fi** standalone connectivity. (c) User

mobility can also impact network performance. To address these issues, various research attempts have been undertaken in recent years. A careful review reveals two major research directions to mitigate these challenges. In one direction, researchers propose enhanced transmitter and receiver architectures such as angle-diversity-transmitter (ADT), angle diversity receiver (ADR), freeform diversity receiver (FDR)^(203,204,205,93,99,91,197,206,201), aiming to improve SINR and mitigate CCI for standalone VLC/Li-Fi systems. On the other hand, problems like light path blockage, user mobility, multi-user association, and network performances are approached as completely different problems where different resource allocation algorithms are applied for an HLWNet considering simple receiver architecture^(207,111,115,208,209,108). However, for future commercialization and use in handheld gadgets, integration of bespoke optical components is the need of the hour⁽¹⁰⁴⁾.

7.2 SYSTEM OVERVIEW

This heterogeneous network employs a noninterfering asymmetric topology, with the down-link and uplink of Li-Fi being facilitated through VLC and infrared, respectively. It has been assumed that the channel state information (CSI)^(210,211) feedback is there but its detailed architecture is beyond the scope of this study. This section provides a concise overview of both Li-Fi and Wi-Fi channel models. Subsequently, an illustration of the system's channel capacity and LOS path blockage is provided.

7.2.1 LiFi CHANNEL MODEL WITH FREEFORM DIVERSITY RECEIVER

In FDR, four identical co-planar receiving units (RU) are placed together in orthogonal orientation with adjacent units as shown in Figure 7.1. Each RU is comprised of a freeform lens called freeform surface element (FSE) and one photodiode packed within a hollow cylindrical base. The architecture of the FDR has already been discussed in last Chapter. However, in

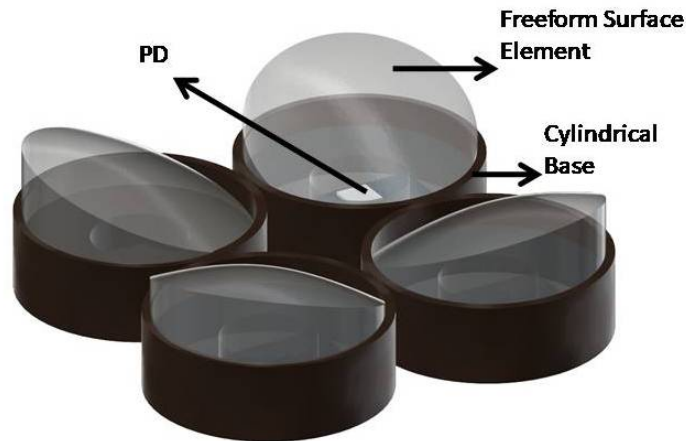


Figure 7.1: FDR structure

Algorithm 1: Computation of FDR Indicator Matrix

Data:

Input the position of i^{th} AP & j^{th} RU position on Communication floor

Result:

Elements of FDR indicator matrix h_{ji}

```

while modulo of  $\left(\frac{i}{2}\right) \neq 0$  do
  if  $\hat{\theta}_{j,i} \leq \left(\frac{\hat{\theta}_W + \hat{\theta}_L}{2}\right)$  then
     $\hat{x}_j^i = h_{CF} \tan \Psi_W$ ;
     $\hat{y}_j^i = h_{CF} \tan \Psi_W \tan \left(\hat{\theta}_{j,i} - \hat{\theta}_W\right)$ ;
  else
     $\hat{x}_j^i = h_{CF} \tan (\Psi_L) \tan \left(\hat{\theta}_W - \hat{\theta}_{j,i}\right)$ ;
     $\hat{y}_j^i = h_{CF} \tan (\Psi_L)$ ;
  end
end
end
while modulo of  $\left(\frac{i}{2}\right) = 0$  do
  if  $\hat{\theta}_{j,i} \leq \left(\frac{\hat{\theta}_W + \hat{\theta}_L}{2}\right)$  then
     $\hat{x}_j^i = h_{CF} \tan (\Psi_W) \tan \left(\hat{\theta}_{j,i} - \hat{\theta}_W\right)$ ;
     $\hat{y}_j^i = h_{CF} \tan (\Psi_W)$ ;
  else
     $\hat{x}_j^i = h_{CF} \tan \Psi_W \tan \left(\hat{\theta}_{j,i} - \hat{\theta}_W\right)$ ;
     $\hat{y}_j^i = h_{CF} \tan \Psi_W$ ;
  end
end
end
  Compute  $\hat{\psi}_{j,u}^i$ ; Compute  $\psi_{j,i}$ ; Compute  $\phi_{j,u}^i$ 
  if  $\psi_{j,i} \leq \phi_{j,u}^i$  then
     $h_{ji} = 1$ ;
  else
     $h_{ji} = 0$ ;
  end
end

```

Table 7.1: FDR indicator matrix parameters definition

N_{AP}	Number of total Li-Fi APs
Γ_{AP}^i	Position of i^{th} AP on xy plane
P_{RU}	Centre position of RU on communication floor
\bar{P}_{RU}	The projection of RU on xy plane (APs plane)
M_{RU}	Number of total RUs
r_f	Semi-diameter of RU
d_d	Distance between P_{RU} and P_{FDR}
$\Psi_L \times \Psi_W$	Quadrilateral FOV of the RU (side of the quadrilateral field making angle with optic axis)
$\widehat{\Psi}$	The projection of FOV of j^{th} RU on the xy plane (APs plane)
$\widehat{\theta}_{j,i}$	Angle between positive x -axis and the line connecting Γ_{AP}^i & \bar{P}_{RU} in xy plane
$\widehat{\psi}_{j,u}^i$	Intersection (x_j^i, y_j^i) point between the side of $\widehat{\Psi}$ and the line connecting Γ_{AP}^i & \bar{P}_{RU} in x - y plane
$\phi_{j,u}^i$	Angle between z -axis and the line connecting Γ_{AP}^i & P_{RU}
$\psi_{j,i}$	Angle between z -axis and the line connecting $\widehat{\psi}_{j,u}^i$ & P_{RU}

order to estimate the performance of this newly surfaced receiver front-end in HLWnet configuration, a proper channel model is required. It has to be noted that the FDR is endowed with a rectangular off-axis FOV ($\Psi_L \times \Psi_W$) instead of a symmetric FOV which is extensively considered in the existing **Li-Fi** channel model. So, in this section, the thrust is given in framing a mathematical framework for the **Li-Fi** channel model using FDR. Due to the off-axis nature, each RU has a distinct azimuthal field in $x - y$ plane bounded by $\widehat{\theta}_L$ and $\widehat{\theta}_W$. This is shown in Figure 7.2. With respect to FDR global position $(x_{FDR}, y_{FDR}, h_{CF})$, coordinates of the j^{th} RU (x_j, y_j, z_j) can be determined as:

$$x_j = x_{FDR} + d_d \cos \left(\frac{\widehat{\theta}_L + \widehat{\theta}_W}{2} \right) \quad (7.1a)$$

$$y_j = y_{FDR} + d_d \sin \left(\frac{\widehat{\theta}_L + \widehat{\theta}_W}{2} \right) \quad (7.1b)$$

$$z_j = h_{CF} \quad (7.1c)$$

where,

$$\widehat{\theta}_W = \frac{360}{M_{RU}}(j - 1) \quad (7.2a)$$

$$\widehat{\theta}_L = \frac{360}{M_{RU}}(j) \quad (7.2b)$$

In the multi-user MIMO environment, all users are equipped with more than one RUs and can access optical signals from multiple **Li-Fi** APs. Now, for the u^{th} user connected with i^{th} AP and receiving a signal using j^{th} RU of FDR, the LOS channel gain can be determined

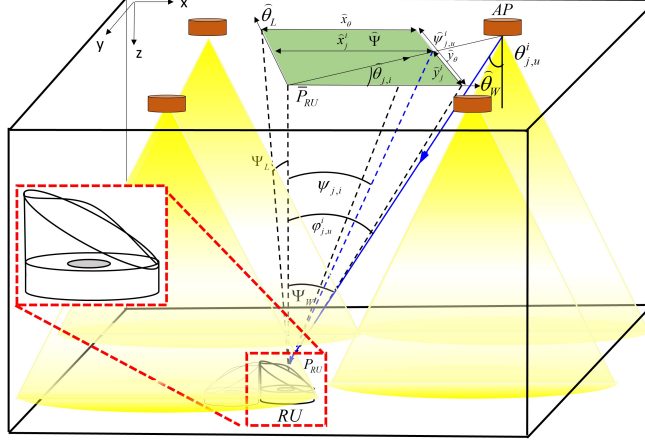


Figure 7.2: LiFi channel and Off-axis quadrilateral FoV of FDR

as:

$$H_{LiFi}^{i,j,u} = \frac{m+1}{2\pi(d_{j,u}^i)^2} \cos^m(\theta_{j,u}^i) \cos(\phi_{j,u}^i) g_c g_f A_{PD} \mathbb{I}_{FDR}(j, i) \quad (7.3)$$

here, $\theta_{j,u}^i$ is the irradiance angle. The optical concentration gain and transmittance of the optical filter are represented by g_c and g_f . $\mathbb{I}_{FDR}(j, i)$ is an element of the indicator matrix that represents the viewing condition of j^{th} RU connected with i^{th} Li-Fi AP. Each element (b_{ji}) of the indicator matrix (\mathbb{I}_{FDR}) is a binary variable and analogous to the rectangular function used in a conventional channel model with symmetrical FOV. The computational procedure of \mathbb{I}_{FDR} is given in Algorithm 1 and Table 7.1 defines the necessary related parameter description.

In general, considering simple PD receivers, the contribution from second and higher-order reflection is very small. In the case of FDR this value reduces further due to off-axis controlled FOV. So, only the first-order reflection is considered to calculate NLOS channel gain. The first-order channel gain can be segmented into two distinct parts A) AP to a very small part of the wall B) Wall to RU of FDR. For the first segment, ie from AP to wall, angle of irradiance & angle of incidence are θ_w^i & ϑ_w^i . Similarly, for 2^{nd} segment, these angles are $\vartheta_{j,u}^w$ and $\phi_{j,u}^w$ respectively. Now the NLOS channel gain is expressed as:

$$H_{NLOS}^{i,j,u} = \int_{A_W} \frac{\rho_W(m+1)}{2(\pi d_w^i d_{j,u}^w)^2} A_{FSE} \cos^m(\theta_w^i) g_f g_c \cos(\vartheta_w^i) \cos(\vartheta_{j,u}^w) \cos(\phi_{j,u}^w) dA_W \quad (7.4)$$

here A_W denotes the area of wall within the rectangular FOV of a specific RU. d_w^i and $d_{j,u}^w$ are the Euclidean distance between i^{th} AP to small patch of wall and wall to j^{th} RU of user u. The total channel gain of the LiFi system is computed as:

$$H_{LiFi}^{i,j,u} = H_{LOS}^{i,j,u} + H_{NLOS}^{i,j,u} \quad (7.5)$$

So, the received optical power by j^{th} RU of user u is determined as:

$$P_{rx}^{i,j,u} = H_{LiFi}^{i,j,u} P_{tx}^i \quad (7.6)$$

Considering, a frequency-independent constant optical to electrical conversion efficiency, the **SINR** due to i^{th} **Li-Fi** AP experienced by user u can be computed as follows:

$$\eta_{LiFi}^{i,u} = \max_j \left(\frac{\left(\gamma_{oe} P_{rx}^{i,j,u} \right)^2}{\sum_{i' \in I_{AP}, i' \neq i} \left(\gamma_{oe} P_{rx}^{i',j,u} \right)^2 + N_{total}} \right) \quad (7.7)$$

7.2.2 WiFi CHANNEL MODEL

In this study, only one RF channel is used. So, the **CCI** is zero for obvious reasons. However, the downlink transmission spectrum can be divided into more than one non-overlapping sub-channels to accommodate all WiFi/RF APs without any **CCI**. From the previous study, it is well established that the WiFi channel gain mainly depends on large-scale and small-scale fading loss. However, the dominance of large-scale fading loss is more compared to small-scale fading gain that follows an identical Rayleigh distribution with a variance of 2.46 dB^(2.12).

The WiFi channel gain, at the centre frequency f_c can be modelled as^(2.12),

$$G_{i,u}(f_c) = \sqrt{10^{(-0.1L(d_{i,u}))}} h_r \quad (7.8)$$

here,

$L(d_{i,u})$ = Large scale fading gain for a user u with separation distance $d_{i,u}$

h_r = Small scale fading gain

The Large scale fading gain is computed as:

$$L(d_{i,u}) = \begin{cases} L_{FS}(d_{i,u}) + X_{SF} & \text{when } d_{i,u} < d_{BP} \\ L_{FS}(d_{BP}) + 35 \log \left(\frac{d_{i,u}}{d_{BP}} \right) + X_{SF} & \text{when } d_{i,u} \geq d_{BP} \end{cases} \quad (7.9)$$

Here $L_{FS}(d)$ is the free space path loss for a distance d , given as:

$$L_{FS}(d) = 20 \log_{10}(d) + 20 \log_{10}(f_c) - 147.5 \quad (7.10)$$

X_{SF} is the shadowing loss modeled as a random variable with Gaussian distribution, mean zero and standard deviation σ_s . Here, d_{BP} is the breakpoint distance. Since no interference for RF is encountered; the **SINR** is analogous to SNR and it can be defined as follows:

$$\eta_{WiFi}^{i,u} = \frac{|G_{i,u}(f_c)|^2 P_{tx}^{WiFi}}{N_{WiFi} B_{WiFi}} \quad (7.11)$$

7.2.3 CHANNEL CAPACITY

In general, the channel capacity of any RF and LiFi communication system can be bounded by Shannon's principle. However, in the case of LiFi system, high-speed reliable communication is not the only design criterion. The same optical transmitters are also used for lighting purposes as well. So, energy-efficient quality illumination design is the other lookout that can be achieved when required horizontal illuminance with high overall uniformity is obtained as per standard, that too with reduced lighting power density. In the presence of daylight or depending on the user's activity, dimming of light sources is quite a common strategy to save energy. In that case, tighter bounds on channel capacity may be considered for lower transmitted power⁽²¹³⁾. When the user u is connected with i^{th} AP, the channel capacity is determined as:

$$r_{i,u} = \begin{cases} B_{WiFi} * \log_2 (1 + \eta_{WiFi}^{i,u}) & \text{for WiFi AP} \\ \frac{B_{LiFi}}{2} * \log_2 \left(1 + \frac{e}{2\pi} \eta_{LiFi}^{i,u}\right) & \text{for LiFi AP} \end{cases} \quad (7.12)$$

7.2.4 LOS PATH BLOCKAGE

In reality, the LOS path of the LiFi channel can be blocked by some non-transparent objects like furniture, appliances, or human bodies. The probability of LOS path blockage increases when the users are in motion inside the indoor environment. In this study, FDR is considered as a LiFi-receiving front-end where more than 99% of received optical power comes by LOS path. This occurs due to customized receiver design using freeform optics. So, hardly any connectivity exists with the corresponding AP if the LOS path is blocked. Thus it can be modeled with a binary variable, $O_{i,u}^{(k)}$. Two parameters are considered to characterize this random event, a) occurrence rate and b) occupation rate^(111,207). The frequency of light-path blockage is defined by the first parameter. A high occurrence rate often leads to an increase in the handover number while the second parameter impedes the link status. The occupation rate determines how long the blockage will persist. As the blockage is unpredictable and random in nature the Poisson point process (PPP) is preferred to mathematically model this event.

7.3 MOBILITY MODEL AND SCENARIO

7.3.1 RANDOM WAYPOINT MODEL

Random Waypoint (RWP) mobility model^(214,215) has been adopted in this study where users move in a random direction through a straight path from the starting node ($P_{n_{wp}-1}$) to the end or destination node ($P_{n_{wp}}$). Each destination node is considered as the starting node for the next waypoint. A random pause time ($T_{pause}^{n_{wp}}$) is also considered at the end node. Hence, mathematically the RWP model is characterized by an infinite chain of quadruple: $\{(P_{n_{wp}-1}, P_{n_{wp}}, S_{n_{wp}}, T_{pause}^{n_{wp}}) | n_{wp} \in \mathbb{N}_{wp}\}$. Here, n_{wp} is the movement index and $S_{n_{wp}}$ denoted as speed for the n_{wp}^{th} movement. The coordinates of all the successive waypoints are selected

randomly within the network area. The transition time for each movement can be computed as,

$$T_{tran}^{n_{wp}} = \frac{d_{n_{wp}}}{S_{n_{wp}}} \quad (7.13)$$

where,

$$d_{n_{wp}} = \|P_{n_{wp}-1} - P_{n_{wp}}\| \quad (7.14)$$

Now, considering the pause time, the total elapsed time between two consecutive waypoints is given by:

$$T_{total}^{n_{wp}} = T_{tran}^{n_{wp}} + T_{pause}^{n_{wp}} \quad (7.15)$$

7.3.2 SCENARIO FORMULATION

A uniform distribution with an upper ($S_{n_{wp}}^{max}$) and lower limit ($S_{n_{wp}}^{min}$) is considered in this study to estimate the speed of the users within the simulation environment. Based on the user's speed and pause time, four different scenarios have been sketched out. Out of these four scenarios, three scenarios are framed with constant user speed while the remaining one attains variable user speed and pause time.

SCENARIOS WITH CONSTANT USER SPEED

Three scenarios have been considered in this mode: a) Low mobility scenario (*ScenLM*) b) Average mobility scenario (*ScenAM*) c) High mobility scenario (*ScenHM*). For all these scenarios, every user moves at a constant speed with a fixed pause time. The upper and lower limits of $S_{n_{wp}}$ are kept at a fixed value in these scenarios to fit with the mobility model. A speed of 0.1 m/s has been considered for *ScenLM*. In cases of *ScenAM* and *ScenHM* the user's speed is 0.5 m/s and 0.8 m/s respectively.

SCENARIOS WITH VARIABLE USER SPEED

Random mobility scenario (*ScenRM*) has been framed within this category where users can move with variable speed. However, during each excursion, the speed of any user remains constant for a short period. The maximum speed ($S_{n_{wp}}^{max}$) is set at 0.8m/s where the minimum speed ($S_{n_{wp}}^{min}$) is kept at 0.1m/s. The upper and lower limit of pause time ($T_{pause}^{n_{wp}}$) is considered as 0 and 10 second respectively.

7.4 DISTRIBUTED RESOURCE ALLOCATION

In a dynamic HLWNet, the mobile/stationary user is either connected to Wi-Fi or served by **Li-Fi** AP for each quasi-static state. So, proper utilization of distributed APs with multi-node receiver structures is always a challenging task. Throughout this chapter, single-AP association is considered and it has been assumed that the channel state information remains the same in between two quasi-static states. Two different resource allocation strategies have been implemented to compute both the system throughput and average user throughput.

7.4.1 MAXIMIZING SYSTEM THROUGHPUT WITH OPTIMAL RESOURCE ALLOCATION

The prime objective of the optimal resource allocation (ORA) policy is to maximize the overall system throughput. This technique is also known as the conventional load-balancing technique^(215,216). Let c denote the type of network connectivity for a user. At k^{th} quasi-static state the total system throughput ($\mathbb{R}_{sys}^{(k)}$) is computed as:

$$\mathbb{R}_{sys}^{(k)} = \sum_c \chi_{c,u}^{(k)} \sum_{u \in U_i} \sum_i r_{i,u}^{(k)} \chi_{i,u}^{(k)} z_{i,u}^{(k)} O_{i,u}^{(k)} \quad (7.16)$$

here, $\chi_{c,u}^{(k)} = 1$ signifies that network type c serves the user u while $\chi_{c,u}^{(k)} = 0$ means otherwise; Likewise $\chi_{i,u}^{(k)} = 1$ means that the user u is served by the i^{th} AP. $O_{i,u}^{(k)}$ is the blockage indicating binary variable that accept a value 0 when the u^{th} user's connectivity is lost with the i^{th} AP. $z_{i,u}^{(k)}$ is the proportion of time that the i^{th} AP allocates to user u . Now, the proportional resource allocation method is adopted where the AP connectivity variable (χ) and the proportion of time variable (z) for each user are determined by solving a mixed integer optimization problem. The optimization problem is framed as:

$$\begin{aligned} & \text{maximise } \mathbb{R}_{sys}^{(k)} \\ & \text{subject to } \chi_{i,u}^{(k)} \in \{0, 1\}, \forall i, u; \\ & O_{i,u}^{(k)} \in \{0, 1\}, \forall i, u; \\ & \chi_{c,u}^{(k)} \in \{0, 1\}, \forall c, u; \\ & \sum_i \chi_{i,u}^{(k)} = 1, \forall u; \\ & \sum_u \chi_{i,u}^{(k)} z_{i,u}^{(k)} \leq 1, \forall i; \end{aligned} \quad (7.17)$$

7.4.2 RULE BASED RESOURCE ALLOCATION (RBRA)

Effective resource management is the key to exploiting the maximum benefits of a heterogeneous network. The achievable system throughput not only depends on the efficiency of the resource allocation algorithm but is also influenced by the distribution of **Li-Fi** APs and receiver geometry. Existing resource allocation techniques always consider symmetric FOV single PD receivers. Thus, frequent handover occurs when users walk in and out at overlapping zones of **Li-Fi** attocells. Interestingly, this area of overlapping zone depends on **Li-Fi** AP distribution and also with their radiation pattern. The probability of handover increases with the rise in overlapping zones. Here, all **Li-Fi** APs are configured in such a way that they can accomplish the lighting requirement as per ISO standard. However, the other influencing parameter (receiver geometry) is customized in this study. As FDR is endowed with off-axis rectangular FOV instead of symmetrical FOV, the overlapping region reduces substantially from the receiver's perspective. Thus the ping-pong effect of handover is relatively less. Maximum handover occurs as a consequence of the mixed integer non-linear optimization process described in the previous section.

In contrast with ORA, the rule-based resource allocation (RBRA) technique doesn't go for throughput maximization instead it looks for limiting the handover number and computational complexity. A simple rule-based policy has been adopted where each user is initially connected to an AP with the best channel capacity. Both the horizontal and vertical handover occur following the signal strength strategy with an exception. When the WiFi channel is unoccupied, then only some user switches to WiFi to exploit the entire bandwidth of the LiFi-WiFi network. The detailed scheme is illustrated through Algorithm 2.

Algorithm 2: Rule Based Resource Allocation Scheme

Input: $r_{i,u}, O_{i,u}$
Output: $\chi_{i,u}, z_{i,u}$

- 1: Initialization
 - for** each user u **do**
 - find the AP corresponds to maximum $r_{i,u} O_{i,u}, i \in I$
 - $\chi_{j,u} \leftarrow 0 \quad \forall j \neq i$
 - $\chi_{i,u} \leftarrow 1$
 - end for**
- 2: Compute total no. of user N_U^i connected to i^{th} AP
 - $\forall i \in I$
- 3: **if** $N_U^{WiFi} = 0$ and $N_U^{LiFi} > 2$ **then**
 - find the LiFi AP ($i^{LiFi} = \tilde{i}$) with maximum host association
 - end if**
- 4: Identify the user ($u = \tilde{u}$) with maximum $r_{i,\tilde{u}}$
- 5: Switch the user (\tilde{u}) to WiFi AP
 - $\chi_{\tilde{i},\tilde{u}} \leftarrow 0$
 - $\chi_{i^{WiFi},\tilde{u}} \leftarrow 1$
- 6: **for** each user u **do**
 - Compute $z_{i,u} = 1/N_U^i$
 - end for**
- 7: **return** $\chi_{i,u}, z_{i,u} \quad \forall u$

7.4.3 USER THROUGHPUT

Depending upon the resource allocation techniques described in the above sections both vertical and horizontal handover may occur in two neighbouring quasi-static states. As a result, the effective throughput of all the users and the system are reduced further. Considering the horizontal (t_{HHO}) and vertical handover (t_{VHO}) overhead, the handover efficiency $\zeta_{i,u}^{(k)}$ is calcu-

lated as⁽²¹⁵⁾:

$$\zeta_{i,u}^{(k)} = \begin{cases} \left(1 - \frac{t_{HHO}}{T_{qs}}\right)^+ & \text{for HHO} \\ \left(1 - \frac{t_{VHO}}{T_{qs}}\right)^+ & \text{for VHO} \\ 1 & \text{otherwise} \end{cases} \quad (7.18)$$

here, the function $[\cdot]^+$ correspond to $\max(\cdot, 0)$. Now, incorporating the handover delay, the average user throughput can be estimated as:

$$\mathbb{R}_u^{avg} = \frac{1}{N_k N_U} \left[\sum_k \sum_{u \in U} \mathbb{R}_{i,u}^{eff} \right] \quad (7.19)$$

here, N_k is the total no. of iterations within a specific simulation interval and $\mathbb{R}_{i,u}^{eff}$ denotes the effective user data rate in k^{th} quasi-static state given as:

$$\mathbb{R}_{i,u}^{eff} = r_{i,u}^{(k)} \min \left(z_{i,u}^{(k)}, \zeta_{i,u}^{(k)} \right) \quad (7.20)$$

Aggregating all the user throughput associated with different transmitting nodes, the effective system throughput is computed by:

$$\mathbb{R}_{sys}^{eff} = \sum_c \chi_{c,u}^{(k)} \sum_{u \in U_i} \sum_i r_{i,u}^{(k)} \chi_{i,u}^{(k)} \min \left(z_{i,u}^{(k)}, \zeta_{i,u}^{(k)} \right) O_{i,u}^{(k)} \quad (7.21)$$

7.5 HLWNET QUALITY OF SERVICE

Apart from system throughput, maintaining high quality in data traffic is essential for delivering a satisfactory user experience concerning accuracy, completeness, timeliness, and resource allocation. In different real-time communication and network applications, quality of service (QoS) encompasses these issues with regard to latency, throughput, packet loss, and jitter. In this study, the network performance of our proposed HLWNet framework is also investigated with FDR in terms of packet loss ratio, latency, and fairness index.

7.5.1 PACKET LOSS RATIO

Packet loss refers to the failure of one or more data packets to reach their destination within any communication network. Packet loss may occur due to overflow of buffer and also for network congestion. In a temporary overload situation, packets may be dropped to alleviate the congestion and prioritize other traffic. In the present study, the network may be degraded or congested due to light-path blockage or frequent handover. So, investigating the system performance at the packet level is very important to have a clear understanding. It has been assumed that the packet arrival (λ) follows a Poisson process as in the case of an $M/M/1$ queueing system.

Let us consider $R_{i,u}^A$ denotes the data arrival rate of the user u connected with i^{th} AP (Li-Fi/WiFi) and $R_{i,u}^{eff}$ represents the effective link capacity. For any quasi-static state k , the effective link capacity of any user is obtained from Eq.7.20. Considering the effective link capacity, user u needs time $\tau_{i,u}$ to receive $R_{i,u}^A$ bits, given as:

$$\tau_{i,u} = R_{i,u}^A / R_{i,u}^{eff} \quad (7.22)$$

The packet-loss ratio (Υ_i) of every users connected with i^{th} AP are equal⁽¹⁴⁾,

ie ($\Upsilon_{u_1,i} = \Upsilon_{u_2,i} = \dots = \Upsilon_{u_n,i}$) and it is given by:

$$\Upsilon_i = \max \left(1 - \frac{L_B}{L_B + L_P} \left(\sum_{u \in U_i} \tau_{i,u} \right)^{-1}, 0 \right) \quad (7.23)$$

here L_B is the buffer size and L_P is the average packet size of the received data. The average packet loss ratio of our proposed LiFi system may be computed as:

$$\Upsilon_{sys} = \frac{\sum_i \Upsilon_i \left(\sum_{u \in U_i} R_{i,u}^A \right)}{\sum_i \sum_{u \in U_i} R_{i,u}^A} \quad (7.24)$$

7.5.2 LATENCY

Considering all the users connected with i^{th} AP, the net data arrival rate associated with the same AP can be expressed as:

$$\lambda_i = \frac{1}{L_P} \sum_{u \in U_i} R_{i,u}^A \quad (7.25)$$

Now, the service rate S_i can be calculated as:

$$S_i = \frac{\lambda_i}{\sum_{u \in U_i} \tau_{i,u}} \quad (7.26)$$

If L_W is the average size of data waiting for service (only when L_W is less than the buffer size) then the packet latency of i^{th} AP can be computed as:

$$\Gamma_i = L_W \frac{\sum_{u \in U_i} R_{i,u}^A}{\sum_{u \in U_i} R_{i,u}^{eff} R_{i,u}^A} \quad (7.27)$$

where L_W is calculated as:

$$L_W = L_P \frac{\lambda_i}{S_i - \lambda_i} = \frac{L_P}{\left(\sum_{u \in U_i} \tau_{i,u} \right)^{-1} - 1} \quad (7.28)$$

The above expression is only valid when the service rate is greater than the arrival rate. For the sake of computation, the above equation can be restructured as:

$$L_W = \frac{L_P}{\max \left(\left(\sum_{u \in U_i} \tau_{i,u} \right)^{-1} - 1, 0 \right)} \quad (7.29)$$

The average value of latency encountered by all the users allocated with different APs is computed as:

$$\Gamma_{sys}^{avg} = \frac{\sum_i \Gamma_i \left[(1 - \Upsilon)_i \sum_{u \in U_i} R_{i,u}^A \right]}{\sum_i \left[(1 - \Upsilon)_i \sum_{u \in U_i} R_{i,u}^A \right]} \quad (7.30)$$

7.5.3 FAIRNESS INDEX

In a hybrid LiFi-WiFi network, optimized resource allocation may improve the overall system throughput but often it fails to look after the user's interest to maximize their individual benefits that can be quantitatively assessed by determining Jain's fairness index. However, allocating all the users with indistinguishable benefits may reduce the system throughput. So, always there exists a trade-off between system throughput and Jain's index⁽²¹⁷⁾. In order to evaluate the effectiveness of ORA and RBRA with our proposed system, the Jain's Fairness Index is also determined in this work. It is given as:

$$JF = \frac{\left(\sum_{u=1}^{N_u} R_{i,u}^{eff} \right)^2}{N_u \sum_{u=1}^{N_u} \left(R_{i,u}^{eff} \right)^2} \quad (7.31)$$

7.6 RESULTS AND ANALYSIS

An indoor environment with 25 m^2 of floor area, 4 **Li-Fi** APs, and one **Wi-Fi** AP is considered in this study. For simplification, the optical reuse factor for each LiFi AP is taken as 1. Within the network space, multiple moving users (4 to 14) are connected with the HLWNet. This is further considered that each user is equipped with FDR & height of the communication floor (b_{CF}) is 0.8m from the floor. Considering the scenarios mentioned in Section 5, Monte Carlo

Table 7.2: HLWNet Simulation Parameters

Parameters	Value
Dimension of network space, $(L \times W \times H)$	$5m \times 5m \times 3m$
Transmitted power (WiFi AP), P_{tx}^{WiFi}	$20dBm$
Transmitted optical power (LiFi AP), P_{tx}	$4.22W$
Area of each PD at RU, A_{PD}	1 cm^2
Optical concentrator gain (FSE), g_c	8.36
Responsivity of detector, γ_{pe}	$0.53A/W$
Transmission coefficient of optical filter, g_f	1
Rectangular FOV of RU, $(\Psi_L \times \Psi_W)$	$28.9^\circ \times 28.9^\circ$
Duration of quasi-static state, T_q	$1s$
Horizontal handover overhead, t_{HHO}	$300ms$
Vertical handover overhead, t_{VHO}	$500ms$
PSD of noise in WiFi, N_{WiFi}	$-174dBm/Hz$
Optical Bandwidth (LiFi), B_{LiFi}	$40MHz$
RF Bandwidth (WiFi), B_{WiFi}	$20MHz$
Buffer size, L_B	$128KB$
Average packet size, L_P	$1KB$

simulations are performed with 2-minute simulation time for each iteration. The remaining parameters are listed in Table 7.2.

7.6.1 SINR DISTRIBUTION

Due to its excellent **SINR** performance and compact nature, FDR is used in this study as a **Li-Fi** signal-receiving front-end. As 4 **Li-Fi** AP along with 4 RU is considered (MIMO configuration), I have followed SSS technique at (21×21) grid points to estimate the **Li-Fi SINR**. The **SINR** distribution for both **Li-Fi** and Wi-Fi connectivity is shown in Figure 7.3. Despite having multiple **Li-Fi** APs and their associated **CCI**, it can be observed that in terms of average spatial **SINR**, LiFi with FDR can provide more than 2 times better performance.

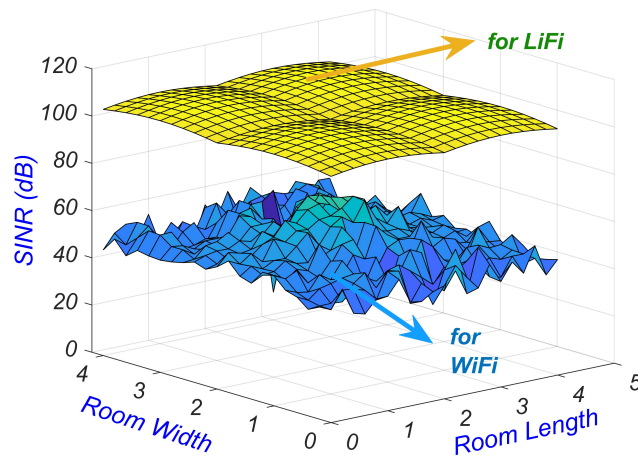


Figure 7.3: SINR distribution

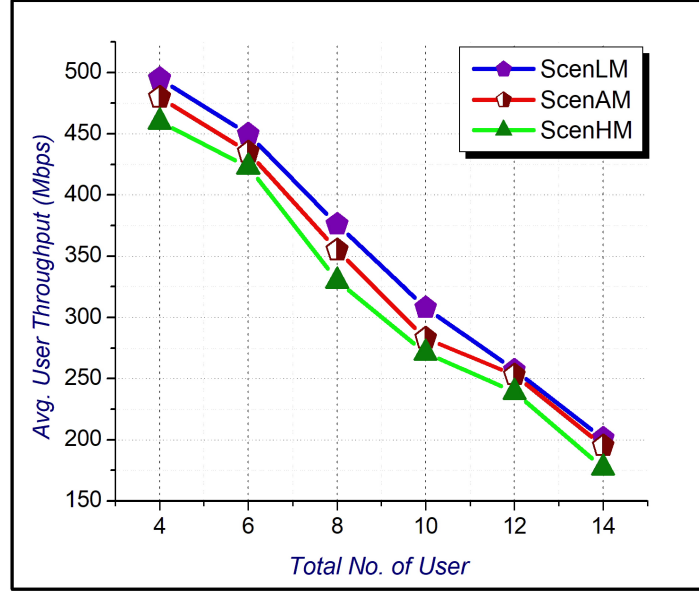


Figure 7.4: Effect of increasing no. of user on average user throughput

7.6.2 EFFECT OF NO. OF USERS

In Figure 7.4, the average user throughput is plotted against an increasing number of users when there is no LOS blockage. Three specific observations have been noticed considering three different mobility scenarios and optimal resource allocation. First, the average user throughput gradually decreases irrespective of mobility scenario with an increase in the number of users from 4 to 14. When $N_U = 4$, near about 500 Mbps average throughput is observed for *ScenLM*. However, with the increased number of users, resource sharing increases which in turn reduces the value of the proportion of time variable illustrated in Sec 3. Still, more than 200 Mbps average user throughput is ensured (when $N_U = 14$) for *ScenLM* scenario. Second, around 7 to 12 % reduction in the average user throughput can be observed with higher user speed (*ScenHM*). This occurs due to the increasing number of handovers. Finally, the overall system throughput improved gradually with the increase in N_U . When N_U is small, often all the LiFi APs are not connected with at least one user. This occurs due to the off-axis nature of FDR-receiving units in pursuit of less CCI. As a result, some bandwidth remains unutilized. However, as the number of users increases, all APs get involved in data transmission resulting in greater utilization of resources. The overall system throughput increases from 1980 Mbps to 3094 Mbps for *ScenLM*. The maximum value of system throughput for *ScenAM* and *ScenHM* scenarios are 3030 and 2730 Mbps respectively. Considering the variable user speed and pause time (*ScenRM*) the average user throughput for different N_U is shown in Figure 7.5. A maximum 14% reduction is observed when LOS blockage is taken into consideration.

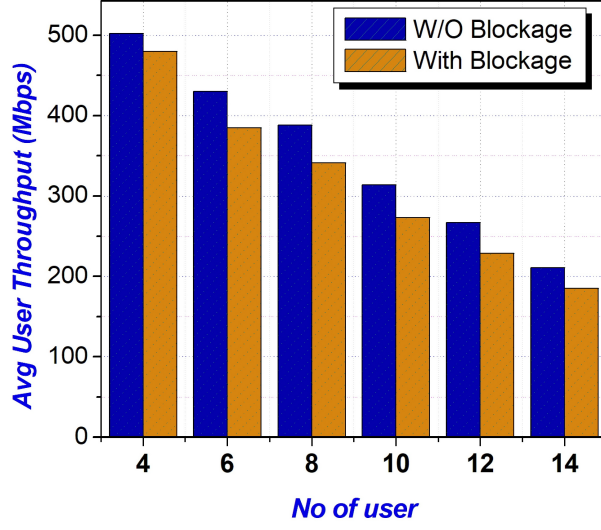
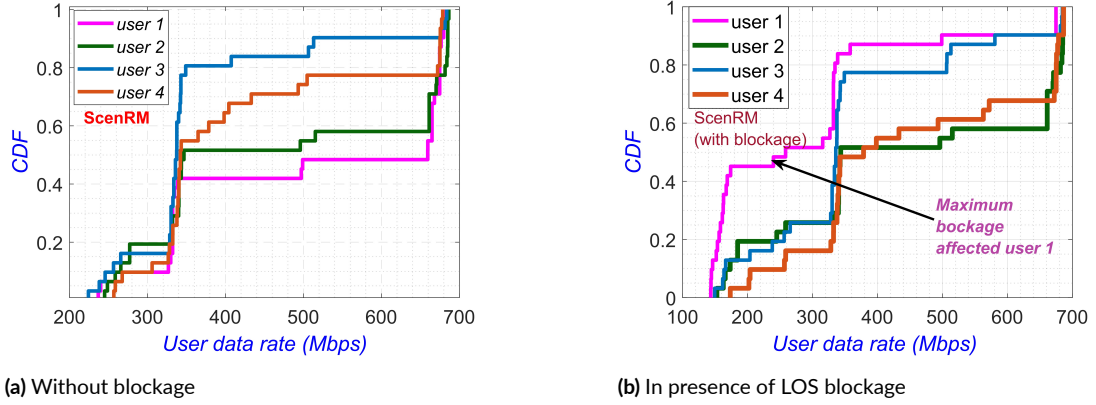


Figure 7.5: Average user throughput as a function of N_U and blockage (ScenRM)



(a) Without blockage

(b) In presence of LOS blockage

Figure 7.6: Cumulative density function of achieved user data rate for $N_U = 4$

7.6.3 IMPACT OF LOS BLOCKAGE

Any obstruction in the LOS path of the LiFi channel may temporarily degrade the network performance depending upon the fierceness of blockage. In this section, the individual user data rate with and without LOS blockage has been studied and compared. In *ScenRM* (with and without blockage) users are moving with variable speed and a gamma-distributed blockage occurrence rate. Keeping the occupation rate fixed at 0.4, the performances for a small and comparatively large number of users are investigated. ($N_U = 4, 10$). When $N_U = 4$, the CDF of the individual user's throughput is depicted in Figure 7.6. Without any LOS blockage (Figure 7.6a), user 1 (U_1) enjoys the best data rate as dissimilarity is there among different users in terms of data rate. This is due to non-uniform user distribution over the network area and optimal resource allocation at different quasi-static states. When the LOS blockage is encountered the same user (U_1) is highly affected. This is shown in Figure 7.6b. The outage probability of achieving a threshold data rate of 500 Mbps suddenly increases from 0.48 to

0.88 when blockage is encountered. However, a more than 150 Mbps data rate is always ensured for the most affected user. The rest of the users (U_2, U_3, U_4) are rarely affected by LOS blockage and at least 300 Mbps of data rate is achieved for a 70% simulation period even in the presence of blockage. However, there may be some confusion about whether U_2, U_3 , and U_4 are consistently less affected by LOS blockage. The answer is no. To calculate the average user throughput, the simulation was repeated 100 times, with the average taken across all simulations. Each simulation included 120 quasi-static states. The CDF of user data rates shown in Figure 7.6b corresponds to a single simulation instance. In other simulations, different users might experience varying levels of impact, as the occurrence of blockages is entirely random.

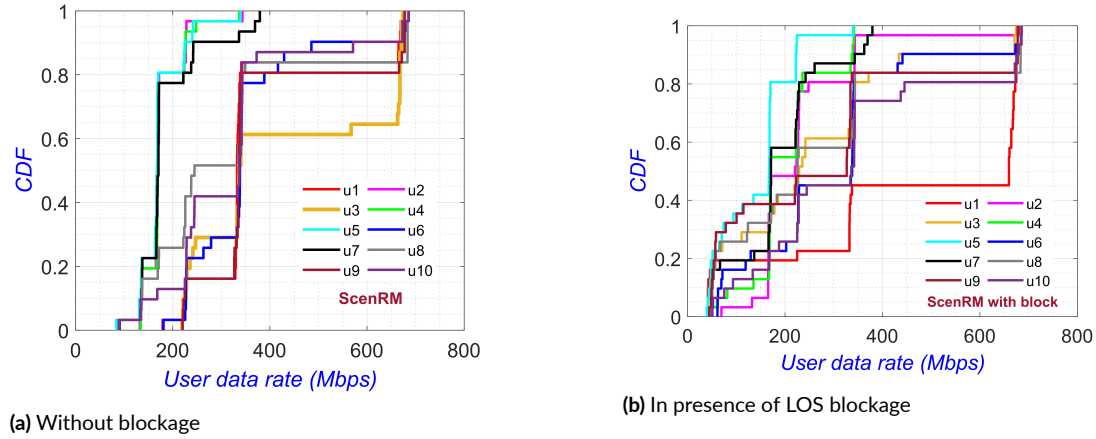


Figure 7.7: Cumulative density function of achieved user data rate for $N_U = 10$

For $N_U = 10$, the individual user performance (shown in Figure 7.7) is a bit low due to high user density and bandwidth sharing. Also, the fairness of the overall system resources is reduced compared with $N_U = 4$. This issue is separately addressed in the subsequent section. Looking closely at Figure 7.7a reveals that U_2, U_5 , and U_7 are offered with a lesser share of the overall system throughput and avail less than 200 Mbps data rate almost for the entire period. Understandably, it occurs due to the inhomogeneous clustering of allocated users with a particular access point. Figure 7.7b shows the performances of all users ($N_U = 10$) in the presence of LOS blockage. As mentioned earlier, in Figure 7.7a and Figure 7.7b the occupation rate is kept constant. Figure 7.8 depicts the impact of variable occupation rate on average user throughput. The maximum rate of degradation in average user throughput occurs when the occupation rate exceeds 0.6, ie LOS path is blocked for a prolonged period. In spite of such blockage severity, more than 300 Mbps and 180 Mbps average user throughput has been achieved for $N_U = 6$ and $N_U = 12$ respectively.

7.6.4 EVALUATION OF QUALITY OF SERVICE

The packet loss ratio is shown in Figure 7.9 as a function of the data arrival rate. Here, the total number of users with *ScenRM* is varied between 2 to 10, each with block and without blockage mode. It has been assumed that the data arrival rate is a Poisson-distributed random variable. It can be observed that the packet loss is almost zero within 150 Mbps data rate for

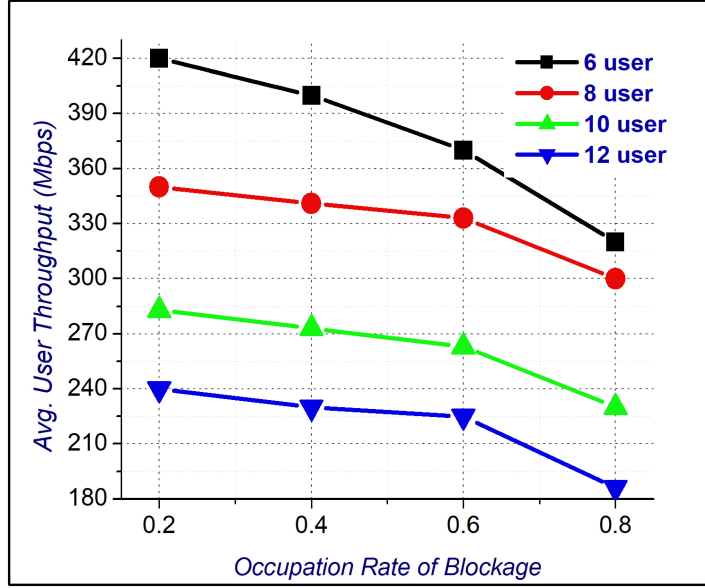


Figure 7.8: Impact of occupation rate of blockage on user throughput

$N_U = 4$. In the presence of LOS blockage maximum of 110 Mbps data arrival rate can be tackled without any packet loss. However, the packet loss increases gradually with an increase in number of users. In the presence of blockage, nearly 29% packet loss can be observed for 200 Mbps data arrival rate when $N_U = 10$. The latency for the HIWNet at different data arrival rates is presented in Figure 7.10 before it saturates. For 4 and 6 users the latency is in the order of microseconds, but for the higher number of users, it increases up to 1 milliseconds. At 200 Mbps arrival rate, latency is 1.5 ms and 2.1 ms respectively for $N_U = 10$ and $N_U = 10$.

It has to be noted that, the optimal resource allocation method has been applied so far to maximize the overall system throughput in every quasi-static state. However, if rule-based resource allocation (RBRA) is used instead of ORA, the overall data traffic quality can be improved, as illustrated in the following section.

7.6.5 QoS IMPROVEMENT WITH RBRA

This subsection validates the influence of RBRA algorithm from four different perspectives.

PACKET LOSS:

To start with, the packet loss considering RBRA is depicted in Figure 7.11. With no loss of generality, 6 and 10 users are taken as examples. In the case of 6 users, the packet loss is substantially reduced, both in the presence of LOS blockage or without blockage. The decrement with respect to ORA is shown with a vertical error bar. It can be observed that the reduction in packet loss gradually increases with the arrival rate, reaches a peak, and finally diminishes slowly. A maximum reduction of 91% is observed at 160 Mbps data arrival rate. However, in the presence of blockage, this decrement is restricted to 25%. When $N_U = 10$ and blockage

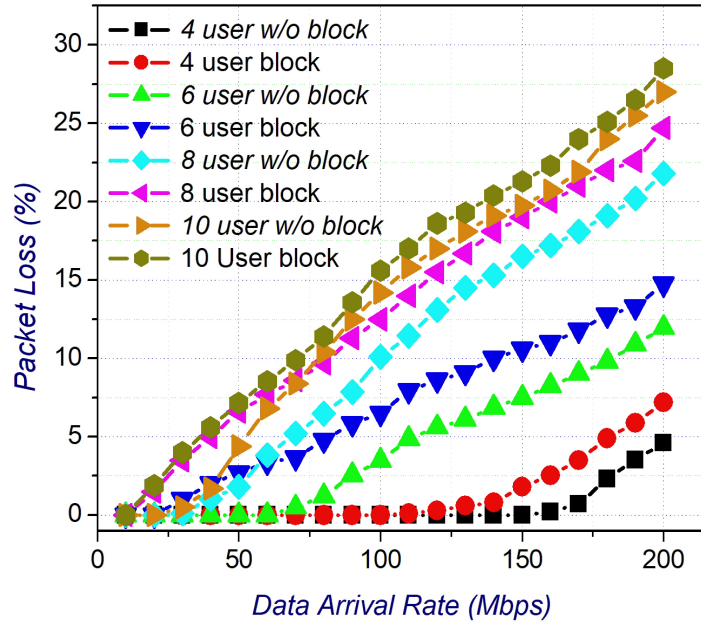


Figure 7.9: Packet loss against data arrival rate ($N_U = 4, 6, 8, 10$)

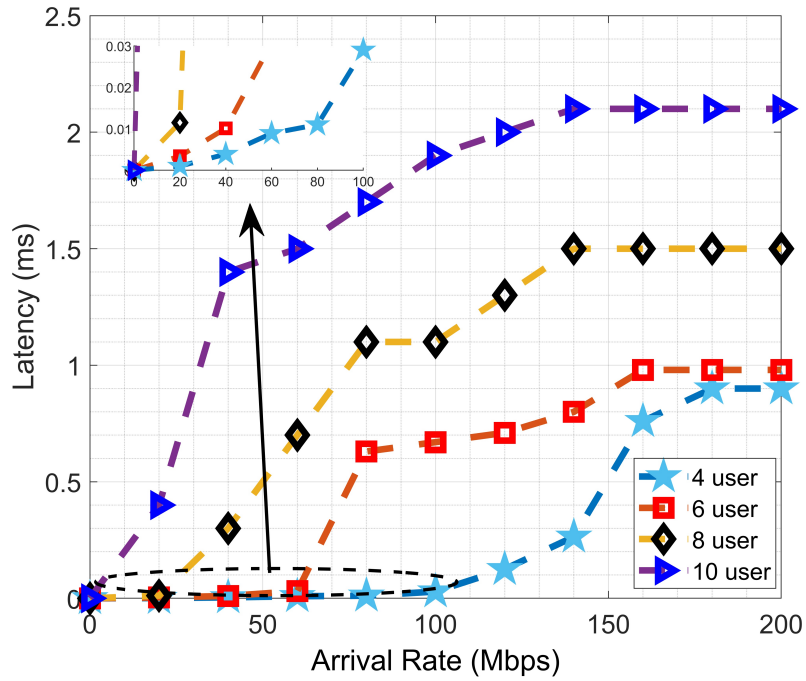


Figure 7.10: Latency versus data arrival rate ($N_U = 4, 6, 8, 10$)

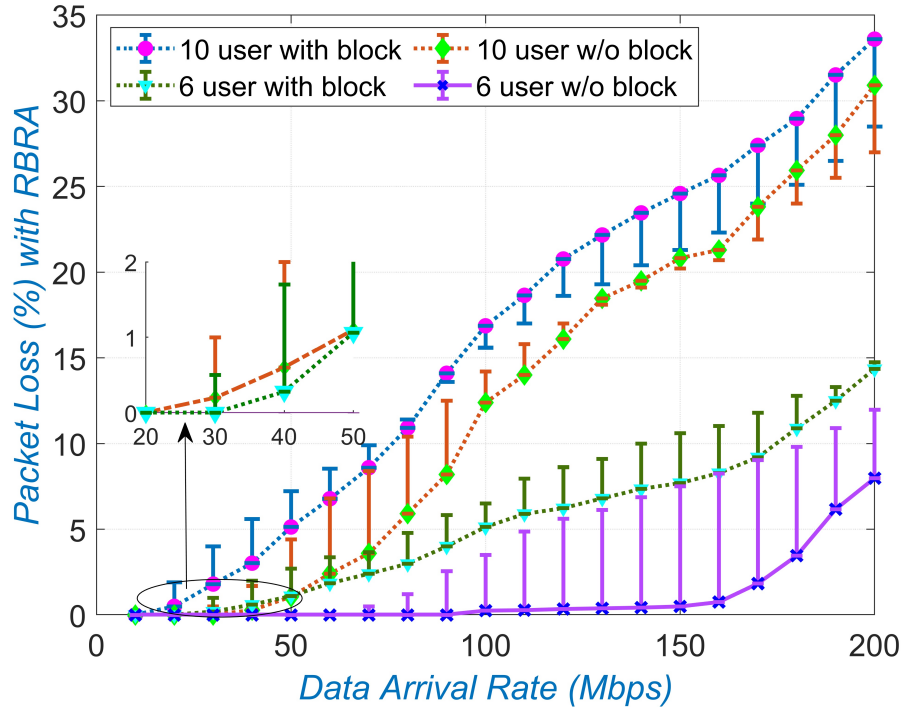
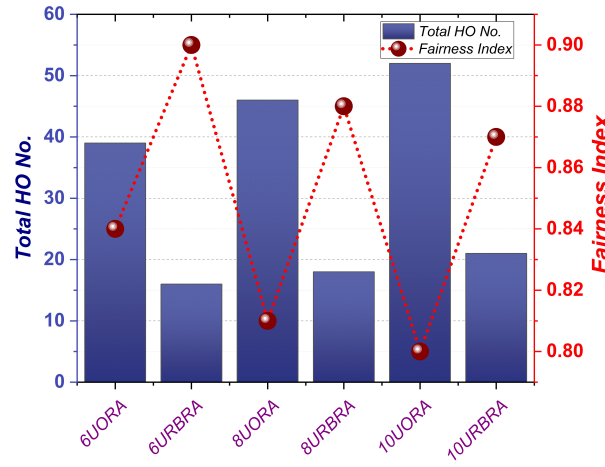


Figure 7.11: Packet loss using RBRA with respect to ORA ($N_U = 6, 10$)

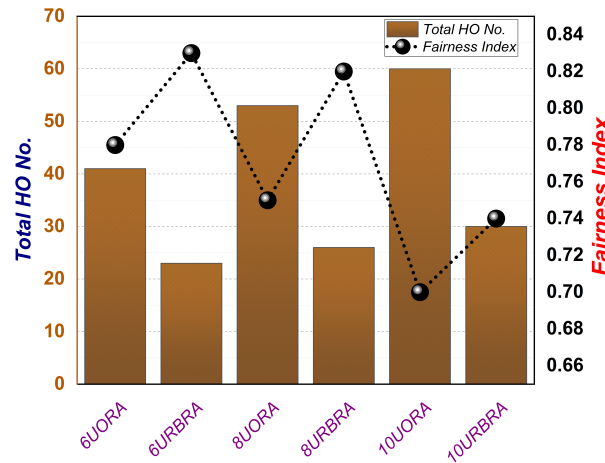
is absent, the gap between the two RA techniques is not so much, especially after 120 Mbps of arrival rate. At 200 Mbps, an increment of 13% is observed. So, it can be presumed that the RBRA offers better performance in most cases, especially when user density is less. Even with high user density it performs better for a low data arrival rate.

FAIRNESS INDEX:

Secondly, the average fairness index of the network is estimated and compared considering both ORA and RBRA. It is shown in Figure 7.12. Figure 7.12a provides the results for the *ScenRM* scenario without any blockage while Figure 7.12b appraises the blockage condition for the same scenario. In both cases, 6, 8, and 10 users are considered. When $N_U = 6$ and ORA is adopted (6UORA), the fairness index is 0.84 in the absence of LOS blockage. However, using the RBRA it increases to 0.9 (6URBRA). Even in the presence of blockage and a higher no of users, the fairness index always improves with RBRA. For 10URBRA 5.7% improvement in fairness index is observed under blockage condition while in the case of 6URBRA, this increment is 6.4%. Due to the reduced number of handovers, it is possible to achieve such improvement. The total number of handovers for each case is also shown in the same figure.



(a) Without LOS blockage



(b) Considering LOS blockage

Figure 7.12: Reduction in HO and improvement in fairness index adopting RBRA

COMPLEXITY:

In terms of algorithmic complexity, the RBRA is considered simpler when contrasted with ORA. In the case of ORA, the complexity is heightened as it employs Mixed-Integer Non-Linear Programming (MINLP) to maximize system throughput. This optimization approach introduces both combinatorial complexities associated with optimizing discrete variable sets and challenges related to managing non-linear functions. On the other hand, RBRA adopts logical decision-based resource distribution.

To compare these two resource allocation techniques, two metrics namely McCabe complexity and execution time complexity are employed. 10-user random mobility scenario is considered as a reference. McCabe complexity, also known as cyclomatic complexity, is a metric used to quantify the complexity of a software algorithm or program. It provides a numerical

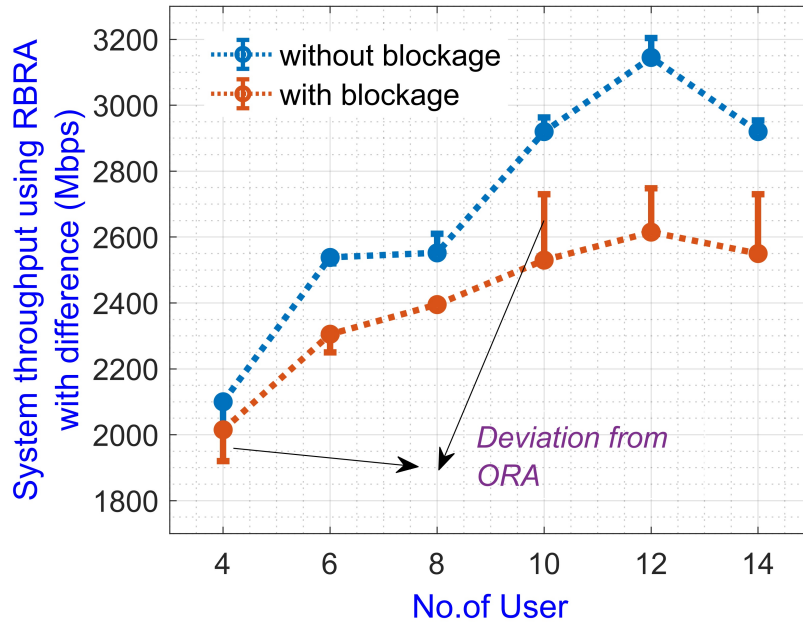


Figure 7.13: System Throughput using RBRA with respect to ORA

measure of the number of linearly independent paths through a program's source code. The ORA exhibits a cyclomatic complexity value of 16, whereas the RBRA possesses only a quarter of this cyclomatic complexity value. In terms of execution time complexity, RBRA is 89 times faster than ORA. Specifically, ORA requires 8.47 seconds for execution, while RBRA completes its execution in a significantly shorter time, taking only 0.0948 seconds.

SYSTEM THROUGHPUT:

Thus far, RBRA has offered notable enhancements concerning packet loss, fairness index, and algorithmic complexity. However, its impact on system throughput yields varied results. The effective system throughput (\mathbb{R}_{sys}^{eff}) is improved a bit using RBRA when a lesser number of users ($N_U \leq 6$) are associated with the network and blockage severity is low. But, as the user density and acuteness of blockage increase ORA performs better. However, the deviation is restricted to a maximum of 2% in the absence of light path blockage. The RBRA technique with FDR offers 2538 Mbps of \mathbb{R}_{sys}^{eff} when $N_U = 6$. The system throughput slowly increases to 2552 Mbps and 2920 Mbps when $N_U = 8$ and 10 respectively. Considering the LOS blockage, a maximum 14% deviation in \mathbb{R}_{sys}^{eff} is observed.

7.6.6 ADVANCEMENT BEYOND PRIOR RESEARCH

The outstanding performance in this proposed system featuring FDR has been noted, particularly when employing the RBRA technique. This approach surpasses ORA in terms of all network parameters and complexity. However, varied outcomes are obtained in terms of system throughput. But, most significantly these values of system throughput (with RBRA)

Table 7.3: Comparative outcome of existing studies

Ref.	No. of User	User Mobility	Path Blockage	System Throughput (Mbps)	User Throughput (Mbps)	Packet Loss (%)	Latency (ms)	Fairness Index
Ref. ⁽²⁰⁸⁾	1	Yes	No	×	71	×	×	×
Ref. ⁽²⁰⁹⁾	1	Yes	No	×	35-70	×	×	×
Ref. ⁽¹¹⁷⁾	50-200	Yes	No	×	30-80	×	×	×
Ref. ⁽¹¹¹⁾	2-14	Yes	Yes	450 (10 user)	×	×	×	1
Ref. ⁽¹¹⁴⁾	2-16	No	Yes	100-300 (5 user)	×	29 (5 user)	6.2 (5 user)	0.84 (5 user)
Ref. ⁽¹⁰⁷⁾	4-12	No	Yes	800-1200	60-130	×	×	×
Ref. ⁽¹⁰⁸⁾	2-14	Yes	Yes	350-750	×	×	×	×
This Study (With RBRA)	4-14	Yes	Yes	2012-2550	182-480	6.23 (6 User)	0.94 (6 User)	0.83 (6 User)

are way above the reported state-of-the-art research in this direction. Even with a higher frequency reuse factor and complex resource allocation algorithm, a maximum of 1200 Mbps system throughput has been reported where almost every study considers a single PD receiver. However, incorporating FDR in conjunction with our proposed RBRA could result in a system throughput that is more than twice as high.

The comparative outcome from different studies is presented in Table 7.3. Only a single study⁽¹¹⁴⁾ in this direction addresses nearly all service parameters. However, unlike our case, it does not account for user mobility. The network parameters are compared at an overall arrival rate of 600 Mbps, considering 5 users as reported in⁽¹¹⁴⁾. This is equivalent to a data arrival rate of 120 Mbps for each user. Even considering both the user mobility and potential light path blockages, the proposed system outperforms the existing studies.

7.7 SUMMARY

Within the confines of this chapter, a thorough examination of the FDR is conducted, specifically in the context of light path blockage scenarios. The investigation extends to multiple users exhibiting random mobility within the framework of a Hybrid **Li-Fi** and WiFi Network (HLWNet). The primary contributions of this study can be succinctly summarized as follows:

- A LiFi channel model with FDR is proposed where off-axis and rectangular FOV is contemplated instead of symmetrical FOV.
- By embracing this channel model, the performance of a hybrid **Li-Fi**-Wi-Fi system has been assessed under various multi-user mobility scenarios, particularly in the presence of light path blockage.

- An innovative rule-based resource allocation algorithm is introduced, demonstrating a superiority over existing optimal resource allocation techniques in terms of overall network performance.
- Furthermore, an investigation has been conducted on the data service quality of HLWNet, taking into account packet loss, latency, and fairness index, while considering handover overload scenarios.

7.8 RESEARCH OUTPUT

The findings from this chapter are reported in the following research publications:

- **Chatterjee, S., Sabui, D. & Roy, B. (2024).** “On the Performance of Hybrid LiFi-RF Network Using Freeform Based Angle Diversity Receiver,” In 2024 3rd *International Conference on Control, Instrumentation, Energy & Communication (CIEC)* IEEE.
DOI: doi.org/10.1109/CIEC59440.2024.10468220
- **Chatterjee, S., Sabui, D., Prakash, A., & Roy, B.(2024).** Mobility aware blockage management of a multi-user multi-cell hybrid Li-Fi Wi-Fi system with freeform diversity receiver. *Optics Communications*, 130487.
DOI: doi.org/10.1016/j.optcom.2024.130487

“My goal is simple. It is a complete understanding of the universe, why it is as it is, and why it exists at all.”

Stephen Hawking

8

Conclusions, Limitations and Future Research

8.1 SUMMARY AND CONCLUSIONS

To address the burgeoning demand for various wireless communication applications amid the surge in mobile data traffic, Visible Light Communication (VLC) and its networked counterpart, **Li-Fi**, have emerged as promising green communication technologies, offering ubiquitous connectivity. While recent research in this domain has witnessed notable advancements in communication performance metrics such as modulation schemes, BER, and Signal-to-Noise Ratio (SNR), a critical aspect has often been overlooked— the primary purpose of using optical access points, which is not only to facilitate communication but also to provide lighting solutions with appropriate horizontal illuminance and uniformity. In the realm of sustainable and smart building designs, the integration of time-varying daylight with data-enabled artificial sources presents an opportunity to conserve energy and enhance connectivity. This proposed research deals with the current research gaps in indoor **VLC** system design, particularly from a lighting perspective. The primary objectives are to address the dual requirements of communication and illumination performances, offering harmonious and effective solutions. By focusing on the integration of lighting considerations into **VLC** system design, this research seeks to contribute to a more comprehensive and sustainable approach to meet the evolving needs of modern optical wireless communication applications.

Chapter 3 introduces an innovative strategy for mitigating ambient light noise in an indoor **VLC** system. The suggested approach involves incorporating Forward Error Correction (FEC) techniques with a data rate of 100 Mb/s . The evaluation of communication and illumination performance takes place within a realistic indoor environment. DIALux simulation results reveal that the proposed system achieves an average horizontal illuminance of 363 Lux and an overall uniformity (U_0) of 0.841 , meeting the recommended standards outlined in

international lighting guidelines. The arrangement of luminaires and the receiver architecture, coupled with FEC, effectively limits the signal-to-noise ratio variation to a maximum of 4.28 dB across different receiver locations, surpassing previous outcomes. Additionally, the relationship between signal-to-noise ratio, ambient light interference, and BER is established. MATLAB simulations demonstrate that the proposed system exhibits superior BER performance (on the order of 10^{-8}) even with ambient light interference, ensuring seamless user mobility throughout the indoor space. As a continuation of this investigation, a more authentic indoor setting resembling an office environment with cubicles and corridors is taken into account. The associated lighting and communication performances in this realistic workspace are then assessed and analyzed.

Chapter 4 introduces an energy-efficient indoor Visible Light Communication (VLC) system designed to incorporate daylight through a suitable dimming control mechanism. The proposed VLC architecture demonstrates significant energy savings, with a maximum of 37.29% power conservation achieved under optimal ambient daylight conditions. The dimming control mechanism for the transmitter is implemented using a continuous current reduction technique. This study thoroughly investigates and analyzes the communication and illumination performances of the system across various ambient daylight conditions. The experimentally obtained average horizontal illuminance over the task area aligns with ISO recommendations. Consistently, an almost constant illuminance of approximately 300 lux is recorded, closely matching the theoretical model. The optical receiver's waveform retrieval capability is examined in the presence of daylight interference, revealing a close resemblance between the received and transmitted waveforms with data-rate of 100 kbps. Furthermore, BER in the order of 10^{-10} is observed under different dimming conditions. Also, the recorded short-term flicker severity index during data transmission is 0.67, demonstrating conformity with the guidelines established by the International Electrotechnical Commission (IEC).

Chapter 5 comprehensively investigates the impact of luminaire placement on both LOS & NLOS VLC channels. The study delves into diverse transmitter configurations and meticulously examines their effects, ultimately presenting a well-balanced solution for optimal channel allocation under illumination constraints. A pivotal outcome of this research lies in the innovative methodology proposed to enhance SINR performance while adhering to lighting recommendations. The AHP weighted Technique for Order of Preference by Similarity to Ideal Solution (TOPSIS) optimization framework serves as a robust tool in achieving this objective. Among the three luminaire arrangements considered, the 2×2 deployment scheme with a 39-degree receiver Field of View (FoV) emerges as the most favorable, boasting the highest closeness coefficient. The corresponding optimal HPBW is determined to be 95 degrees. The results indicate a remarkable 27 dB improvement in average SINR, coupled with a negligible reduction in the overall uniformity of horizontal illuminance. Notably, this enhancement in SINR is achieved through the implementation of a straightforward receiver architecture employing a single PD.

Chapter 6 delves into the significance of using angle diversity receivers. Unlike the single PD counterparts, this diversity technique proves highly effective in enhancing SINR performance, even in the presence of luminaires with a high HPBW. Consequently, there is a marked improvement in the uniformity of horizontal illuminance. Our focus lies in opti-

mizing a hemispheric ADR for the purpose of minimizing spatial **SINR** fluctuations. This study introduces a pioneering methodology, jointly optimizing the receiver's FOV and inclination angle to confine **SINR** fluctuations within a significant threshold. The system utilizes the SBC scheme for dynamic channel selection within the MIMO system during reception. Importantly, the proposed HADR outperforms the state-of-the-art ADR, particularly in the realm of reducing spatial **SINR** deviation.

Chapter 7 meticulously explores the feasibility and potential of integrating FDR technology into a multi-cell HLWNet. Distinguishing itself from angle diversity receiver, FDR, a more compact and enhanced version of ADR, demonstrates superior capabilities in mitigating **CCI** and elevating **SINR**. This work employs a specialized optical front-end with a rectangular FOV in lieu of a conventional receiver configuration, conducting thorough testing across various mobility-aware multi-user scenarios. Four distinct scenarios, shaped by mobility and pause time considerations, evaluate performance both in the presence of random blockage and without blockage. To facilitate this assessment, a **Li-Fi** channel model incorporating FDR is proposed. Results exhibit a substantial enhancement in throughput performance compared to state-of-the-art research. Furthermore, the study explores network quality of service metrics, including packet loss, latency, and fairness index. Notably, the application of FDR in conjunction with the proposed Receiver-Based Rate Adaptation (RBRA) algorithm showcases heightened robustness in network performance when compared to the conventional load balancing technique. This tailored solution serves as a crucial milestone in charting the future research trajectory for commercializing FDR technology. Despite the significant contributions made, the study suggests potential extensions, such as examining mobility scenarios with random receiver orientation and investigating the efficacy of various optical front-ends within HLWNet, incorporating reflective intelligent surfaces. Customization and further research endeavors in this domain are deemed essential for the prospective integration of this heterogeneous technology into the evolving **Li-Fi** ecosystem.

8.2 LIMITATIONS AND FUTURE RESEARCH

To craft an effective indoor **VLC** system, this thesis thoroughly examines key factors pertaining to both communication and illumination perspectives. All these investigations are conducted within an individual capacity, primarily relying on simulation-based approaches, and undertaken without external funding or financial support. Nevertheless, it is essential to emphasize that practical considerations play a crucial role in solidifying the proposed solutions. The firm establishment of these solutions can only be achieved through collaborative efforts across multiple domains, working together with the shared goal of designing a finished product.

A simple on-off keying technique has been used in Section 3.3.2 to design a forward error-corrected transmitter. However, a more sophisticated optical orthogonal frequency division multiplexing technique can be adopted. OFDM is known for its high spectral efficiency and is well-suited for multi-path environments. In the future, we are planning to establish a **VLC/Li-Fi** test bed where the influence of ambient light can be practically investigated for different modulation techniques. Moreover, investigation has been performed on horizontal

illuminance and overall uniformity as lighting parameters. The lighting quality of LEDs is intricately tied to variations in the driving current, directly influencing chromaticity and color rendering properties. Any fluctuations in the driving current can bring about alterations in lighting quality, impacting not only visual perception but also bearing significance for associated health and psychological effects^(2.18,2.19). Additionally, undesirable shifts in LED chromaticity may contribute to a decline in LED efficiency, a phenomenon commonly known as the droop effect. Hence, understanding and controlling driving current variations is crucial for maintaining optimal lighting quality and efficient LED performance. So, an in-depth exploration of CCT and CRI at the time of data transfer will contribute valuable insights to the overall understanding of lighting quality.

The concept of designing an energy-efficient daylight-integrated **VLC** system holds the potential for extension into a multi-cell framework. Chapter 3 introduces the idea of an energy-efficient dimmable **VLC** system, while Chapter 4 provides an in-depth exploration of **CCI** in a multi-cell environment. By merging these concepts, a practical and realistic **VLC** system can be devised to not only harness energy efficiency but also effectively address challenges posed by **CCI** in a multi-cell setting. This integrated approach aims to enhance the overall performance and sustainability of **VLC** systems, offering a comprehensive solution to the demands of modern communication environments. This topic will be studied in our future research. Chapter 4 delves into the study of the optimal transmitter and receiver configuration, taking into account a fixed height of the working plane at 0.85m. While this provides valuable insights, it is acknowledged that in practical scenarios, the height of the working plane can vary within a range. Such variations may impact the optimal receiver's FOV and the transmitter's semi-angle. Additionally, the room's shape presents another influencing factor. Consequently, further research becomes imperative to identify the optimal solution, considering these practical variables. A more comprehensive investigation will contribute to a nuanced understanding of the optimal configuration under real-world conditions, enhancing the applicability of the findings.

To improve the **SINR** without sacrificing the uniformity of illuminance, different receiver diversity plays an important role. Thus, in this thesis, work has been done on the design of hemispheric ADR and the potential use of an FDR in a multi-user HLWNet framework. Even though a few practical issues like light-path blockage, and mobility have been addressed, other important factors like random receiver orientation remain untouched. Here, we assume that the receiver is always in a vertically upright position. However, the receiver orientation often changes in practice, particularly in the case of handheld gadgets. This variability poses a tangible barrier to the advancement of **Li-Fi** for commercial use. The performance of hybrid Li-Fi/Wi-Fi system has not been tested for large dimension of room in this study. This can be considered as a potential direction for future work. Additionally, the technology faces a significant obstacle in enhancing the frequency response of optical front-end devices in both transmitter and receiver components which limit the achievable data rates. To maximize the utilization of optical spectrum resources, it is imperative to persist in the innovation of high-bandwidth electrical-to-optical conversion devices (optical sources) and optical-to-electrical conversion devices (optical detectors) reaching into the hundreds of gigahertz range.

“You cannot hope to build a better world without improving the individuals. To that end, each of us must work for his own improvement and, at the same time, share a general responsibility for all humanity, our particular duty being to aid those to whom we think we can be most useful.”

Marie Curie



Other Publications On VLC

This chapter comprises a compilation of research papers distinct from the original contributions presented in this thesis. The research outputs of this thesis (publications related to the thesis) have been previously mentioned. Nonetheless, it is pertinent to incorporate other relevant contributions within the realm of Visible Light Communication (VLC), which significantly bolster the groundwork in this field, especially the last chapter.

Journal Publications

1. Sabui, D., **Chatterjee, S.**, Prakash, A., Roy, B., Khan, G. S., (2022), "Design of an off-axis freeform diversity receiver to improve SINR performance of a multi-cell VLC system". Optics Communications, 510, 127937.
2. Sabui, D., Mishra, V., **Chatterjee, S.**, Roy, B., Khan, G. S., (2023), "Freeform based compact receiver front-end for indoor multi-cell VLC system: Fabrication, optical characterization and associated challenges". Optik, 274, 170539.
3. Sabui, D., **Chatterjee, S.**, Khan, G. S., (2024), "Impact of different receiver geometry on reconfigurable intelligent surface assisted multi-cell VLC system in presence of light path blockage". Applied Optics 63, no. 10 : 2404-2414.

Proceedings in International Conferences

1. Sabui, D., **Chatterjee, S.**, Prakash, A., Roy, B., Khan, G. S. (2022, October), "An improved angular diversity receiver structure for indoor VLC system using off-axis freeform

optics”, in Novel Optical Systems, Methods, and Applications XXV (Vol. 12216, pp. 164-168). SPIE.

2. Sabui, D., **Chatterjee, S.**, Mishra, V., Roy, B., Khan, G. S. (2023, September), ”Compact monolithic freeform Fresnel receiver front-end for Li-Fi application: a step forward”, in International Optical Design Conference 2023 (Vol. 12798, pp. 7-8). SPIE.
3. Sabui, D., **Chatterjee, S.**, Khan, G. S., ”Multicell VLC System and Reconfigurable intelligent surfaces: Connecting the dots ”, In 2024 3rd *International Conference on Control, Instrumentation, Energy & Communication (CIEC)* IEEE.

References

- [1] P. Sharma, “Evolution of mobile wireless communication networks-1g to 5g as well as future prospective of next generation communication network,” *International Journal of Computer Science and Mobile Computing*, vol. 2, no. 8, pp. 47–53, 2013.
- [2] M. U. A. Siddiqui, H. Abumarshoud, L. Bariah, S. Muhaidat, M. A. Imran, and L. Mohjazi, “Urrlc in beyond 5g and 6g networks: An interference management perspective,” *IEEE Access*, vol. 11, pp. 54639–54663, 2023.
- [3] J. L. C. Bárcena, P. Ducange, F. Marcelloni, G. Nardini, A. Noferi, A. Renda, F. Ruffini, A. Schiavo, G. Stea, and A. Virdis, “Enabling federated learning of explainable ai models within beyond-5g/6g networks,” *Computer Communications*, vol. 210, pp. 356–375, 2023.
- [4] L. P. Rachakonda, M. Siddula, and V. Sathya, “A comprehensive study on iot privacy and security challenges with focus on spectrum sharing in next-generation networks (5g/6g/beyond),” *High-Confidence Computing*, p. 100220, 2024.
- [5] P. McEnroe, S. Wang, and M. Liyanage, “A survey on the convergence of edge computing and ai for uavs: Opportunities and challenges,” *IEEE Internet of Things Journal*, vol. 9, no. 17, pp. 15435–15459, 2022.
- [6] L. DeNardis, *The Internet in everything*. Yale University Press, 2020.
- [7] W. Rafique and J. Qadir, “Internet of everything meets the metaverse: Bridging physical and virtual worlds with blockchain,” *Computer Science Review*, vol. 54, p. 100678, 2024.
- [8] M. Mehrnoush, C. Hu, and C. Aldana, “AR/VR Spectrum Requirement for Wi-Fi 6E and Beyond,” *IEEE Access*, vol. 10, pp. 133016–133026, 2022.
- [9] M. Rüßmann, M. Lorenz, P. Gerbert, M. Waldner, J. Justus, P. Engel, and M. Harnisch, “Industry 4.0: The future of productivity and growth in manufacturing industries,” *Boston consulting group*, vol. 9, no. 1, pp. 54–89, 2015.
- [10] M. Kinoshita, T. Yamazato, H. Okada, T. Fujii, S. Arai, T. Yendo, and K. Kamakura, “Motion modeling of mobile transmitter for image sensor based I2V-VLC, V2I-VLC, and V2V-VLC,” in *2014 IEEE Globecom Workshops (GC Wkshps)*, pp. 450–455, IEEE, 2014.

- [11] P. S. R. Henrique and R. Prasad, *6G: The Road to the Future Wireless Technologies 2030*. CRC Press, 2022.
- [12] A. E. Ibhaze, P. E. Orukpe, and F. O. Edeko, "High capacity data rate system: Review of visible light communications technology," *Journal of Electronic Science and Technology*, vol. 18, no. 3, p. 100055, 2020.
- [13] C. Chen, H. Yang, P. Du, W.-D. Zhong, A. Alphones, Y. Yang, and X. Deng, "User-centric mimo techniques for indoor visible light communication systems," *IEEE Systems Journal*, vol. 14, no. 3, pp. 3202–3213, 2020.
- [14] T. Cogalan and H. Haas, "Why would 5G need optical wireless communications?," in *2017 IEEE 28th Annual International Symposium on Personal, Indoor, and Mobile Radio Communications (PIMRC)*, pp. 1–6, IEEE, 2017.
- [15] H. Haas, M. S. Islim, C. Chen, and H. Abumarshoud, *An Introduction to Optical Wireless Mobile Communication*. Artech House, 2021.
- [16] A. K. Majumdar, *Optical wireless communications for broadband global internet connectivity: fundamentals and potential applications*. Elsevier, 2018.
- [17] A.-M. Căilean and M. Dimian, "Current challenges for visible light communications usage in vehicle applications: A survey," *IEEE Communications Surveys & Tutorials*, vol. 19, no. 4, pp. 2681–2703, 2017.
- [18] L. E. M. Matheus, A. B. Vieira, L. F. Vieira, M. A. Vieira, and O. Gnawali, "Visible light communication: concepts, applications and challenges," *IEEE Communications Surveys & Tutorials*, vol. 21, no. 4, pp. 3204–3237, 2019.
- [19] P. H. Pathak, X. Feng, P. Hu, and P. Mohapatra, "Visible light communication, networking, and sensing: A survey, potential and challenges," *IEEE communications surveys & tutorials*, vol. 17, no. 4, pp. 2047–2077, 2015.
- [20] H. Burchardt, N. Serafimovski, D. Tsonev, S. Videv, and H. Haas, "VLC: Beyond point-to-point communication," *IEEE Communications Magazine*, vol. 52, no. 7, pp. 98–105, 2014.
- [21] T. Fath, C. Heller, and H. Haas, "Optical wireless transmitter employing discrete power level stepping," *Journal of Lightwave Technology*, vol. 31, no. 11, pp. 1734–1743, 2013.
- [22] F. A. Umrani, F. A. Dahri, A. W. Umrani, and H. B. Mangrio, "The internet of LED: Indoor visible light communication using LED as transmitter and receiver," in *2018 21st International Symposium on Wireless Personal Multimedia Communications (WPMC)*, pp. 75–78, IEEE, 2018.

- [23] S. Idris, U. Mohammed, J. Sanusi, and S. Thomas, "Visible light communication: a potential 5G and beyond communication technology," in *2019 15th international conference on electronics, computer and computation (ICECCO)*, pp. 1–6, IEEE, 2019.
- [24] J. Guaña-Moya, M. Román Cañizares, P. Palacios Játiva, I. Sánchez, D. Ruminot, and F. V. Lobos, "Comprehensive survey on vlc in e-healthcare: Channel coding schemes and modulation techniques," *Applied Sciences*, vol. 14, no. 19, p. 8912, 2024.
- [25] C. Jenila and R. Jeyachitra, "Green indoor optical wireless communication systems: Pathway towards pervasive deployment," *Digital Communications and Networks*, vol. 7, no. 3, pp. 410–444, 2021.
- [26] S. Vappangi and V. Mani, "Concurrent illumination and communication: A survey on Visible Light Communication," *Physical Communication*, vol. 33, pp. 90–114, 2019.
- [27] E. Zolala, M. A. Dastgheib, H. Beyranvand, and J. A. Salehi, "Towards more energy efficient vlc networks: A study on space division multiplexing and smart lighting," *IEEE Transactions on Green Communications and Networking*, 2024.
- [28] W. Matthews, Z. Ahmed, W. Ali, and S. Collins, "A 3.45 Gigabits/s SiPM-based OOK VLC receiver," *IEEE Photonics Technology Letters*, vol. 33, no. 10, pp. 487–490, 2021.
- [29] C. Yeh, C. W. Chow, C. Gu, B. Guo, Y. Chang, J. Weng, and M. Wu, "400 Mbit/s OOK green-LED visible light communication with low illumination," *Optical and Quantum Electronics*, vol. 50, pp. 1–5, 2018.
- [30] V. Dixit and A. Kumar, "Error analysis of L-PPM modulated MIMO based multi-user NOMA-VLC system with perfect and imperfect SIC," *Applied Optics*, vol. 61, no. 4, pp. 858–867, 2022.
- [31] M. Tahir and A. B. Siddique, "Optimal brightness-rate control using VR-MPPM and its spectral analysis for VLC system," *IEEE communications letters*, vol. 16, no. 7, pp. 1125–1128, 2012.
- [32] M. Kumari, A. Sheetal, and R. Sharma, "Performance analysis of symmetrical and bidirectional 40 Gbps TWDM-PON employing m-QAM-OFDM modulation with multi-color LDs based VLC system," *Optical and quantum electronics*, vol. 53, pp. 1–29, 2021.
- [33] S. Dimitrov and H. Haas, *Principles of LED light communications: towards networked Li-Fi*. Cambridge University Press, 2015.
- [34] X. Huang, F. Yang, C. Pan, and J. Song, "Pre-distorted enhanced ADO-OFDM for hybrid VLC networks: A mutual-interference-free approach," *IEEE Photonics Journal*, vol. 12, no. 2, pp. 1–12, 2020.
- [35] Y. Zhao, Z. Zeng, H. Cao, and C. Chen, "Enhanced transmitter designs for indoor mimo-vlc systems," *Optics Communications*, p. 131279, 2024.

- [36] D. Lin, F. Yi, G. Yongliang, and M. Guizani, "Design of protograph ldpc-coded mimo-vlc systems with generalized spatial modulation," *China Communications*, vol. 21, no. 3, pp. 118–136, 2024.
- [37] D. Hutt, K. Snell, and P. Belanger, "Alexander Graham Bell's PHOTOPHONE," *Optics and Photonics News*, vol. 4, no. 6, pp. 20–25, 1993.
- [38] S. Nakamura, "Background story of the invention of efficient blue InGaN light emitting diodes," *International Journal of Modern Physics B*, vol. 29, no. 32, p. 1530016, 2015.
- [39] T. Komine and M. Nakagawa, "Fundamental analysis for visible-light communication system using led lights," *IEEE transactions on Consumer Electronics*, vol. 50, no. 1, pp. 100–107, 2004.
- [40] R. Wan, L. Wang, J. Huang, X. Yi, H.-C. Kuo, and J. Li, "Improving the modulation bandwidth of GaN-based light-emitting diodes for high-speed visible light communication: countermeasures and challenges," *Advanced Photonics Research*, vol. 2, no. 12, p. 2100093, 2021.
- [41] A. Khalid, G. Cossu, R. Corsini, P. Choudhury, and E. Ciaramella, "1-gb/s transmission over a phosphorescent white led by using rate-adaptive discrete multitone modulation," *IEEE photonics journal*, vol. 4, no. 5, pp. 1465–1473, 2012.
- [42] G. Cossu, A. Khalid, P. Choudhury, R. Corsini, and E. Ciaramella, "3.4 gbit/s visible optical wireless transmission based on rgb led," *Optics express*, vol. 20, no. 26, pp. B501–B506, 2012.
- [43] E. F. Schubert, *Light-emitting diodes (2018)*. E. Fred Schubert, 2018.
- [44] J. J. McKendry, R. P. Green, A. Kelly, Z. Gong, B. Guilhabert, D. Massoubre, E. Gu, and M. D. Dawson, "High-speed visible light communications using individual pixels in a micro light-emitting diode array," *IEEE Photonics Technology Letters*, vol. 22, no. 18, pp. 1346–1348, 2010.
- [45] J. J. McKendry, D. Massoubre, S. Zhang, B. R. Rae, R. P. Green, E. Gu, R. K. Henderson, A. Kelly, and M. D. Dawson, "Visible-light communications using a CMOS-controlled micro-light-emitting-diode array," *Journal of lightwave technology*, vol. 30, no. 1, pp. 61–67, 2011.
- [46] M. S. Islim, R. X. Ferreira, X. He, E. Xie, S. Videv, S. Viola, S. Watson, N. Bamiedakis, R. V. Pentty, I. H. White, *et al.*, "Towards 10 Gb/s orthogonal frequency division multiplexing-based visible light communication using a GaN violet micro-LED," *Photonics Research*, vol. 5, no. 2, pp. A35–A43, 2017.

- [47] E. Xie, R. Bian, X. He, M. S. Islam, C. Chen, J. J. McKendry, E. Gu, H. Haas, and M. D. Dawson, "Over 10 Gbps VLC for long-distance applications using a GaN-based series-biased micro-LED array," *IEEE Photonics Technology Letters*, vol. 32, no. 9, pp. 499–502, 2020.
- [48] F. Xu, P. Qiu, T. Tao, P. Tian, X. Liu, T. Zhi, Z. Xie, B. Liu, and R. Zhang, "High bandwidth semi-polar InGaN/GaN micro-LEDs with low current injection for visible light communication," *IEEE Photonics Journal*, vol. 15, no. 1, pp. 1–4, 2023.
- [49] M. Monavarian, A. Rashidi, and D. Feezell, "A Decade of Nonpolar and Semipolar III-Nitrides: A Review of Successes and Challenges," *physica status solidi (a)*, vol. 216, no. 1, p. 1800628, 2019.
- [50] L. Yu, L. Wang, Z. Hao, Y. Luo, C. Sun, B. Xiong, Y. Han, J. Wang, and H. Li, "High-speed micro-LEDs for visible light communication: Challenges and progresses," *Semiconductor Science and Technology*, vol. 37, no. 2, p. 023001, 2021.
- [51] K. Rajabi, J. Wang, J. Jin, Y. Xing, L. Wang, Y. Han, C. Sun, Z. Hao, Y. Luo, K. Qian, *et al.*, "Improving modulation bandwidth of c-plane GaN-based light-emitting diodes by an ultra-thin quantum wells design," *Optics express*, vol. 26, no. 19, pp. 24985–24991, 2018.
- [52] M. Meneghini, C. De Santi, A. Tibaldi, M. Vallone, F. Bertazzi, G. Meneghesso, E. Zanoni, and M. Goano, "Thermal droop in III-nitride based light-emitting diodes: Physical origin and perspectives," *Journal of applied Physics*, vol. 127, no. 21, 2020.
- [53] M. Usman, S. Malik, M. A. Khan, and H. Hirayama, "Suppressing the efficiency droop in AlGaIn-based UVB LEDs," *Nanotechnology*, vol. 32, no. 21, p. 215703, 2021.
- [54] E. Xie, C. Chen, C. Ouyang, J. Hill, J. J. McKendry, Y. Zhang, E. Gu, J. Herrnsdorf, H. Haas, and M. D. Dawson, "GaN-based series hybrid LED array: a dual-function light source with illumination and high-speed visible light communication capabilities," *Journal of Lightwave Technology*, 2023.
- [55] D. Karunatilaka, F. Zafar, V. Kalavally, and R. Parthiban, "Led based indoor visible light communications: State of the art," *IEEE communications surveys & tutorials*, vol. 17, no. 3, pp. 1649–1678, 2015.
- [56] S.-M. Kim and J.-S. Won, "Simultaneous reception of visible light communication and optical energy using a solar cell receiver," in *2013 International Conference on ICT Convergence (ICTC)*, pp. 896–897, IEEE, 2013.
- [57] Z. Wang, D. Tsonev, S. Videv, and H. Haas, "Towards self-powered solar panel receiver for optical wireless communication," in *2014 IEEE International Conference on Communications (ICC)*, pp. 3348–3353, IEEE, 2014.

- [58] Z. Wang, D. Tsonev, S. Videv, and H. Haas, "On the design of a solar-panel receiver for optical wireless communications with simultaneous energy harvesting," *IEEE Journal on Selected areas in Communications*, vol. 33, no. 8, pp. 1612–1623, 2015.
- [59] J. M. Kahn and J. R. Barry, "Wireless infrared communications," *Proceedings of the IEEE*, vol. 85, no. 2, pp. 265–298, 1997.
- [60] M. R. Ghaderi, "LiFi and hybrid WiFi/LiFi indoor networking: From theory to practice," *Optical Switching and Networking*, vol. 47, p. 100699, 2023.
- [61] "IEEE standard for local and metropolitan area networks: Short range optical wireless communication," standard, Jan. 2018.
- [62] F. Che, L. Wu, B. Hussain, X. Li, and C. P. Yue, "A fully integrated IEEE 802.15.7 visible light communication transmitter with on-chip 8-W 85% efficiency boost LED driver," *Journal of Lightwave Technology*, vol. 34, no. 10, pp. 2419–2430, 2016.
- [63] R. Mesleh, H. Elgala, and H. Haas, "Optical spatial modulation," *Journal of Optical Communications and Networking*, vol. 3, no. 3, pp. 234–244, 2011.
- [64] R. Deng, J. He, M. Chen, and Y. Zhou, "Experimental demonstration of a real-time gigabit OFDM-VLC system with a cost-efficient precoding scheme," *Optics Communications*, vol. 423, pp. 69–73, 2018.
- [65] Y. Yang, C. Chen, P. Du, X. Deng, J. Luo, W.-D. Zhong, and L. Chen, "Low complexity OFDM VLC system enabled by spatial summing modulation," *Optics Express*, vol. 27, no. 21, pp. 30788–30795, 2019.
- [66] M. G. Al-Hamiri and H. J. Abd, "Enhancing the performance of lifi communication with ostbc, qam, and ofdm: High-capacity, low-complexity transceiver design," *Results in Optics*, vol. 16, p. 100675, 2024.
- [67] M. Kumari, M. Banawan, V. Arya, and S. K. Mishra, "Investigation of ofdm-based hspn using front-end lifisystem for 5g networks," in *Photonics*, vol. 10, p. 1384, MDPI, 2023.
- [68] J. Gholipour, K. L. Bober, M. Hinrichs, and V. Jungnickel, "Compressed sensing for feedback generation in ofdm based lifi systems," in *2023 IEEE Wireless Communications and Networking Conference (WCNC)*, pp. 1–6, IEEE, 2023.
- [69] A. A. Abdulkafi, M. Y. Alias, and Y. S. Hussein, "Performance analysis of DCO-OFDM in VLC system," in *2015 IEEE 12th Malaysia International Conference on Communications (MICC)*, pp. 163–168, IEEE, 2015.
- [70] Y. Jiang, Y. Wang, P. Cao, M. Safari, J. Thompson, and H. Haas, "Robust and low-complexity timing synchronization for DCO-OFDM LiFi systems," *IEEE Journal on Selected Areas in Communications*, vol. 36, no. 1, pp. 53–65, 2017.

- [71] E. Panayirci, E. B. Bektaş, and H. V. Poor, "Physical layer security with dco-ofdm-based vlc under the effects of clipping noise and imperfect csi," *IEEE Transactions on Communications*, 2024.
- [72] H. T. Alrakah, T. Z. Gutema, S. Sinanovic, and W. O. Popoola, "PAPR reduction in DCO-OFDM based WDM VLC," *Journal of Lightwave Technology*, vol. 40, no. 19, pp. 6359–6365, 2022.
- [73] R. Yang, S. Ma, Z. Xu, H. Li, X. Liu, X. Ling, X. Deng, X. Zhang, and S. Li, "Spectral and energy efficiency of DCO-OFDM in visible light communication systems with finite-alphabet inputs," *IEEE Transactions on Wireless Communications*, vol. 21, no. 8, pp. 6018–6032, 2022.
- [74] R. Bai, S. Hranilovic, and Z. Wang, "Low-complexity layered ACO-OFDM for power-efficient visible light communications," *IEEE Transactions on Green Communications and Networking*, vol. 6, no. 3, pp. 1780–1792, 2022.
- [75] I. Stefan, H. Elgala, and H. Haas, "Study of dimming and LED nonlinearity for ACO-OFDM based VLC systems," in *2012 IEEE Wireless Communications and Networking Conference (WCNC)*, pp. 990–994, IEEE, 2012.
- [76] R. Bai and S. Hranilovic, "Absolute value layered ACO-OFDM for intensity-modulated optical wireless channels," *IEEE Transactions on Communications*, vol. 68, no. 11, pp. 7098–7110, 2020.
- [77] M. R. H. Mondal, "Comparison of dco-ofdm, ado-ofdm, hdc-ofdm and hnc-ofdm for optical wireless communications," *Journal of Optical Communications*, vol. 42, no. 2, pp. 325–340, 2021.
- [78] S.-K. Lee, T.-Y. Chen, and C.-C. Lee, "Regarding a pre-distorted ADO-OFDM system as a DCO-OFDM system for visible light communications," *IEEE Access*, vol. 9, pp. 154651–154658, 2021.
- [79] W.-W. Hu, "An Energy-Efficient ADO-OFDM System for Optical Wireless Communication," *IEEE Photonics Journal*, 2023.
- [80] S. M. Hameed, S. M. Abdulsatar, and A. A. Sabri, "Performance enhancement for visible light communication based ADO-OFDM," *Optical and Quantum Electronics*, vol. 53, no. 6, p. 339, 2021.
- [81] A. Mirvakili, V. J. Koomson, M. Rahaim, H. Elgala, and T. D. Little, "Wireless access test-bed through visible light and dimming compatible OFDM," in *2015 IEEE Wireless Communications and Networking Conference (WCNC)*, pp. 2268–2272, IEEE, 2015.
- [82] Q. Wang, Z. Wang, and L. Dai, "Asymmetrical hybrid optical OFDM for visible light communications with dimming control," *IEEE Photonics Technology Letters*, vol. 27, no. 9, pp. 974–977, 2015.

- [83] R. J. Godwin, K. Veena, and D. S. Kumar, "Performance analysis of direct detection Flip-OFDM for VLC system," in *2016 International Conference on Emerging Trends in Engineering, Technology and Science (ICETETS)*, pp. 1–5, IEEE, 2016.
- [84] M. Kafafy, Y. Fahmy, and M. Khairy, "Multi-cell VLC system design under illumination and communication constraints," *Optical Switching and Networking*, vol. 34, pp. 23–34, 2019.
- [85] T. Little, M. Rahaim, I. Abdalla, E. Lam, R. Mcallister, and A. M. Vegni, "A multi-cell lighting testbed for VLC and VLP," in *2018 Global LiFi Congress (GLC)*, pp. 1–6, IEEE, 2018.
- [86] T. V. Pham and A. T. Pham, "Coordination/cooperation strategies and optimal zero-forcing precoding design for multi-user multi-cell VLC networks," *IEEE Transactions on Communications*, vol. 67, no. 6, pp. 4240–4251, 2019.
- [87] S. Naser, L. Bariah, S. Muhaidat, M. Al-Qutayri, M. Uysal, and P. C. Sofotasios, "Interference management strategies for multiuser multicell MIMO VLC systems," *IEEE Transactions on Communications*, vol. 70, no. 9, pp. 6002–6019, 2022.
- [88] H. B. Eldeeb, H. A. Selmy, H. M. Elsayed, and R. I. Badr, "Interference mitigation and capacity enhancement using constraint field of view adr in downlink vlc channel," *IET Communications*, vol. 12, no. 16, pp. 1968–1978, 2018.
- [89] A. Ibrahim, T. Ismail, K. F. Elsayed, M. S. Darweesh, and J. Prat, "Resource allocation and interference management techniques for OFDM-based VLC atto-cells," *IEEE access*, vol. 8, pp. 127431–127439, 2020.
- [90] M. Hosney, H. A. Selmy, A. Srivastava, and K. M. Elsayed, "Interference mitigation using angular diversity receiver with efficient channel estimation in mimo vlc," *IEEE Access*, vol. 8, pp. 54060–54073, 2020.
- [91] Z. Chen, D. A. Basnayaka, X. Wu, and H. Haas, "Interference mitigation for indoor optical attocell networks using an angle diversity receiver," *Journal of Lightwave Technology*, vol. 36, no. 18, pp. 3866–3881, 2018.
- [92] C. Chen, W.-D. Zhong, H. Yang, S. Zhang, and P. Du, "Reduction of sinr fluctuation in indoor multi-cell vlc systems using optimized angle diversity receiver," *Journal of Lightwave Technology*, vol. 36, no. 17, pp. 3603–3610, 2018.
- [93] M. Román Cañizares, P. Palacios Játiva, C. A. Azurdia-Meza, S. Montejo-Sánchez, and S. Céspedes, "Impact of diversity combining schemes in a multi-cell VLC system with angle diversity receivers," *Photonic Network Communications*, vol. 43, no. 1, pp. 13–22, 2022.
- [94] A. Upadhyay, "Investigation of RIS Enabled Mixed RF/VLC Relaying with Interference," *Physical Communication*, vol. 55, p. 101920, 2022.

- [95] G. A. Romero-Munoz and K. Lee, "Performance enhancement using decentralised co-operative transmission in an MISO-VLC system," *IET Optoelectronics*, vol. 14, no. 1, pp. 30–36, 2020.
- [96] S. H. Younus, A. A. Al-Hameed, A. T. Hussein, M. T. Alresheedi, and J. M. Elmirghani, "WDM for multi-user indoor VLC systems with SCM," *IET Communications*, vol. 13, no. 18, pp. 3003–3011, 2019.
- [97] A. T. Hussein and J. M. Elmirghani, "Mobile multi-gigabit visible light communication system in realistic indoor environment," *Journal of Lightwave Technology*, vol. 33, no. 15, pp. 3293–3307, 2015.
- [98] H. Liu, X. Gong, M. Huang, Y. Chen, X. Yuan, K. Chen, and S. Yang, "Joint AP grouping and user clustering for interference management in Cell-Free VLC network," *Optics & Laser Technology*, vol. 156, p. 108465, 2022.
- [99] C. Chen, W.-D. Zhong, D. Wu, and Z. Ghassemlooy, "Wide-fov and high-gain imaging angle diversity receiver for indoor sdm-vlc systems," *IEEE Photonics Technology Letters*, vol. 28, no. 19, pp. 2078–2081, 2016.
- [100] M. F. Ali, D. N. K. Jayakody, and Y. Li, "Recent trends in underwater visible light communication (UVLC) systems," *IEEE Access*, vol. 10, pp. 22169–22225, 2022.
- [101] R. Salam, V. A. Bohara, and A. Srivastava, "Smart element allocation strategies for dynamic optical irls in underwater wireless communication," *IEEE Transactions on Vehicular Technology*, 2024.
- [102] B. Anitha Vijayalakshmi, A. Senthil Kumar, V. Kavitha, and D. Ravikumar, "Transmitting patient's health care information using LEDs in hospitals through VLC technology," *Journal of Optics*, pp. 1–8, 2024.
- [103] G. Pan, J. Ye, C. Zhang, J. An, H. Lei, Z. Ding, and M. S. Alouini, "Secure cooperative hybrid VLC-RF systems," *IEEE Transactions on Wireless Communications*, vol. 19, no. 11, pp. 7097–7107, 2020.
- [104] H. Haas, L. Yin, C. Chen, S. Videv, D. Parol, E. Poves, H. Alshaer, and M. S. Islam, "Introduction to indoor networking concepts and challenges in lifi," *Journal of Optical Communications and Networking*, vol. 12, no. 2, pp. A190–A203, 2020.
- [105] F. Wang, F. Yang, J. Song, and Z. Han, "Access frameworks and application scenarios for hybrid VLC and RF systems: State of the art, challenges, and trends," *IEEE Communications Magazine*, vol. 60, no. 3, pp. 55–61, 2022.
- [106] S. Zargari, M. Kolivand, S. A. Nezamalhoseini, B. Abolhassani, L. R. Chen, and M. H. Kahaei, "Resource allocation of hybrid VLC/RF systems with light energy harvesting," *IEEE Transactions on Green Communications and Networking*, vol. 6, no. 1, pp. 600–612, 2021.

- [107] I. Abdalla, M. B. Rahaim, and T. D. Little, "Interference mitigation through user association and receiver field of view optimization in a multi-user indoor hybrid RF/VLC illuminance-constrained network," *IEEE Access*, vol. 8, pp. 228779–228797, 2020.
- [108] X. Wu, C. Chen, and H. Haas, "Mobility management for hybrid LiFi and WiFi networks in the presence of light-path blockage," in *2018 IEEE 88th Vehicular Technology Conference (VTC-Fall)*, pp. 1–5, IEEE, 2018.
- [109] S. Paramita, A. Bhattacharya, R. Ahmad, V. A. Bohara, and A. Srivastava, "Flow-based rate maximization for link aggregation enabled hybrid lifi-wifi network," *IEEE Transactions on Vehicular Technology*, pp. 1–13, 2024.
- [110] S. Abdel-Razeq, H. B. Salameh, and S. Mdardas, "Indoor hybrid wifi/lifi wireless networks (ihwnets): Architecture, channel models, state of the art, and future directions," in *2024 International Conference on Multimedia Computing, Networking and Applications (MCNA)*, pp. 8–14, IEEE, 2024.
- [111] X. Wu and H. Haas, "Mobility-aware load balancing for hybrid lifi and wifi networks," *Journal of Optical Communications and Networking*, vol. 11, no. 12, pp. 588–597, 2019.
- [112] X. Wu and H. Haas, "Access point assignment in hybrid LiFi and WiFi networks in consideration of LiFi channel blockage," in *2017 IEEE 18th international workshop on signal processing advances in wireless communications (SPAWC)*, pp. 1–5, IEEE, 2017.
- [113] R. Ahmad, M. D. Soltani, M. Safari, A. Srivastava, and A. Das, "Reinforcement learning based load balancing for hybrid LiFi WiFi networks," *IEEE Access*, vol. 8, pp. 132273–132284, 2020.
- [114] X. Wu and D. C. O'Brien, "QoS-driven load balancing in hybrid LiFi and WiFi networks," *IEEE Transactions on Wireless Communications*, vol. 21, no. 4, pp. 2136–2146, 2021.
- [115] M. Asad and S. Qaisar, "Energy efficient QoS-based access point selection in hybrid WiFi and LiFi IoT networks," *IEEE Transactions on Green Communications and Networking*, vol. 6, no. 2, pp. 897–906, 2021.
- [116] D. N. Anwar, R. Ahmad, H. Bany Salameh, H. Elgala, and M. Ayyash, "Performance analysis of neural network-based unified physical layer for indoor hybrid lifi–wifi flying networks," *Neural Computing and Applications*, vol. 35, no. 34, pp. 24179–24189, 2023.
- [117] Z. Zeng, M. D. Soltani, X. Wu, and H. Haas, "Access point selection scheme for LiFi cellular networks using angle diversity receivers," in *2019 IEEE Wireless Communications and Networking Conference (WCNC)*, pp. 1–6, IEEE, 2019.
- [118] E. Khorov and I. Levitsky, "Current status and challenges of li-fi: IEEE 802.11 bb," *IEEE Communications Standards Magazine*, vol. 6, no. 2, pp. 35–41, 2022.

- [119] J. Gancarz, H. Elgala, and T. D. Little, "Impact of lighting requirements on vlc systems," *IEEE Communications Magazine*, vol. 51, no. 12, pp. 34–41, 2013.
- [120] M. Figueiredo, L. N. Alves, and C. Ribeiro, "Lighting the wireless world: The promise and challenges of visible light communication," *IEEE Consumer Electronics Magazine*, vol. 6, no. 4, pp. 28–37, 2017.
- [121] A. A. Dowhuszko, M. C. Ilter, and J. Hämäläinen, "Visible light communication system in presence of indirect lighting and illumination constraints," in *ICC 2020-2020 IEEE International Conference on Communications (ICC)*, pp. 1–6, IEEE, 2020.
- [122] C. Gong, S. Li, Q. Gao, and Z. Xu, "Power and rate optimization for visible light communication system with lighting constraints," *IEEE transactions on signal processing*, vol. 63, no. 16, pp. 4245–4256, 2015.
- [123] H. Wu, Q. Wang, J. Xiong, and M. Zuniga, "SmartVLC: Co-designing smart lighting and communication for visible light networks," *IEEE Transactions on Mobile Computing*, vol. 19, no. 8, pp. 1956–1970, 2019.
- [124] S. Chatterjee and D. Sabui, "Daylight integrated indoor vlc architecture: an energy-efficient solution," *Transactions on Emerging Telecommunications Technologies*, vol. 31, no. 9, p. e3800, 2020.
- [125] K. Sindhubala and B. Vijayalakshmi, "Design and performance analysis of visible light communication system through simulation," in *2015 international conference on computing and communications technologies (ICCCT)*, pp. 215–220, IEEE, 2015.
- [126] F.-L. Chang, W.-W. Hu, D.-H. Lee, and C.-T. Yu, "Design and implementation of anti low-frequency noise in visible light communications," in *2017 international conference on applied system innovation (ICASI)*, pp. 1536–1538, IEEE, 2017.
- [127] T. Adiono, A. Pradana, R. V. W. Putra, and S. Fuada, "Analog filters design in vlc analog front-end receiver for reducing indoor ambient light noise," in *2016 IEEE asia pacific conference on circuits and systems (APCCAS)*, pp. 581–584, IEEE, 2016.
- [128] Q. N. Pham, V. P. Rachim, J. An, and W.-Y. Chung, "Ambient light rejection using a novel average voltage tracking in visible light communication system," *Applied Sciences*, vol. 7, no. 7, p. 670, 2017.
- [129] S. Rajagopal, R. D. Roberts, and S.-K. Lim, "Ieee 802.15. 7 visible light communication: modulation schemes and dimming support," *IEEE Communications Magazine*, vol. 50, no. 3, pp. 72–82, 2012.
- [130] D. Walsh, D. Moodie, I. Mauchline, S. Conner, W. Johnstone, and B. Culshaw, "Practical bit error rate measurements on fibre optic communications links in student teaching laboratories," in *9th International Conference on Education and Training in Optics and Photonics (ETOP)*, Marseille, France, Paper ETOP021, 2005.

- [131] Z. Wang, C. Yu, W.-D. Zhong, J. Chen, and W. Chen, "Performance of a novel led lamp arrangement to reduce snr fluctuation for multi-user visible light communication systems," *Optics express*, vol. 20, no. 4, pp. 4564–4573, 2012.
- [132] F. R. Gfeller and U. Bapst, "Wireless in-house data communication via diffuse infrared radiation," *Proceedings of the IEEE*, vol. 67, no. 11, pp. 1474–1486, 1979.
- [133] I. O. for Standardization, "Lighting of work places – Part 1: Indoor," standard, International Organization for Standardization, Geneva, CH, Mar. 2002.
- [134] J. L. Lindsey, *Applied illumination engineering*. Prentice Hall, 1997.
- [135] D. A. Miller, "Establishing optimal wave communication channels automatically," *Journal of Lightwave Technology*, vol. 31, no. 24, pp. 3987–3994, 2013.
- [136] M. S. Chowdhury, W. Zhang, and M. Kavehrad, "Combined deterministic and modified monte carlo method for calculating impulse responses of indoor optical wireless channels," *Journal of Lightwave Technology*, vol. 32, no. 18, pp. 3132–3148, 2014.
- [137] J. R. Barry, J. M. Kahn, W. J. Krause, E. A. Lee, and D. G. Messerschmitt, "Simulation of multipath impulse response for indoor wireless optical channels," *IEEE journal on selected areas in communications*, vol. 11, no. 3, pp. 367–379, 1993.
- [138] J. H. Choi, S. W. Koo, and J. Y. Kim, "Influence of optical path difference on visible light communication systems," in *2009 9th international symposium on communications and information technology*, pp. 1247–1251, IEEE, 2009.
- [139] X. Zhang, K. Cui, M. Yao, H. Zhang, and Z. Xu, "Experimental characterization of indoor visible light communication channels," in *2012 8th international symposium on communication systems, networks & digital signal processing (CSNDSP)*, pp. 1–5, IEEE, 2012.
- [140] Y. Hong, J. Chen, Z. Wang, and C. Yu, "Performance of a precoding mimo system for decentralized multiuser indoor visible light communications," *IEEE Photonics journal*, vol. 5, no. 4, pp. 7800211–7800211, 2013.
- [141] H. Farahneh, S. M. Kamruzzaman, and X. Fernando, "Differential receiver as a denoising scheme to improve the performance of v2v-vlc systems," in *2018 IEEE international conference on communications workshops (ICC Workshops)*, pp. 1–6, IEEE, 2018.
- [142] M. Tomlinson, C. J. Tjhai, M. A. Ambroze, M. Ahmed, M. Jibril, M. Tomlinson, C. J. Tjhai, M. A. Ambroze, M. Ahmed, and M. Jibril, "Historical convolutional codes as tail-biting block codes," *Error-Correction Coding and Decoding: Bounds, Codes, Decoders, Analysis and Applications*, pp. 289–298, 2017.
- [143] H. Ma and J. Wolf, "On tail biting convolutional codes," *IEEE Transactions on Communications*, vol. 34, no. 2, pp. 104–111, 1986.

- [144] B. Vucetic and J. Yuan, *Turbo codes: principles and applications*, vol. 559. Springer Science & Business Media, 2012.
- [145] J. J. Kong and K. K. Parhi, "Interleaved convolutional code and its viterbi decoder architecture," *EURASIP Journal on Advances in Signal Processing*, vol. 2003, no. 13, pp. 1–7, 2003.
- [146] F. Chan and D. Haccoun, "Adaptive viterbi decoding of convolutional codes over memoryless channels," *IEEE Transactions on Communications*, vol. 45, no. 11, pp. 1389–1400, 1997.
- [147] R. Johannesson and K. S. Zigangirov, *Fundamentals of convolutional coding*. John Wiley & Sons, 2015.
- [148] T. Zhang, J. Zhou, Z. Zhang, Y. Lu, F. Su, and Y. Qiao, "Dimming control systems based on low-paprr scfdm for visible light communications," *IEEE Photonics Journal*, vol. 10, no. 5, pp. 1–11, 2018.
- [149] Y. Zuo and J. Zhang, "Energy-efficient optimization design for the multi-color led based visible light communication systems under illumination constraints," *Applied Sciences*, vol. 9, no. 1, p. 1, 2018.
- [150] I. Din and H. Kim, "Energy-efficient brightness control and data transmission for visible light communication," *IEEE photonics technology letters*, vol. 26, no. 8, pp. 781–784, 2014.
- [151] J. Okumura, Y. Kozawa, Y. Umeda, and H. Habuchi, "Hybrid PWM/DPAM dimming control for digital color shift keying using RGB-LED array," *IEEE Journal on Selected Areas in Communications*, vol. 36, no. 1, pp. 45–52, 2017.
- [152] F. Zafar, D. Karunatilaka, and R. Parthiban, "Dimming schemes for visible light communication: the state of research," *IEEE Wireless Communications*, vol. 22, no. 2, pp. 29–35, 2015.
- [153] M. S. Islim, S. Videv, M. Safari, E. Xie, J. J. McKendry, E. Gu, M. D. Dawson, and H. Haas, "The impact of solar irradiance on visible light communications," *Journal of Lightwave Technology*, vol. 36, no. 12, pp. 2376–2386, 2018.
- [154] A. R. Ndjiongue and H. C. Ferreira, "An overview of outdoor visible light communications," *Transactions on Emerging Telecommunications Technologies*, vol. 29, no. 7, p. e3448, 2018.
- [155] IEC-61000-3-3, "Electromagnetic compatibility (EMC)," standard, International Electrotechnical Commission, Geneva, Switzerland, Mar. 2005.
- [156] Lumileds Holding B.V., *LUXEON rebel ES Datasheet*, 5 2016. Rev. 2.

- [157] CIE-So10:2005, “Photometry—The CIE system of physical photometry,” standard, International Organization for Standardization, Geneva, CH, Mar. 2005.
- [158] LM3414-Datasheet, *1A 60W common anode capable constant current Buck LED driver*. Texas Instruments, 5 2010. Rev. 2.
- [159] T. Instruments, *Monolithic photodiode and single-supply transimpedance amplifier*. Texas Instruments, 1994.
- [160] V. Siliconix, *Silicon PIN Photodiode*. Vishay Siliconix, 5 2006. Rev. 2.
- [161] E. Säckinger, *Analysis and design of transimpedance amplifiers for optical receivers*. John Wiley & Sons, 2017.
- [162] A. Gupta and M. Brandt-Pearce, “Receiver design for shot noise limited mimo fso/uv communication systems,” in *2012 IEEE Globecom Workshops*, pp. 1183–1187, IEEE, 2012.
- [163] Y. Chen, C. W. Sung, S.-W. Ho, and W. S. Wong, “Ber analysis and power control for interfering visible light communication systems,” *Optik*, vol. 151, pp. 98–109, 2017.
- [164] L. Yin, X. Wu, and H. Haas, “Indoor visible light positioning with angle diversity transmitter,” in *2015 IEEE 82nd Vehicular Technology Conference (VTC2015-Fall)*, pp. 1–5, IEEE, 2015.
- [165] M. Saadi, T. Ahmad, M. Kamran Saleem, and L. Wuttisittikulkij, “Visible light communication—an architectural perspective on the applications and data rate improvement strategies,” *Transactions on Emerging Telecommunications Technologies*, vol. 30, no. 2, p. e3436, 2019.
- [166] I. C. on Illumination (CIE), “Technical Report Discomfort Glare in Interior Lighting,” standard, International Commission on Illumination (CIE), Viena, Austria, Jan. 1995.
- [167] T. Keppler, N. Watson, and J. Arrillaga, “Computation of the short-term flicker severity index,” *IEEE Transactions on power delivery*, vol. 15, no. 4, pp. 1110–1115, 2000.
- [168] I. Katzela and M. Naghshineh, “Channel assignment schemes for cellular mobile telecommunication systems: A comprehensive survey,” *IEEE personal communications*, vol. 3, no. 3, pp. 10–31, 1996.
- [169] R. Raj, S. Jaiswal, and A. Dixit, “Optimization of led semi-angle in multipath indoor visible light communication links,” in *2019 IEEE International Conference on Advanced Networks and Telecommunications Systems (ANTS)*, pp. 1–6, IEEE, 2019.
- [170] J. Feng, C. Yang, J. Hou, H. Long, and S. Chen, “Performance enhancement for indoor visible light communication system with an improved inter-symbol interference model using optimized hemispherical optical-angle-diversity-receivers,” *Optics Communications*, vol. 454, p. 124488, 2020.

- [171] K. Cai, M. Jiang, and X. Ma, "Photodetector selection aided multiuser mimo optical ofdm imaging visible light communication system," *IEEE Access*, vol. 4, pp. 9870–9879, 2016.
- [172] G. A. Romero-Munoz, K. Kim, K. Lee, and K. Lee, "Performance analysis of sfbc-fstd in multiple-input single-output-vlc systems with co-channel interference," *IET Optoelectronics*, vol. 12, no. 2, pp. 106–113, 2018.
- [173] F. I. K. Mousa, N. Al Maadeed, K. Busawon, A. Bouridane, and R. Binns, "Secure mimo visible light communication system based on user's location and encryption," *Journal of Lightwave Technology*, vol. 35, no. 24, pp. 5324–5334, 2017.
- [174] Q. Wang, Z. Wang, and L. Dai, "Multiuser mimo-ofdm for visible light communications," *IEEE Photonics Journal*, vol. 7, no. 6, pp. 1–11, 2015.
- [175] L. Xiao, G. Sheng, S. Liu, H. Dai, M. Peng, and J. Song, "Deep reinforcement learning-enabled secure visible light communication against eavesdropping," *IEEE transactions on communications*, vol. 67, no. 10, pp. 6994–7005, 2019.
- [176] X. Ma, F. Yang, S. Liu, and J. Song, "Channel estimation for wideband underwater visible light communication: a compressive sensing perspective," *Optics express*, vol. 26, no. 1, pp. 311–321, 2018.
- [177] A. Burton, Z. Ghassemloooy, S. Rajbhandari, and S.-K. Liaw, "Design and analysis of an angular-segmented full-mobility visible light communications receiver," *Transactions on Emerging Telecommunications Technologies*, vol. 25, no. 6, pp. 591–599, 2014.
- [178] F. Yang, J. Gao, and S. Liu, "Novel visible light communication approach based on hybrid oofdm and aco-ofdm," *IEEE photonics technology letters*, vol. 28, no. 14, pp. 1585–1588, 2016.
- [179] K. Saxena, R. Raj, and A. Dixit, "A novel optimization approach for transmitter semi-angle and multiple transmitter configurations in indoor visible light communication links," in *2018 9th International Conference on Computing, Communication and Networking Technologies (ICCCNT)*, pp. 1–7, IEEE, 2018.
- [180] R. Sharma, A. C. Kumari, M. Aggarwal, and S. Ahuja, "Down-link performance of an led based visible light communication system through dynamic control of semi-angle," *Physical Communication*, vol. 33, pp. 222–230, 2019.
- [181] B. of Indian Standard. India., "National Lighting Code; SP 72," standard, Bureau of Indian Standard. India., India, Jan. 2010.
- [182] R. H. Simons and A. R. Bean, *Lighting engineering: applied calculations*. Routledge, 2008.
- [183] ANSI/IESNA, "Standard File Format for the Electronic Transfer of Photometric Data, LM-63-02," standard, ANSI/IESNA, UK, Jan. 2002.

- [184] Y. Qiu, H.-H. Chen, and W.-X. Meng, "Channel modeling for visible light communications—a survey," *Wireless Communications and Mobile Computing*, vol. 16, no. 14, pp. 2016–2034, 2016.
- [185] R. Heinisch and K. F. Leadford, "Illumination systems design: techniques in transition," in *International Optical Design Conference 1998*, vol. 3482, pp. 378–388, SPIE, 1998.
- [186] X. Wu and H. Haas, "Handover skipping for lifi," *IEEE Access*, vol. 7, pp. 38369–38378, 2019.
- [187] P. Garg and P. K. Sharma, "Interference mitigation technique with coverage improvement in indoor vlc system," *Transactions on Emerging Telecommunications Technologies*, vol. 30, no. 2, p. e3511, 2019.
- [188] H. Deng, C.-H. Yeh, and R. J. Willis, "Inter-company comparison using modified topsis with objective weights," *Computers & Operations Research*, vol. 27, no. 10, pp. 963–973, 2000.
- [189] N. H. Zardari, K. Ahmed, S. M. Shirazi, and Z. B. Yusop, *Weighting methods and their effects on multi-criteria decision making model outcomes in water resources management*. Springer, 2015.
- [190] C.-F. Chen, "Applying the analytical hierarchy process (ahp) approach to convention site selection," *Journal of travel research*, vol. 45, no. 2, pp. 167–174, 2006.
- [191] T. L. Saaty, "Group decision making and the ahp," *The analytic hierarchy process: applications and studies*, pp. 59–67, 1989.
- [192] D. O'Brien, "Multi-input multi-output (mimo) indoor optical wireless communications," in *2009 Conference Record of the Forty-Third Asilomar Conference on Signals, Systems and Computers*, pp. 1636–1639, IEEE, 2009.
- [193] L. Zeng, D. C. O'Brien, H. Le Minh, G. E. Faulkner, K. Lee, D. Jung, Y. Oh, and E. T. Won, "High data rate multiple input multiple output (mimo) optical wireless communications using white led lighting," *IEEE Journal on Selected Areas in Communications*, vol. 27, no. 9, pp. 1654–1662, 2009.
- [194] F. Bohagen, P. Orten, and G. E. Oien, "Design of optimal high-rank line-of-sight mimo channels," *IEEE Transactions on Wireless Communications*, vol. 6, no. 4, pp. 1420–1425, 2007.
- [195] T. Fath and H. Haas, "Performance comparison of mimo techniques for optical wireless communications in indoor environments," *IEEE Transactions on Communications*, vol. 61, no. 2, pp. 733–742, 2012.

- [196] A. Nuwanpriya, S.-W. Ho, and C. S. Chen, "Angle diversity receiver for indoor mimo visible light communications," in *2014 IEEE Globecom Workshops (GC Wkshps)*, pp. 444–449, IEEE, 2014.
- [197] A. Nuwanpriya, S.-W. Ho, and C. S. Chen, "Indoor mimo visible light communications: Novel angle diversity receivers for mobile users," *IEEE Journal on selected areas in communications*, vol. 33, no. 9, pp. 1780–1792, 2015.
- [198] Z. Chen, N. Serafimovski, and H. Haas, "Angle diversity for an indoor cellular visible light communication system," in *2014 IEEE 79th Vehicular Technology Conference (VTC Spring)*, pp. 1–5, IEEE, 2014.
- [199] D. Sabui, S. Chatterjee, A. Prakash, B. Roy, and G. S. Khan, "An improved angular diversity receiver structure for indoor VLC system using off-axis freeform optics," in *Novel Optical Systems, Methods, and Applications XXV*, vol. 12216, pp. 164–168, SPIE, 2022.
- [200] D. Sabui, V. Mishra, S. Chatterjee, B. Roy, and G. S. Khan, "Freeform based compact receiver front-end for indoor multi-cell VLC system: Fabrication, optical characterization and associated challenges," *Optik*, vol. 274, p. 170539, 2023.
- [201] D. Sabui, S. Chatterjee, A. Prakash, B. Roy, and G. S. Khan, "Design of an off-axis freeform diversity receiver to improve sinr performance of a multi-cell vlc system," *Optics Communications*, vol. 510, p. 127937, 2022.
- [202] C.-X. Wang, X. You, X. Gao, X. Zhu, Z. Li, C. Zhang, H. Wang, Y. Huang, Y. Chen, H. Haas, *et al.*, "On the road to 6G: Visions, requirements, key technologies and testbeds," *IEEE Communications Surveys & Tutorials*, 2023.
- [203] M. T. Alresheedi and J. M. Elmirghani, "Hologram selection in realistic indoor optical wireless systems with angle diversity receivers," *Journal of Optical Communications and Networking*, vol. 7, no. 8, pp. 797–813, 2015.
- [204] V. Dixit and A. Kumar, "Performance analysis of angular diversity receiver based MIMO–VLC system for imperfect CSI," *Journal of Optics*, vol. 23, no. 8, p. 085701, 2021.
- [205] P. F. Mmbaga, J. Thompson, and H. Haas, "Performance analysis of indoor diffuse VLC MIMO channels using angular diversity detectors," *Journal of Lightwave Technology*, vol. 34, no. 4, pp. 1254–1266, 2016.
- [206] Z. Zeng, M. D. Soltani, M. Safari, and H. Haas, "Angle diversity receiver in LiFi cellular networks," in *ICC 2019-2019 IEEE International Conference on Communications (ICC)*, pp. 1–6, IEEE, 2019.
- [207] X. Wu, M. D. Soltani, L. Zhou, M. Safari, and H. Haas, "Hybrid LiFi and WiFi networks: A survey," *IEEE Communications Surveys & Tutorials*, vol. 23, no. 2, pp. 1398–1420, 2021.

- [208] X. Wu, D. C. O'Brien, X. Deng, and J.-P. M. Linnartz, "Smart handover for hybrid LiFi and WiFi networks," *IEEE Transactions on Wireless Communications*, vol. 19, no. 12, pp. 8211–8219, 2020.
- [209] G. Ma, R. Parthiban, and N. Karmakar, "An adaptive handover scheme for hybrid LiFi and WiFi networks," *IEEE Access*, vol. 10, pp. 18955–18965, 2022.
- [210] S. Paramita, A. Bhattacharya, V. A. Bohara, and A. Srivastava, "Wiliconnect: A novel csi sharing technique in hybrid wifi/lifi networks," in *2024 IEEE 99th Vehicular Technology Conference (VTC2024-Spring)*, pp. 1–5, IEEE, 2024.
- [211] S. Ma, H. Sheng, J. Sun, H. Li, X. Liu, C. Qiu, M. Safari, N. Al-Dhahir, and S. Li, "Feasibility conditions for mobile lifi," *IEEE Transactions on Wireless Communications*, 2024.
- [212] Y. Wang, D. A. Basnayaka, X. Wu, and H. Haas, "Optimization of load balancing in hybrid LiFi/RF networks," *IEEE Transactions on Communications*, vol. 65, no. 4, pp. 1708–1720, 2017.
- [213] J.-B. Wang, Q.-S. Hu, J. Wang, M. Chen, and J.-Y. Wang, "Tight bounds on channel capacity for dimmable visible light communications," *Journal of Lightwave Technology*, vol. 31, no. 23, pp. 3771–3779, 2013.
- [214] M. D. Soltani, A. A. Purwita, Z. Zeng, C. Chen, H. Haas, and M. Safari, "An orientation-based random waypoint model for user mobility in wireless networks," in *2020 IEEE International Conference on Communications Workshops (ICC Workshops)*, pp. 1–6, IEEE, 2020.
- [215] X. Wu and H. Haas, "Load balancing for hybrid LiFi and WiFi networks: To tackle user mobility and light-path blockage," *IEEE Transactions on Communications*, vol. 68, no. 3, pp. 1675–1683, 2019.
- [216] Y. Wang, X. Wu, and H. Haas, "Load balancing game with shadowing effect for indoor hybrid lifi/rf networks," *IEEE Transactions on Wireless Communications*, vol. 16, no. 4, pp. 2366–2378, 2017.
- [217] A. B. Sediq, R. H. Gohary, R. Schoenen, and H. Yanikomeroglu, "Optimal tradeoff between sum-rate efficiency and jain's fairness index in resource allocation," *IEEE Transactions on Wireless Communications*, vol. 12, no. 7, pp. 3496–3509, 2013.
- [218] R. F. Riemersma-van Der Lek, D. F. Swaab, J. Twisk, E. M. Hol, W. J. Hoogendijk, and E. J. Van Someren, "Effect of bright light and melatonin on cognitive and noncognitive function in elderly residents of group care facilities: a randomized controlled trial," *Jama*, vol. 299, no. 22, pp. 2642–2655, 2008.
- [219] T. Partonen and J. Lönqvist, "Bright light improves vitality and alleviates distress in healthy people," *Journal of Affective disorders*, vol. 57, no. 1-3, pp. 55–61, 2000.

S. Chandra
19-06-2024

19/06/2024
Professor
Electrical Engineering Department
JADAVPUR UNIVERSITY
Kolkata - 700 032